Project THEMIS
Technical Report No. 3

SECONDARY FLOW IN A BOUNDARY LAYER

by

Scott D. Veenhuizen
and
R. N. Meroney

Prepared under
Office of Naval Research
Contract No. N00014-68-A-0493-0001
Project No. NR 062-414/6-6-68(Code 438)
U. S. Department of Defense
Washington, D. C.

Fluid Dynamics and Diffusion Laboratory
College of Engineering
Colorado State University
Fort Collins, Colorado

June 1969

CER68-69SDV-RNM28

ABSTRACT

The secondary flow in the developing boundary layer of a square duct is investigated experimentally. Measurements of the horizontal components of secondary flow were made for free stream velocities of 3, 6.1, and 12.2 m/s, corresponding to Reynolds numbers based upon the hydraulic diameter of 3.6×10^5 , 7.2×10^5 , and 1.4×10^6 at a ratio of L/D_h of 6.7 . Measurements of the developing boundary layer parameters and turbulence quantities in a corner were made for the intermediate Reynolds number.

The secondary flow and turbulence distribution in a corner are discussed and compared with the fully developed flow situation. The results indicate the maximum secondary flow velocity is less than 2% of the free stream velocity, and further, that the secondary flow may encompass the entire cross section.

The turbulence distribution was found to not differ fundamentally from those found in fully developed flow.

A criterion for two dimensionality of wind tunnel flow is examined and a correction for three dimensionality is evaluated from the experimental data.

TABLE OF CONTENTS

TABLE OF CONTENTS - Continued

LIST OF TABLES

LIST OF FIGURES

LIST OF FIGURES - Continued

LIST OF FIGURES - Continued

LIST OF SYMBOLS

Symbol	Definition	Dimensions
a_i	Hot-wire sensitivity for i^{th} component	VT/L
B	Constant	V^2T^m/L^m
b_i	Hot-wire sensitivity for i^{th} component	UT/L
C_f	Skin friction coefficient	
$\overline{C}_f$	Average skin friction coefficient	
C_f^*	Ratio of skin friction coefficient	
D_h	Hydraulic diameter	L
d_i	Half width, height of tunnel cross section	L
E	Mean hot-wire voltage	V
E_o	Mean hot-wire voltage at zero velocity	V
$\overline{e_{i,j}^2}$	Mean square fluctuating hot-wire voltage, i-j plane	V^2
H	Shape factor	
h	Point in free stream	L
i	Index	
j	Index	
K	Momentum integral correction term	
k	Index, constant	
L	Wind tunnel width	L
l	Index	
m	Exponent	
P	Mean pressure	ML/T^2
U	Total velocity	L/T

LIST OF SYMBOLS - Continued

Symbol	Definition	Dimensions
$U_{i,j}$	Resultant of i^{th} and j^{th} mean velocity components	L/T
U_∞	Free stream velocity	L/T
u_i	Turbulent velocity component in i^{th} direction	L/T
$\overline{u_i u_j}$	Time mean of product of u_i and u_j	L^2/T^2
x_i	Spatial coordinate in i^{th} direction	L
x_i'	$d_i - x_i$	L
α	Secondary flow angle	
β	Reference angle	
δ	Boundary layer thickness along centerline	L
δ^*	Displacement thickness	L
ε_{ijk}	Alternating third order permutation tensor	
η	Variable of integration	L
θ	Momentum thickness	L
μ	Dynamic viscosity	M/LT
ν	Kinematic viscosity	L^2/T
ρ	Density	M/L^3
$\tau_{i,j}$	Shear stress tensor component	M/LT^2
τ_o	Shear stress at boundary	M/LT^2
ϕ	Angle of yaw	
ψ	Stream function	L^2/T
Ω_i	Mean vorticity about i^{th} direction	1/T
ω_i	Fluctuating vorticity about i^{th} direction	1/T

Chapter I

INTRODUCTION

Turbulent flow in ducts of noncircular cross section is generally of a three-dimensional nature. The mean velocity vector consists of a primary component in the axial direction and a transverse component in the plane perpendicular to the axial direction. The turbulence properties of these flows are also generally of a three-dimensional nature.

The most obvious characteristic of the three-dimensionality is the now commonly accepted distortion of the lines of constant velocity, or isovels, particularly in the region of a corner. Nikuradse (20) was the first to observe experimentally that the isovels were displaced toward the walls in corner regions and away from the walls at the mid-points between corners of a triangular duct. Some of Nikuradse's results are sketched in Fig. 1. From this fact, Prandtl (23) concluded that a flow component must exist perpendicular to the isovels at points of nonuniform isovel curvature and be directed from the concave side to the convex side of an isovel. The effect of the transverse flow was to convect higher momentum fluid into the corner regions and lower momentum fluid into the center region of the duct at mid-points between corners. These transverse currents have since become known as secondary flows and are generally regarded as superimposed upon the axial mean flow or primary flow.

The effect of the secondary flow on wall shear stress in noncircular ducts is to cause a more uniform distribution around the periphery. Hoagland (12) has measured the wall shear stress in a

square duct with a Preston tube and compared his results with an analytical solution given by Deissler and Taylor (5) wherein secondary flow effects have been neglected. The measured wall shear stress is considerably higher in the region of the corner compared with Deissler and Taylor's result. A more recent numerical solution involving the use of a computer has been given by Liggett, Chiu and Miao (16) in which the wall shear stress in the corner was calculated accounting for secondary flow. This result was compared by the authors with Hoagland's experimental values and found to be more realistic, Fig. 2.

Further effects of the three-dimensional nature of turbulent flow in noncircular ducts are of engineering interest. In the corners of a rectangular duct, the heat transfer coefficients have been found to be as much as thirty percent higher than the predicted values for uniform wall temperatures (5).

Sediment transport in rivers and canals is another example where secondary flow effects are significant. Delleur and McManus (7) have measured the primary velocity profiles in an open channel flow. Their results show an isovel distortion in the corner regions indicating secondary flows similar to those observed in the corners of rectangular wind tunnels. Leopold (14) describes ribbons of sediment moving along the floor of an open channel attributed to secondary flows.

The above effects are due to the local characteristics of the turbulent flow field and any solution to the above problems will have to account for secondary flows to not only be qualitatively correct, but to be quantitatively correct.

With the exception of one study performed by Pletcher and McManus (22) on the entrance region of a rectangular duct, the previous studies of secondary flows have been restricted to the fully developed flow case. The present investigation is intended to examine further the case of a developing turbulent flow, in particular the boundary layer developing along the floor of a wind tunnel with the emphasis placed upon experimentally determining the regions of secondary flow and gaining a greater understanding of the three-dimensional nature of a developing turbulent boundary layer.

Chapter II

ANALYTICAL BACKGROUND

In this chapter the basic equations will be presented in a general form for later reference. Subsequently the case of secondary flow for fully developed flow systems will be described. Much of the description will follow that presented in previous work but it will be included here for completeness and for emphasis. Next, the case of the developing boundary layer is described and compared to the fully developed flow case. The remainder of the chapter is devoted to summarizing significant measurements.

2.1 Generalized Governing Equations

The equations governing a general flow are the turbulent Navier-Stokes equations of motion and the equation of continuity. Under the restrictions of steady and incompressible flow, the momentum equation is in tensor notation

$$\rho U_j \frac{\partial U_i}{\partial x_j} = - \frac{\partial P}{\partial x_i} + \mu \frac{\partial^2 U_i}{\partial x_j \partial x_j} - \rho \frac{\partial}{\partial x_j} (\overline{u_i u_j}) \qquad (2\text{-}1)$$

for $i, j=1, 2,$ and 3. The U_i are the mean velocities in the three coordinate directions defined in Fig. 3 and the last term is the apparent Reynolds' stresses. The other symbols have their standard meaning.

Similarly, the continuity equation for the mean flow is

$$\frac{\partial U_i}{\partial x_i} = 0 \qquad (2\text{-}2)$$

and for the turbulent components, it is

$$\frac{\partial u_i}{\partial x_i} = 0 \quad . \tag{2-3}$$

Equations (2-1) through (2-3) with the appropriate boundary conditions do not form a complete set of equations from which a solution could be obtained. Missing is a relationship between the turbulent shear stresses and the mean velocities. At this time an adequate relationship is not available, thus, an analytic solution is not possible.

By operating on equation (2-1) with the curl operator and manipulating with the continuity equations, the vorticity equation may be obtained. It is

$$\rho U_k \frac{\partial \Omega_\ell}{\partial x_k} - \rho \Omega_k \frac{\partial U_\ell}{\partial x_k} = \varepsilon_{ji\ell} \frac{\partial}{\partial k_j \partial x_k} (-\rho \overline{u_i u_k}) + \mu \frac{\partial^2 \Omega_\ell}{\partial x_k \partial x_k} \tag{2-4}$$

where $\Omega_\ell = \varepsilon_{ji\ell} \frac{\partial U_i}{\partial x_j}$ is the mean vorticity vector about the ℓ direction and $\varepsilon_{ji\ell}$ is the alternating third order permutation tensor. A turbulent vorticity can be defined analogous to the mean vorticity from which

$$\varepsilon_{ji\ell} \frac{\partial}{\partial x_j \partial x_k} (-\rho \overline{u_i u_k}) = - \rho \overline{u_k \frac{\partial \omega_\ell}{\partial x_k}} + \rho \overline{\omega_k \frac{\partial u_\ell}{\partial x_k}} \tag{2-5}$$

where as above $\omega_\ell = \varepsilon_{ji\ell} \frac{\partial u_i}{\partial x_j}$.

Derivations of the above equations can be found in Hinze (11).

Although the complete turbulent Navier-Stokes equations cannot presently be solved, much information can be gained from an examination

of their terms together with some simplifications due to the geometry of the flow.

2.1.1 Fully Developed Flow: Momentum Equations - When the flow is fully developed, some simplification of the governing equations is possible. For the case here, fully developed flow is taken to mean that all variables are constant in the axial, or mean flow direction, i.e., derivatives in the x_1 direction are zero. With this simplification equation (2-1) through equation (2-4) can be written

$$\left.\begin{aligned}
\rho U_2 \frac{\partial U_1}{\partial x_2} + \rho U_3 \frac{\partial U_1}{\partial x_3} &= -\frac{\partial P}{\partial x_1} + \mu\left(\frac{\partial^2 U_1}{\partial x_2^2} + \frac{\partial^2 U_1}{\partial x_3^2}\right) \\
&\quad - \rho \frac{\partial}{\partial x_2}(\overline{u_1 u_2}) - \rho \frac{\partial}{\partial x_3}(\overline{u_1 u_3}) \\
\rho U_2 \frac{\partial U_2}{\partial x_2} + \rho U_3 \frac{\partial U_2}{\partial x_3} &= -\frac{\partial P}{\partial x_2} + \mu\left(\frac{\partial^2 U_2}{\partial x_2^2} + \frac{\partial^2 U_2}{\partial x_3^2}\right) \\
&\quad - \rho \frac{\partial}{\partial x_2}(\overline{u_2^2}) - \rho \frac{\partial}{\partial x_3}(\overline{u_2 u_3}) \\
\rho U_2 \frac{\partial U_3}{\partial x_2} + \rho U_3 \frac{\partial U_3}{\partial x_3} &= -\frac{\partial P}{\partial x_3} + \mu\left(\frac{\partial^2 U_3}{\partial x_2^2} + \frac{\partial^2 U_3}{\partial x_3^2}\right) \\
&\quad - \rho \frac{\partial}{\partial x_2}(\overline{u_2 u_3}) - \rho \frac{\partial}{\partial x_3}(\overline{u_3^2})
\end{aligned}\right\} \qquad (2\text{-}6)$$

where the components of equation (2-1) have been written out for the three coordinate directions. The continuity equations are written as

$$\left.\begin{aligned} &\frac{\partial U_2}{\partial x_2} + \frac{\partial U_3}{\partial x_3} = 0 \\ \text{and} \quad &\\ &\frac{\partial u_2}{\partial x_2} + \frac{\partial u_3}{\partial x_3} = 0 \end{aligned}\right\} \qquad (2\text{-}7)$$

General solutions to equations (2-6) and (2-7) appear to be as unapproachable as solutions to the full equations. It is interesting to note, however, that several attempts at solving these equations for the case of fully developed secondary flow in a corner have met with some success. Delleur and McManus (7) attempted to obtain a solution by a simplified mathematical flow model for an open channel utilizing an assumed mixing length relation between the mean velocity gradients and the turbulent shearing stresses. Their model evidently was overly simplified for their solution does not agree with any experimental measurements.

More recently Liggett, Chiu and Miao (16) used a semi-theoretical approach wherein the axial equation of motion was transformed into an equation in coordinates corresponding to the isovels of the mean axial flow and their perpendiculars. The measured axial mean velocity profiles were used with von Kármán's equation for shear in a finite difference form of the transformed equations of motion to obtain a numerical solution from a computer for the flow in a 90^{o} corner. The difficulty with this method is that the isovel distribution must be very accurately determined since the coordinate transformation to be made must be determined in an analytical form from these measurements. The example computed by the authors appears to

give reasonable results but is very cumbersome and not well suited to other applications. Their computer solution did compare very favorably with their experimental measurements for a 90^{o} "V" open channel. The method was extended later by Chiu and McSparran (4) to an open channel with sediment transport. Again, the results were favorable.

2.1.2 Fully Developed Flow: Vorticity Equation - The vorticity equation has been discussed by many investigators of secondary flows for the fully developed flow case. What is included here is a summary of the important contributions from these discussions and an analysis to determine the apparent conditions under which secondary flows cannot exist and under which secondary flows can exist.

The vorticity equation for fully developed flow is from equation (2-4)

$$\rho U_2 \frac{\partial \Omega_1}{\partial x_2} + \rho U_3 \frac{\partial \Omega_1}{\partial x_3} = \frac{\partial^2}{\partial x_2 \partial x_3} (\overline{\rho u_3^2} - \overline{\rho u_2^2}) - \left(\frac{\partial^2}{\partial x_2^2} - \frac{\partial^2}{\partial x_3^2} \right) \rho \overline{u_2 u_3} + \mu \left(\frac{\partial^2 \Omega_1}{\partial x_2^2} + \frac{\partial^2 \Omega_1}{\partial x_3^2} \right) \qquad (2\text{-}8)$$

which does not include the axial mean velocity. The interpretation of vorticity is that of angular rotation of a fluid element about some axis. Equation (2-8) is a description of the rotational behavior of a fluid element in the plane perpendicular to the axial direction. The terms on the left side represent the convection of mean vorticity in the plane by the mean lateral velocities and the last term on the

right hand side represents the diffusion and dissipation of mean vorticity by the viscous forces. The remaining terms on the right side are due to the turbulent nature of the flow. The first of these involves the normal turbulent intensities and the second involves the turbulent shear stress, and are commonly thought of as the source of vorticity production.

If $U_2 = U_3 = 0$ there is no secondary flow by definition, and there is no axial vorticity since $\Omega_1 = \partial U_3/\partial x_2 - \partial U_2/\partial x_3$. Conversely, when $\Omega_1 = 0$, U_2 and U_3 then satisfy Laplaces two-dimensional equation and therefore must also be zero; hence, zero vorticity implies the absence of secondary flow; consequently, the left side of equation (2-8) vanishes. Vanishing of the left side of equation (2-8) provides a restrictive condition on the turbulent stress terms of equation (2-8) that is

$$\frac{\partial^2}{\partial x_3 \partial x_2} \left(\overline{u_3^2} - \overline{u_2^2}\right) - \left(\frac{\partial^2}{\partial x_3^2} - \frac{\partial^2}{\partial x_2^2}\right) \overline{u_2 u_3} = 0 \quad . \tag{2-9}$$

When turbulent stress terms are set equal to zero as in equation (2-9), and the stream function, ψ , is introduced such that $U_2 = \partial\psi/\partial x_3$ and $U_3 = -\partial\psi/\partial x_2$, then equation (2-8) transforms to

$$\frac{\partial\psi}{\partial x_2}\left[\frac{\partial^2}{\partial x_2^2}\left(\frac{\partial\psi}{\partial x_3}\right) + \frac{\partial^2}{\partial x_3^2}\left(\frac{\partial\psi}{\partial x_3}\right)\right] - \frac{\partial\psi}{\partial x_3}\left[\frac{\partial^2}{\partial x_2^2}\left(\frac{\partial\psi}{\partial x_2}\right) + \frac{\partial^2}{\partial x_3^2}\left(\frac{\partial\psi}{\partial x_2}\right)\right]$$

$$+ \nu \frac{\partial^2}{\partial x_2^2}\left(\frac{\partial^2\psi}{\partial x_2^2} + \frac{\partial^2\psi}{\partial x_3^2}\right) + \nu \frac{\partial^2}{\partial x_3^2}\left(\frac{\partial^2\psi}{\partial x_2^2} + \frac{\partial^2\psi}{\partial x_3^2}\right) = 0 \quad . \tag{2-10}$$

Maslen (19) utilized the boundary conditions $\partial\psi/\partial x_3 = \partial\psi/\partial x_2 = 0$ at the boundaries to show that ψ satisfies Laplace's two-dimensional equation and is therefore constant throughout the flow, which implies $U_2 = U_3 = 0$. Equation (2-9), therefore provides a necessary and sufficient condition for the nonexistence of secondary flows. Equation (2-8), without the terms of equation (2-9), is the laminar vorticity equation which Maslen used to show that secondary currents cannot exist in steady, fully developed laminar flow.

Einstein and Li (8) also discussed equation (2-8) and arrived at the same conclusion, equation (2-9), from physical arguments as did Brundrett and Baines (2).

The condition under which secondary flows do, or do not exist in steady, fully developed flow is thus completely determined by equation (2-9). The conditions under which equation (2-9) vanishes may be stipulated, but the conditions for which it does not vanish are much more complicated. Obviously equation (2-9) vanishes identically for laminar flow which is the case analyzed by Maslen.

When the flow is turbulent, but isotropic and homogeneous $\overline{u_3^2} = \overline{u_2^2}$ and the first term in equation (2-9) is zero. The lateral correlations are zero by definition, thus the second term is zero, and equation (2-9) vanishes.

For steady, fully developed flow in a straight circular tube the lateral correlations $\overline{u_1u_3}$, $\overline{u_3u_1}$, $\overline{u_2u_3}$ and $\overline{u_3u_2}$ are zero, and $\overline{u_1u_2} = \overline{u_2u_1}$, thus the last term in equation (2-9) is zero. The transverse intensities $\overline{u_3^2}$ and $\overline{u_2^2}$ approach equal values at the centerline of the tube, but near the wall they are not equal. From

symmetry arguments, the mixed derivatives are equal and thus, the first term in equation (2-9) is also zero. Because of symmetry of the turbulence field, secondary flows cannot exist in steady, fully developed turbulent circular tube flow.

2.1.3 Fully Developed Flow: Stress Tensor - Arguments of symmetry similar to those mentioned for circular tube flow have been used by Gessner (10) to predict the boundaries of secondary flow cells in fully developed square duct flow. Brundrett and Baines (2) gave a similar discussion and extended it to determine the terms of the turbulent stress tensor at different locations in the cross section of a square duct.

The bisectors of the walls, the bisectors of the corners, or diagonals, and the centerline are locations where simplified forms of the tensor may be written by inspection when considering conditions of symmetry at these locations. By inspection of the conditions shown in Fig. 4, the tensor has the following forms at the designated locations.

On centerline
$$\begin{pmatrix} \overline{u_1^2} & 0 & 0 \\ 0 & \overline{u_2^2} & 0 \\ 0 & 0 & \overline{u_2^2} \end{pmatrix} \tag{2-11}$$

On corner diagonal
$$\begin{pmatrix} \overline{u_1^2} & \overline{u_1 u_2} & \overline{u_1 u_2} \\ \overline{u_1 u_2} & \overline{u_2^2} & \overline{u_2 u_3} \\ \overline{u_1 u_2} & \overline{u_2 u_3} & \overline{u_2^2} \end{pmatrix} \tag{2-12}$$

$$\text{On } x_2 \text{ axis} \quad \begin{pmatrix} \overline{u_1^2} & \overline{u_1 u_2} & 0 \\ \overline{u_1 u_2} & \overline{u_2^2} & 0 \\ 0 & 0 & \overline{u_3^2} \end{pmatrix} \tag{2-13}$$

$$\text{On } x_3 \text{ axis} \quad \begin{pmatrix} \overline{u_1^2} & 0 & \overline{u_1 u_3} \\ 0 & \overline{u_2^2} & 0 \\ \overline{u_1 u_3} & 0 & \overline{u_3^2} \end{pmatrix} \tag{2-14}$$

Brundrett and Baines (2) designated the turbulent terms of equation (2-9) as the turbulent vorticity production terms in accordance with Townsend (27) and commented that if the second of the two turbulence terms were smaller than the first, then vorticity in region I of Fig. 4 would be negative. Experimental evaluation of the two terms by Brundrett and Baines has shown this to be true. The physical action of each of the turbulence vorticity production terms has been discussed by Einstein and Li (8) with the gradients of the term $\overline{u_3^2} - \overline{u_2^2}$ interpreted as a fluctuating normal pressure, which when unbalanced creates a rotation of a fluid element. The term $\overline{u_2 u_3}$ is interpreted as a turbulent shear stress on a surface in the x_1-x_3 plane directed in the x_2 direction, or on a surface in the x_1-x_2 plane directed in the x_3 direction. An unbalance in the gradient of this last term also would produce a rotation of a fluid element. Tracy (28) argues that this last term is a result of the vorticity and would be zero if there were no vorticity, and thus the only terms which can produce rotation are the normal intensity terms.

2.2 Developing Flow

The developing flow case to be described in the following section is much more complex than the fully developed flow discussed above. This type of flow is found in the entrance regions of non-circular wind tunnels and is characterized by two regions of flow; the potential core or free stream, and the boundary layers which develop along the walls. The complexity of this flow over that just discussed is due to several fundamental differences.

The entrance conditions greatly influence the characteristics of the flow in the potential core region, and to a lesser extent, in the boundary layers. The turbulence characteristics of the free stream are dependent upon the characteristics of the fluid before it enters the duct, and it also depends upon the physical structures which are located in the entrance. Although correlations between the entrance conditions and the turbulence characteristics directly downstream from them have been studied, it has never been determined how to relate them to solutions of the flow field. The entrance conditions at the beginning of the boundary layer affect their properties for some distance downstream, although, at sufficient distances from the beginning these effects decay and the boundary layer approaches an equilibrium boundary layer.

Interaction between the free stream and the outer edges of the boundary layer creates further complications. Intermittency of turbulence is a characteristic of this interaction between the two regimes about which little is actually known, except that it is

dependent upon the free stream turbulence level and upon the external pressure gradient of the free stream.

2.2.1 Developing Flow: Momentum Equations - The mathematical description of secondary flow in a three-dimensional boundary layer becomes extremely complex due to two complications. The simplification that was accomplished earlier for fully developed flow is no longer allowed, and there now exists an upper boundary to the boundary layer which distinguishes the boundary layer from the free stream. On either side of this external boundary exist two decidedly different regimes of flow. In the most general sense, however, equations (2-1) and (2-3) are applicable on either side of this boundary and through this external boundary.

In general, equations (2-1) and (2-3) cannot be simplified and must be dealt with in their entirety. The simplification used in section 2.1 no longer applies since the variables are now allowed to vary in the x_1 direction. Boundary layer approximations to reduce the complexity of the equations of motion are not applicable because these approximations generally assume the flow field to be of a two-dimensional nature. Three-dimensional boundary layer equations have been developed by Mager (18) and Sears (25), but these apply specifically to the region of the boundary layer and are restricted to regions away from any wall effects. Indications are that the secondary flow is not limited to the boundary layer, but exists simultaneously in the free stream and in the boundary layer. Introducing secondary flow of this nature into the boundary layer equations would require modification of the boundary conditions of the external

boundary of the boundary layer in the form of making these conditions be of a functional nature, thereby increasing the degree of the complexity for solution.

2.2.2 Developing Flow: Vorticity Equation - It is interesting to consider the vorticity equation for the case of a developing flow. As mentioned above, the simplification afforded by the vanishing of x_1 derivatives is no longer allowed. Without this simplification, equation (2-4) must be taken in its entirety. The equation for vorticity in the x_1 direction is

$$U_1 \frac{\partial \Omega_1}{\partial x_1} + U_2 \frac{\partial \Omega_1}{\partial x_2} + U_3 \frac{\partial \Omega_1}{\partial x_3}$$

$$- \Omega_1 \frac{\partial U_1}{\partial x_1} - \Omega_2 \frac{\partial U_1}{\partial x_2} - \Omega_3 \frac{\partial U_1}{\partial x_3} = \nu \nabla^2 \Omega_1 + \frac{\partial^2}{\partial x_2 \partial x_3} (\overline{u_3^2} - \overline{u_2^2})$$

$$- \left(\frac{\partial^2}{\partial x_2^2} - \frac{\partial^2}{\partial x_3^2} \right) \overline{u_2 u_3} + \frac{\partial^2}{\partial x_1 \partial x_3} (\overline{u_1 u_2})$$

$$- \frac{\partial^2}{\partial x_1 \partial x_2} (\overline{u_1 u_3}) \qquad (2\text{-}15)$$

which now contains the axial mean velocity and its gradients on the left side. The additional terms on the left involving the velocity gradients, $\Omega_k \, \partial U_1 / \partial x_k$, are terms describing the change in vorticity due to the stretching or contracting of a stream tube. Additional terms appearing on the right side involve two turbulent shear terms, the gradients of which are no longer zero in the axial direction. The other additional terms appearing are the axial convection of axial

vorticity and axial dissipation of axial vorticity. The equations for mean vorticity in the lateral directions are

$$\left.\begin{aligned} U_1 \frac{\partial \Omega_2}{\partial x_1} + U_2 \frac{\partial \Omega_2}{\partial x_2} + U_3 \frac{\partial \Omega_2}{\partial x_3} - \Omega_1 \frac{\partial U_2}{\partial x_1} - \Omega_2 \frac{\partial U_2}{\partial x_2} - \Omega_3 \frac{\partial U_2}{\partial x_3} \\ = \nu \nabla^2 \Omega_2 + \frac{\partial^2}{\partial x_1 \partial x_3} (\overline{u_3^2} - \overline{u_1^2}) + \left(\frac{\partial^2}{\partial x_1^2} - \frac{\partial^2}{\partial x_3^2} \right) \overline{u_1 u_3} \\ + \frac{\partial^2}{\partial x_1 \partial x_3} (\overline{u_2 u_3}) - \frac{\partial^2}{\partial x_3 \partial x_2} (\overline{u_1 u_2}) \end{aligned}\right\} \quad (2\text{-}16)$$

and

$$\left.\begin{aligned} U_1 \frac{\partial \Omega_3}{\partial x_1} + U_2 \frac{\partial \Omega_3}{\partial x_2} + U_3 \frac{\partial \Omega_3}{\partial x_3} - \Omega_1 \frac{\partial U_3}{\partial x_1} - \Omega_2 \frac{\partial U_3}{\partial x_2} - \Omega_3 \frac{\partial U_3}{\partial x_3} = \\ = \nu \nabla^2 \Omega_3 + \frac{\partial^2}{\partial x_1 \partial x_2} (\overline{u_1^2} - \overline{u_2^2}) + \left(\frac{\partial^2}{\partial x_2^2} - \frac{\partial^2}{\partial x_1^2} \right) \overline{u_1 u_2} + \frac{\partial^2}{\partial x_2 \partial x_3} (\overline{u_1 u_3}) \\ - \frac{\partial^2}{\partial x_1 \partial x_3} (\overline{u_2 u_3}) \quad . \end{aligned}\right\}$$

In addition to equation (2-4) for vorticity, a continuity equation for mean vorticity is available (13). It is

$$\frac{\partial \Omega_1}{\partial x_1} + \frac{\partial \Omega_2}{\partial x_2} + \frac{\partial \Omega_3}{\partial x_3} = 0 \quad . \qquad (2\text{-}17)$$

As in the continuity equation for velocity, if all the terms are zero, then a constant uniform vorticity field exists. If one of the terms is non-zero, then at least two of them must be non-zero, that is, there must be a change in mean vorticity in two directions simultaneously. If the flow is considered to enter a square duct with zero

vorticity, then vorticity will develop and continue to change until the condition of fully developed flow is attained. Under the restriction of equation (2-17), the vorticity must develop simultaneously in at least two directions, and by symmetry in a square duct, it must develop in all three coordinate directions when considering the complete cross section. Assuming that the total vorticity vector is zero when the flow enters the duct, equation (2-17) indicates that the vorticity in the lateral directions must change in an opposite sense to that of the axial vorticity. Discussions by Gessner (10) and Brundrett and Baines (2) indicate that the axial vorticity is limited to cells in the cross section for fully developed flow which are bounded by the coordinate axes and the corner bisectors. They have further indicated, and substantiated by measurement, that the axial vorticity is of different sign, depending upon which of these cells is being considered. In consideration of the above discussion then, it would seem that the lateral vorticity should change sign in a corresponding manner. The flow is indeed complex.

2.2.3 Developing Flow: Stress Tensor - The arguments of symmetry that were applied in section 2.1.2 to the square duct for fully developed flow are also valid for a square duct with developing flow since the agreements were based strictly upon geometrical considerations. The only change which occurs is due to the nature of the turbulence of the entering flow. If the entering flow is considered to be laminar, then the stress components are zero by definition until the boundary layer is reached. If the entering flow is turbulent, then the tensors presumably would take the form of (2-11)

unless the positions considered were in the boundary layer. Under this kind of a restriction it would be natural to conclude that the secondary flow is limited to the regions of the boundary layer since the terms in the vorticity equation attributed to vorticity production involve the difference of the turbulent stresses $\overline{u_3^2}$ and $\overline{u_2^2}$ which are presumably equal in this region. Evidently secondary flows are not limited to the boundary layers only as experimental measurements by Pletcher and McManus (22) indicate the presence of secondary flow components in the free stream region of a developing flow. In this case the tensors would assume the forms already given.

2.3 Additional Literature

In addition to the theoretical material contributed to the subject of secondary flow by those authors which have already been mentioned, a substantial amount of experimental measurements concerning secondary flows have been contributed. Table I contains a summary of the experimental studies that have been performed and published on secondary flow which this author has encountered during the present investigation. Included in this tabulation is the present study.

With the exception of the study conducted by Pletcher and McManus, the studies listed in Table I all deal with fully developed flows. This fact coupled with the degree of success evident on a theoretical level, as exemplified by the preceding section, provided the stimulus for an experimental program to examine the secondary flow in a boundary layer. This program is described in the next chapter.

Chapter III

EXPERIMENTAL PROGRAM AND PROCEDURES

The experimental work was performed in the rectangular test section of the large U.S. Army Micrometeorological wind tunnel in the Fluid Dynamics and Diffusion Laboratory at Colorado State University. The primary objective of the experiment was to examine secondary flow in the developing boundary layer along the floor of this tunnel. In this chapter are described the tunnel facility, the instrumentation, and the measurement techniques.

3.1 Wind Tunnel

The U.S. Army Micrometeorological wind tunnel, Fig. 5, was designed to simulate atmospheric boundary layer effects. The test section of approximately 30 meters in length constituted one side of the recirculating system with the driving motor and heating-cooling coils located on the opposite side. Air left the three meter diameter, four bladed airplane propeller, passed through the heating-cooling coils and turned through two 90 degree corners with turning vanes to a stilling chamber. From the stilling chamber the air passed through four fine mesh screens of stainless steel mesh having a wire diameter of 0.19 millimeters and 9.45 by 9.45 meshes per square centimeter, through a nine to one contraction and entered the test section. Around the entrance to the 1.8 by 1.8 meter test section was a gravel roughness 1.3 centimeters high and 1.2 meters in length followed by a 3.8 centimeter high sawtooth fence used to trip the boundary layer.

The test section gradually expanded in width at the rate of 2.54 centimeters every 2.44 meters to maintain a zero pressure gradient the length of the test section. Variation of the pressure gradient was possible with the adjustable ceiling. Following the test section, two more 90 degree corners with turning vanes brought the flow back to the drive motor.

In addition, the test section was equipped with a carriage device which allowed remote placing of probes in the flow and traversing of the cross section. Casters, which ran on rails fixed to the inside walls of the test section, Fig. 6, were mounted on the carriage and allowed it to be positioned at any desired cross section. Variable speed D.C. motors were mounted on the carriage to provide horizontal and vertical motion of the carriage boom which was equipped with potentiometers to monitor the respective positions of each motion. Positioning of the carriage was through a control unit located outside of the wind tunnel.

Air speed through the tunnel was controlled by means of the variable speed D.C. drive motor with a variable pitch airplane propeller. A more detailed description of this facility has been given by Plate and Cermak (21).

3.2 Instrumentation

3.2.1 Secondary Flow Instrumentation - For secondary flow direction measurements, a rotating constant temperature hot-wire anemometer technique similar to that used by Hoagland (12), Gessner (10), and Brundrett and Baines (2) was utilized. This

technique employed the following physical characteristic of the hot-wire: when a hot wire operated at constant temperature is parallel to the flow direction, a minimum heat loss from the wire to the fluid occurs, and therefore, a minimum voltage output is obtained. Yawing of the wire about the position where the wire is parallel to the flow direction produces, for a well constructed hot wire, a voltage output which is symmetrical about the flow direction, Fig. 7. To determine the flow direction the hot wire is rotated either clockwise, or counterclockwise, about an axis which is normal (usually the probe axis) to the wire axis until the wire is yawed approximately twenty degrees from the approximate direction of flow and the voltage output is recorded. The wire is then rotated in the opposite direction until the same angle of yaw is approximately achieved, Fig. 8. The second yaw angle is determined exactly by matching the voltage output with the value recorded from the first yaw position, thus the flow direction is determined by half the total angular change from, for example, the clockwise yaw position to the counterclockwise yaw position. Accuracy of the method is limited by the turbulence level of the flow passing by the wire (6) and, to a greater degree, by the ability to accurately determine the angular position of the hot wire itself.

Angular measurements, from which the horizontal components of secondary flow were determined, required a reference direction from which to measure the angles to the flow direction. Pletcher and McManus (22) indicated that the flow in the entrance region of their duct was not symmetrical and, therefore, the flow direction did not

necessarily parallel the geometrical centerline of the duct at points located on the centerline. In the wind tunnel used in this study (see previous section), the flow was not fully developed and was required to turn two 90 degree corners before entering the test section. In addition, preliminary mean velocity measurements indicated that the flow was skewed relative to the direction of the centerline in the boundary layer. For these reasons, the primary reference direction was initially chosen as the geometrical centerline of the tunnel with the direction of the free stream to be determined relative to the tunnel centerline. The reference position of the hot wire was then defined as the position in which the hot wire was parallel to the geometrical centerline of the tunnel. All flow direction angles were then measured relative to this reference.

Preliminary attempts at determining the reference position of hot wire employed a direct observation of the hot-wire filament through a surveyor's transit telescope to align the probe with the line of sight of the transit. The transit was a K & E with an internal focus and magnification of twenty-four. The hot-wire filament was a platinum wire 10.2 microns in diameter and 13 millimeters in length mounted on a probe with prongs 2.6 centimeters in length, Fig. 9. Accuracy of repositioning the wire was ± 1/4 degree with respect to the centerline of the tunnel.

To achieve greater accuracy in aligning the hot wire, either a longer wire, or greater magnification was necessary. In an effort to achieve both, another technique was developed which involved projecting a shadow of two wires side by side on a screen through a lens,

the hot-wire filament itself and another wire used as a secondary reference line, Figs. 10 and 11. The secondary reference line was a platinum wire 10.2 microns in diameter stretched across two supports 12.7 centimeters apart. It was aligned by the transit with the centerline of the tunnel. A quartz iodide spot lamp was used as the light source. The light was positioned above the two wires and reflected from a mirror past the two wires through a 50 millimeter camera lens focused on a screen located on the ceiling of the tunnel, producing images of the two wires. The hot wire was then rotated until the two images on the tunnel ceiling were parallel, thus the hot wire was parallel with the centerline of the tunnel.

The spot lamp, lens, and secondary reference line were fixed to the tunnel carriage as a unit and could be removed and replaced without disturbing the hot wire probe and its support, Fig. 11. Accuracy of aligning the secondary reference line with the transit was consistently within ± 0.02 degrees of rotation and the accuracy of aligning the hot wire with the secondary reference wire was consistently within ± 0.03 degrees of rotation. Repeatability of measuring a flow direction with the complete system was experimentally determined to be within ± 0.05 degrees of rotation. For later reference, this technique is designated the shadow-graph technique. A more complete discussion of the technique above, and below, is given in Appendix A.

The following method of probe alignment was used to measure the flow direction from which the horizontal components of the total velocity vector were calculated. The free stream direction in the

tunnel was used as the reference direction for determining the reference position of the hot-wire probe. This reference was used since preliminary measurements in the free stream of the tunnel using the shadow-graph technique indicated that the free stream direction coincided with the geometrical centerline of the tunnel.

To determine the reference position of the probe, hereafter called the zero position, the probe was positioned in the free stream in the approximate center of the tunnel, Fig. 12. The exact location of the probe in the tunnel during this operation was known each time the probe was zeroed, but it varied depending upon where the probe was to be positioned for a flow direction measurement after the zeroing operation. The zero position was found by first adjusting the line of sight of the transit to the centerline of the tunnel. The secondary reference wire used in the shadow-graph technique, which had been mounted on the base of the probe rotating stand, was then aligned with the transit. The hot wire was then rotated in the free stream, the voltage output of which determined the zero position relative to the rotating stand. All of the zeroing operations were performed with a free stream velocity of 6.1 meters per second.

With the zero position of the probe established, the transit was then aligned on a line parallel with the centerline and passing through one of the data positions. The rotating stand was then aligned with the transit using the secondary reference wire fixed to the base of the stand, repositioning the probe in a known position relative to the free stream direction, but at a point in the cross section of the tunnel where the flow direction was to be determined.

After the flow direction had been determined, the probe was again placed in the free stream and re-zeroed. Comparison of the initial zero with the final zero indicated reproduction of the zero position within ± 0.05 degrees of rotation.

For angle measurements the probe was mounted in a 33 centimeter holder 6.35 millimeters in diameter held in a vertical position above the floor. A plastic union coupled the holder to the output shaft of a gear train connected to a variable speed D.C. motor. Gear reduction from the motor to the probe was 4550:1 in two steps of 70:1 and 65:1. A ten-turn, 1000 ohm linear potentiometer was connected through a gear to the first reduction in the gear train. The potentiometer, excited at 1.000 volts with a 1.5 volt dry cell battery and voltage divider, allowed the angular position of the probe to be determined to ± 0.04 degrees. The motor-gear mechanism and probe were mounted on a heavy stand with 30 centimeter legs threaded through the base. The legs were utilized because it was feared that the secondary flow might be affected by any obstacle placed on the floor of the tunnel that was of finite height. The legs raised the base from the floor to reduce blockage effects near the boundary, Fig. 12. Vertical attitude of the probe on the stand was established with the transit, and the attitude of the stand was maintained with a portable precision bubble tube placed on the base. The height of the probe above the floor of the tunnel was adjustable to within 2 millimeters.

The instrumentation associated with the secondary flow measurements is shown in Fig. 13. A block diagram of the system is given in Fig. 14.

3.2.2 Mean Velocity and Turbulence Instrumentation - For the determination of the mean velocity profiles and the longitudinal turbulence intensity a single hot wire was used normal to the flow in a horizontal position. The wire used was a 5.1 micron diameter tungsten wire approximately 2.5 millimeters in length. The probe to which the wire was silver soldered was similar to the probe used for angular measurements, Fig. 9.

An x-wire probe was used for the measurement of Reynolds' stresses. The probe and holder were made by Disa, models 55A32 145 and 55A30, respectively, Fig. 9. The tungsten wires were 5.1 micron diameter and each was approximately 2.5 millimeters in length. Considerable effort was expended to orient the wires at right angles to each other.

The hot wires were operated with Colorado State University Constant Temperature Hot-Wire Anemometers, model HW300B (9). The root-mean-square values were recorded from a B and K, model 2409 true RMS meter. These instruments used to measure the turbulent quantities are shown in Fig. 15, the block diagram is given in Fig. 16.

A 3.2 millimeter outside diameter pitot static probe Type PAC-12-KL from United Sensor and Control Corporation was used in conjunction with a Transonics Equibar Type 120 electronic manometer to monitor the free stream velocity and to make several velocity profile surveys. This pitot static tube was compared with the one calibrated by Tieleman (26) and later used by Zoric (31) as a velocity standard. The present probe was considered sufficiently accurate to serve as a velocity standard for the present study. The hot wires described

above were calibrated using this pitot static probe as the standard. The calibrations were performed in the free stream of the tunnel where the turbulence level was a minimum.

For surveys with the probes across the tunnel cross section, the probes were mounted on the remote control carriage of the tunnel.

3.3 Measurements

Mean velocity profiles were taken on the centerline of the test section at stations 3.0, 6.1, 9.1, 10.7, 12.2 and 13.7 meters from the sawtooth roughness with the pitot static tube for a free stream velocity of 6.1 meters per second. The data from the electronic manometer were recorded on an electronic x-y recorder and mean values were obtained graphically from the recorded data.

The remainder of the data were obtained at a station 12.2 meters from the sawtooth roughness and in one quadrant of the cross section. The quadrant studied was the lower right-hand quadrant of the cross section when observing it in the stream-wise direction.

Vertical mean velocity profiles were obtained at points across the test quadrant with the single hot wire for free stream speeds of 3.0, 6.1 and 12.2 meters per second. The mean values were obtained graphically from a continuous recording obtained with an electronic x-y recorder.

Turbulence measurements were obtained in the test quadrant for a free stream velocity of 6.1 meters per second. The longitudinal intensity was obtained from the single, normal hot wire. The RMS values were recorded directly from the B and K true RMS meter.

Reynolds stresses were determined using the x-wire at the same points in the test quadrant as for the longitudinal intensities. The x-wire was positioned in the two planes normal to the axial direction, thus only seven components of the stress tensor were determined.

Horizontal components only of the secondary flow were measured using the long, single rotating wire in the test quadrant. Mean values of the turbulent voltage signal from the anemometer were obtained using an electronic integrator of the same design as that described by Tieleman (26). The horizontal secondary flow components were determined for these free stream velocities: 3.0, 6.1 and 12.2 meters per second corresponding to Reynolds numbers, $R = U_\infty D_h/\nu$, of 3.6×10^5, 7.2×10^5 and 1.4×10^6. The positions at which data were obtained in the test quadrant are indicated in Fig. 17.

Cahpter IV

RESULTS AND DISCUSSIONS

In this chapter the results of the experimental investigation described in the preceding chapter are presented and discussed.

4.1 Calibrations

Calibrations of the various instruments were obtained whenever a measuring device did not provide data in a direct fashion. Several of the transducers operated in such an indirect manner. The pitot static tube was compared with the one calibrated by Tieleman (26) and found to give identical results. It was subsequently utilized as the velocity standard in this experiment. The hot wires used were calibrated in the free stream region of the wind tunnel with the pitot static tube. A typical plot of the hot-wire response is given in Fig. 20. The hot-wire calibration plots were also fitted to an equation of the form of King's law to facilitate the calculation of the quantities in the turbulent stress tensor. This procedure has been carried out for the wire of Fig. 18 and the results included in the figure.

Calibration of the mechanism for measuring the secondary flow directions consisted of comparing the resulting voltage signal of the linear potentiometer with the number of revolutions of the drive motor determined by a counter, reduced to angular degrees of rotation of the probe through the known gear ratios.

4.2 Boundary Layer Parameters

This experiment was performed in the developing boundary layer of a wind tunnel. As such, it is necessary to specify under what conditions the boundary layer developed and to provide some information which characterizes the particular boundary layer. Velocity profiles were obtained at a series of points on the centerline of the tunnel for a free stream velocity of 6.1 meters per second. The data were obtained on an electronic x-y recorder from the electronic equibar micromanometer in conjunction with a pitot static tube. Traverses were made with the pitot tube from near the floor of the tunnel, through the boundary layer into the free stream. A nondimensional plot of these profiles is presented in Fig. 19. U_1/U_∞ is the ratio of the local mean velocity to the free stream velocity. x_2/δ is the ratio of the vertical coordinate measured from the floor to the boundary layer thickness on the centerline of the tunnel. δ corresponds to the vertical coordinate where the local velocity, U_1, has obtained 99 percent of the free stream velocity, U_∞. Downstream from station 6.1 meters, the condition of centerline similarity is a good assumption.

From these profiles, the several boundary layer parameters were calculated and are tabulated in Table II. These parameters are defined in Appendix B. These parameters have been plotted as functions of x_1 in Fig. 22. The shape factor, H, becomes reasonably constant with a mean of 1.289, which is close to the value of 1.286 for a zero pressure gradient given by von Doenhoff and Tetervin (29).

This may be taken as confirmation of a zero pressure gradient in the region where secondary flow measurements were taken in the cross section.

The momentum thickness, θ, became linear with x_1 after station 9 meters. Von Kármán's momentum integral equation for the condition of a zero pressure gradient is

$$C_f = 2 \frac{d\theta}{dx_1} \quad . \tag{4-1}$$

C_f calculated from (4-1) is given in Table II as 0.00326. Ludwieg and Tillmann (17) have given an empirical relation for the case of a flat plate with zero pressure gradient. They give C_f as

$$C_f = 0.123 \times 10^{-0.678\, H} \left(\frac{U_\infty \theta}{\nu} \right)^{-0.268} \quad . \tag{4-2}$$

The first column of C_f in Table II gives values of C_f computed according to (4-2). The mean value of C_f according to (4-2) over the given stations in Table II, $\overline{C}_f$, has been compared with the value given by (4-2) as $C_f^* = C_f/\overline{C}_f = 1.24$. Zoric (31) and Tieleman (26) have measured these same quantities. C_f^* from Zoric's data ranges from 1.1 to 3.0. In addition to the above measurements, Tieleman also performed shear plate measurements. The shear plate measurements agreed with equation (4-2) and C_f^* was observed to range from 2.5 to three. Tieleman attributed this discrepancy to the three-dimensionality of the flow in the nature of secondary flows, which von Kármán's equation, of course, does not incorporate (see Appendix B).

Clauser's method for determining the friction velocity was applied to the lower portion of the velocity profiles to determine C_f . The second column of C_f in Table II was determined this way.

4.3 Secondary Flow

Secondary flow measurements were performed in a portion of one quadrant (Fig. 17) of the wind tunnel. Profiles of the primary velocity at the station 12.2 meters indicated the mean flow was not symmetrical with respect to the geometrical centerline of the tunnel. There were two aspects of this nonsymmetrical behavior which should be emphasized. First, the mean motion was displaced approximately six to eight centimeters from the centerline of the tunnel as indicated in Fig. 21. It appeared this condition existed throughout the length of the test section of the tunnel. Secondly, the boundary layers on the tunnel boundaries grew at different rates. That is, the boundary layers on the vertical walls differed from that on the floor of the tunnel. Hence, complete symmetry of mean properties about the corner bisector did not exist.

4.3.1 Isovels - From the primary velocity profiles, an isovel map was constructed and is presented in Fig. 21. The penetration of the isovels into the corner and the displacement from the wall at the centerline are characteristic of secondary flow (Fig. 1). Several of the primary velocity profiles are presented in Fig. 22, where the ordinate is normalized by the boundary layer thickness at the centerline. During the course of the experiment, these profiles were measured several times and exhibited consistent repeatability.

Utilizing Clauser's method applied to the lower portion of the velocity profile in the cross section, the distribution of $\tau_o/\overline{\tau}_o$, the wall shear, was determined. Values of C_f in the cross section are given in Table II. The values of $\tau_o/\overline{\tau}_o = C_f/\overline{C}_f$ are plotted in Fig. 2 for comparison with the data from other ducts. Of note is the maintenance of a high wall shear into the corner.

4.3.2 Horizontal Components - The direction of the resultant velocity vector lying in the horizontal, or x_1-x_3 plane, was determined by the rotating hot wire previously described. At each data location, integrated hot-wire signals were obtained at several positions about the flow direction. In each case a minimum of four integrated signals comprised a set. These values were plotted on a rectangular grid with the integrated hot-wire signal as the ordinate and the position voltage as the abscissa, as given in Fig. 23. The complete hot-wire response was assumed to be of the form shown in Fig. 7. For each measurement location in the tunnel cross section, four points on the curve were determined, one on the clockwise side and three, or more, on the counterclockwise side of the direction of flow. Subtracting the original value of position for the clockwise direction from the counterclockwise position that was graphically determined then gave the total included angle of probe rotation about the flow direction. Dividing this by two and subtracting it from the zero position gave the direction of the resultant horizontal velocity vector in terms of voltage of the position. This value in volts was then multiplied by the slope of the calibration curve of the position potentiometer, as determined by a least square curve fitting, yielding

the deviation in degrees of rotation and is the angle α which appears in Fig. 8.

The angle α was then multiplied by the local mean velocity to obtain the velocity component in the x_3 direction. This procedure obviously contains two assumptions, first that the angle in radians equals the sine of the angle, and second, the magnitude of the resultant horizontal velocity vector is given by the magnitude of the component in the x_1 direction as determined in the mean velocity measurements. The first assumption is justified since almost all of the measured angles were less than one degree. The second assumption is reasonable since $|U|^2 = \sum_{i=1}^{3} U_i^2$ and U_3^2 , U_2^2 can be neglected compared with U_1^2 .

The horizontal secondary flow velocities, U_3 , have been plotted in Fig. 24 for each point where they were measured directly. The ordinate is the nondimensional height above the floor, nondimensionalized by the corresponding boundary layer thickness at the centerline. The abscissa is the nondimensional horizontal velocity, nondimensionalized by the free stream or centerline velocity. Figure 25 shows the same plots with the boundary layer thickness replaced by the half height of the tunnel as the nondimensionalizing parameter. The data points appear to collapse better in general in Fig. 24. However, in the corner the data collapses better in Fig. 25. This implies that the flow distribution away from the corner is influenced more by the boundary layers, whereas the flow distribution in the corner is influenced more by the geometry of the corner.

Figure 26 is a plot of the horizontal velocity, U_3/U_∞, versus the lateral coordinate, x_3/d_3, for several values of the vertical coordinate. It is interesting to compare this figure with the sketch of Fig. 27 which is an idealized case representing fully developed flow in a square duct as presented by Hoagland (12), Gessner (10), and Brundrett and Baines (2). In this sketch, no attempt has been made to establish any magnitudes although a reasonable estimate of the abscissa intercepts was attempted. It is interesting to note the similar shape for the corresponding curves.

4.3.3 Calculated Vertical Components - Information of the form of Fig. 26 was used to obtain an estimation of the vertical component of the secondary motion through a graphical integration of the three-dimensional continuity equation.

$$U_2(x_2) = - \int_0^{x_2} \left(\frac{\partial U_1}{\partial x_1} + \frac{\partial U_3}{\partial x_3} \right) d\eta + F(x_1) + G(x_3) \qquad (4\text{-}3)$$

where $F(x_1) = G(x_3) = 0$ since $U_2(0) \equiv 0$. Approximate values of $\partial U_3/\partial x_3$ were obtained graphically from Fig. 34.

An estimation of an average value for $\partial U_1/\partial x_1$ was obtained by differentiating the displacement thickness with respect to x_1 to obtain

$$\frac{\partial U_1}{\partial x_1} = - \frac{U_\infty}{\delta} \frac{\partial \delta^*}{\partial x_1} \qquad (4\text{-}4)$$

Equation (4-3) thus becomes

$$U_2(x_2) = - \int_0^{x_2} \frac{\partial U_3}{\partial x_3} d\eta + \frac{U_\infty}{\delta} \frac{\partial \delta^*}{\partial x_1} x_2 \qquad (4\text{-}5)$$

This equation was used to calculate the vertical component of the secondary flow which is shown in Fig. 28 for different relative positions from the centerline. Also plotted in this figure are two esitmates of the vertical motions on the centerline associated with an equivalent two-dimensional continuity equation using the flat plate, zero pressure gradient, 1/7 power law. Integration of the two-dimensional continuity equation produces

$$U_2(x_2) = \frac{U_\infty}{\delta}\left(\frac{x_2}{\delta}\right)^{8/7}\frac{\partial\delta}{\partial x_1} \quad . \tag{4-6}$$

Values for δ and $\partial\delta/\partial x_1$ were obtained two ways. They were evaluated first from data for δ versus x presented previously; and secondly, they were evaluated from the flat plate relation

$$\frac{\partial\delta}{\partial x_1} = 0.296\left(\frac{U_\infty x_1}{\nu}\right)^{-1/5} \tag{4-7}$$

corresponding to the 1/7 power law for velocity. After inserting equation (4-7) into equation (4-6), the vertical velocity on the centerline is

$$U_2(x_2) = 0.037\left(\frac{x_2}{\delta}\right)^{8/7}\left(\frac{U_\infty x_1}{\nu}\right)^{-1/5} \quad . \tag{4-8}$$

Values of U_2 are plotted in Fig. 28. These values are the two-dimensional equivalent of the data shown in the figure for $x_3/d_3 = 0$. There is an obvious difference between the data from this experiment and that calculated from the 1/7 power law, which is attributed to secondary motions. The vertical velocity has been plotted in Fig. 29 as a function of x_3/d_3 for two values of x_2/d_2. The

distribution is similar to what has been observed except for the region of positive (upward) velocity at $x_3/d_3 = 0.55$. That this region of upward vertical velocity appears is not surprising since the streamlines of secondary flow have generally been observed to be inclined to the boundary, but that it is of the same magnitude as the vertical velocity at the centerline is surprising.

4.3.4 Flow in the Corner - Figure 30 presents a comparison of the measured lateral secondary flow component and the computed vertical secondary flow component. If the secondary flow is symmetric about the corner bisector, the two profiles would be expected to be identical. Figure 30 does not show this to be the case in this investigation. There are three possible explanations for this. The first has been mentioned previously and involves the accuracy with which the vertical components were obtained. Second, the possibility exists that the comparison was made in a region sufficiently removed from the corner such that the distribution is under the influence of the relative boundary layers on the wall and on the floor of the tunnel. Comparison further into the corner was precluded due to equipment limitations. This resulted from the physical dimensions of probe mechanism, which also suggests the third possibility.

An obstacle in the flow near the wall produces an asymmetrical disturbance of the flow field in the vicinity of the obstacle. Consequently, a measurement of horizontal velocity component may consist of a secondary flow component plus a probe-obstacle interference component. Correction procedures for this effect were used by Hoagland (12) and Gessner (10) to correct their data near a wall.

Their corrections were in the form of an experimentally determined curve relating the diameter of the probe and distance from the wall to the angular error due to the presence of the probe. The probe arrangement used in this experiment was more complex than a simple cylinder; nevertheless, an estimation of the effect was obtained from a potential flow calculation of uniform flow around a large cylinder next to a wall. Figure 31 is the result of the calculation compared with the experimental curves obtained by Hoagland (12) and Gessner (10). Calculations were then performed for different points in the flow field to determine the effect of the presence of the probe mechanism. The diameters of each of the component parts of the probe mechanism were used to compute a correction due to that particular component. Superposition of all the corrections did not produce a significant correction, therefore, no corrections were applied to any of the horizontal components. In conclusion, the observed asymmetry in Fig. 30 is attributed to an actual asymmetric behavior of the flow in the corner possibly due to the interaction of the corner region with the respective boundary layer regions.

4.3.5 Comparison with Other Data - A comparison of data from the present experiment and some of those previously mentioned is displayed in Fig. 32. The data from Pletcher and McManus (22) is for fully developed flow, as are the data shown from other investigators, but is from a 3:1 aspect ratio duct. The coordinates for this data were nondimensionalized using only the half width for the minor dimension. The data from the present study is seen to be generally of a larger magnitude at the corresponding height above

the floor, which corresponds to flow away from the wall. Calculations discussed previously indicated this increased magnitude cannot be interpreted as probe blockage. The data of Fig. 32 for $x_3/d_3 = 0.77$ confirms this conclusion as a greater total correction would have to be applied, yet the data near the floor compares favorably, and would require no correction. The flow farther from the floor is very complex due to the interference of the boundary layers along the wall and along the floor.

4.3.6 Resultant Secondary Flow - Figures 33, 34, and 35 display the resultant velocity vector in the x_2-x_3 plane. The three diagrams are for axial velocities of 3, 6.1 and 12.2 meters per second. In the corner the flow is similar for all three velocities; however, farther from the corner ($x_3/d_3 = 0.3$ and $x_2/d_2 = 0.3$). The velocity data is reversed for 3 m/s compared to the 6.1 and 12.2 m/s velocity data. Further, the trend of an increase in velocity magnitude as the floor is approached is also reversed for the 3 m/s data, and a decrease in magnitude is observed. The absolute value of the secondary velocities in this area were very small, indicating weak secondary currents. At the two higher speeds, the secondary flow strengthened and was much better behaved. Of note is the fact that the secondary components are all less than two percent of the free stream speed at the point where they were determined.

In the corner region along the vertical wall ($x_3/d_3 = 0.8$ and $x_2/d_2 = 0.3$) a strong flow away from the wall is observed. Comparison of this region with the same region along the floor (symmetry of the corner) indicates the flow in the two regions are obviously not similar.

The continuity equation for fully developed flow is two-dimensional, thus a single stream function may be defined (see Chapter II) for all cross sections. The corresponding streamlines are closed within each axial section, i.e., the mass flow toward the wall must equal the mass flow away from the wall. Gessner (10) reported that continuity in the cross section was satisfied by his data within 20 percent. Hoagland (12) makes a similar statement. If these streamlines are plotted for the cross section, they provide a graphical picture of the secondary flow cells. Such an exercise is not possible for a developing flow because the streamlines must begin and end upstream and downstream of the cross section under consideration and are not constant from one cross section to the next cross section. Hence, for a specific cross section, the flow toward the wall need not equal the flow away from the wall. This follows from the three-dimensional continuity equation, which requires the change of the boundary layer displacement thickness with succeeding cross sections. Nevertheless, the concept of a cell is an attractive means to describe secondary flows. Figures 33, 34, and 35 present a general pattern of motion in which several zones of the fluid appear to rotate about a longitudinal axis.

The question arises as to whether any secondary flow cell would be limited to the boundary region in developing flows. Figures 26 through 35 appear to imply that secondary flow cells should extend over the entire quadrant of flow and encompass not only the boundary layers, but the free stream as well. Indeed, if the secondary flow were limited to the boundary layers, the horizontal velocity, U_3 ,

should change sign on or near the centerline and should be positive over a significant portion of the boundary layer near the outer edges. This conclusion is also supported by the large magnitude of the vertical velocity at the centerline (upward) and along the corner bisector (downward). Figures 34 and 35 strongly suggest such full section cells since it is apparent that if closed cells are imagined to exist, they must be completed outside the boundary layer. In terms of the turbulence equations of Chapter II, the turbulence level is essentially zero in the free stream, thus the terms for vorticity production cannot exist. This does not preclude connection by the secondary flows themselves or by the interaction of the boundary layer with the free stream. A pressure distribution must accompany the secondary flow in the free stream although it must be small, it precludes the existence of the classical potential flow core. Leutheusser (15) has measured the static pressure distribution in a fully developed flow and found it to vary slightly.

The mean vorticity in the x_1 direction is

$$\Omega_1 = \frac{\partial U_3}{\partial x_2} - \frac{\partial U_2}{\partial x_3} \quad . \tag{4-9}$$

Given the distribution of U_2 and U_3 with respect to x_2 and x_3, values of Ω_1 might be calculated. However, a sufficient amount of data to make the process of taking graphical derivatives reasonably accurate is required. The data herein was not considered sufficient for this purpose.

4.4 Turbulence

Measurements of turbulence were obtained in the same region as the secondary flow measurements for a free stream speed of 6.1 meters per second only. Three hot-wire anemometers were used in conjunction with a single, normal wire and a cross wire, the output from which five of the six terms of the turbulent stress tensor were determined. The signal from the normal hot wire was integrated to obtain a mean voltage and the root-mean-square fluctuation voltage was obtained from each of the wires. The turbulence calculations and measurements are explained further in Appendix C.

Figure 36 is the distribution of $\overline{u}_1^2/U_\infty^2$ in the region of the cross section investigated. The distribution is in general, similar to that given by previous experimenters with two distinct differences. First, the intensity approaches zero at the outer edge of the boundary layer; and second, better symmetry about the corner bisector was observed in the data of the literature.

The existence of the free stream with an essentially zero turbulence level requires that all the turbulence quantities approach zero at the outer edge of the boundary layer. The asymmetry exhibited by $\overline{u}_1^2$ agrees with what has already been mentioned concerning symmetry in the corner. It is interesting to point out that the contours penetrate farther into the corner along the bisector than elsewhere. This penetration into the corner is more severe than what has been observed in fully developed flow. This is because the fluid convected into the corner has little turbulence in it and suppresses the turbulence growing outward from the walls.

The distribution of $\overline{u}_2^2/U_\infty^2$ is given in Fig. 37. The penetration of the corner contours again occurs well off the corner bisector. Figure 37 may be compared with Fig. 38 for the distribution of $\overline{u}_3^2/U_\infty^2$. According to the discussion of Chapter II, Fig. 38 should be a mirror image to Fig. 37 about the corner bisector for a symmetrical flow. This is not satisfied about the corner bisector in Figs. 37 and 38 and it is not evident whether it is satisfied about any other line extending from the corner.

Figure 39 displays the distribution of the turbulent shearing stress $\overline{u_1u_2}/U_\infty^2$. It is typical of previous measurements of such a distribution with the above mentioned exceptions of symmetry. Shown in Fig. 40 is the distribution of $\overline{u_1u_3}/U_\infty^2$. A great deal of confusion apparently exists in the published literature on its distribution in a corner. Gessner (10) presented an exhaustive study of fully developed turbulent flow in a square duct in which measurements of this term were presented in the same form as given here. His data exhibits no change of sign when progressing across the cross section. In contrast, Brundrett and Baines (2) performed an equally exhaustive set of turbulence measurements and indicate a distribution similar to that given here in regard to the variation of the change in sign of the turbulent shearing stress. Tracy (28) has also observed a similar change in sign of this quantity.

Figure 41 shows the distribution of the quantity $\sum_{j=1}^{3} \overline{u_i^2}$ which is equal to the total turbulent kinetic energy per unit mass. It is a direct composite of Figs. 36, 37, and 38 and reflects the characteristics of each. Pletcher and McManus (22) observed that

the direction of secondary flow in the corner region coincided well with grad$(\overline{u_1^2})$. They further speculated that the secondary flow direction in the corner would coincide with the gradient of turbulence energy. Away from the corner, the correlation between the direction of secondary flow and grad$(\overline{u_1^2})$ breaks down as the secondary flow direction changes to become perpendicular to the gradient of turbulence energy.

The distribution of $(\overline{u_3^2} - \overline{u_2^2})/U_\infty^2$ is given in Fig. 42. Symmetry of the flow in the corner requires that along the corner bisector $\overline{u_2^2} = \overline{u_3^2}$, thus $\overline{u_3^2} - \overline{u_2^2}$ should be zero along the bisector. In view of the asymmetry which has been demonstrated, the occurrence of a zero contour along the corner bisector is surprising.

In fully developed flow, the mixed second derivatives of $(\overline{u_3^2} - \overline{u_2^2})/U_\infty^2$, (see equation (2-8)), are called the vorticity production terms. The Laplacian of the turbulent shearing stress $\overline{u_2u_3}$ either makes a positive, negative or zero contribution to the mean vorticity. Brundrett and Baines (2) measured the term $\overline{u_2u_3}$ and found it sufficiently small to be neglected in its contribution to mean vorticity. Tracy (28) argued that the stress could only exist if secondary flow were present; and, that as such, it would not make a positive contribution to the mean vorticity. The distribution of $\overline{u_2u_3}$ was not determined in this experiment. The term that remains in equation (2-8) is $\partial^2(\overline{u_3^2} - \overline{u_2^2})/\partial x_2 \partial x_3$, the production term. Unfortunately, the data presented in Fig. 42 is not sufficiently accurate, or abundant, to give any validity to the process

of graphically obtaining second derivatives. Thus, the actual production term has not been determined.

Under the condition of developing flow, other terms remain undetermined herein from the axial mean vorticity equation, as seen in equation (2-15). Again, second derivatives are required, one of which is the space derivative in the axial direction which was not measured.

Chapter V

CONCLUSIONS AND RECOMMENDATIONS FOR FURTHER STUDY

Secondary flow has been studied in a region along the floor of a wind tunnel with a developing boundary layer. The differences which exist between the fully developed flow case and the developing flow case have been discussed in terms of the equations which describe the fluid motions and in terms of the physical motion of the fluid. Experimental information of the existing secondary flow has been obtained and discussed. Turbulence measurements in a corner region have also been obtained and discussed.

5.1 Conclusions

In summary, as a consequence of the results and discussions of this study the following conclusions are appropriate:

1) Secondary flows do exist in the entrance region of this wind tunnel facility with an L/D_h ratio of only 6.7 at the high Reynolds numbers of 3.6×10^5 to 1.4×10^6.

2) The maximum secondary velocity measured was less than two percent of the free stream velocity in all cases studied.

3) The secondary flows found do not differ fundamentally from those which have been found in ducts of various aspect ratios with fully developed flows. In the vicinity of the corner the secondary flow is into the corner along the corner bisector. This tendency is stronger farther into the corner and weaker farther out from the corner along the corner bisector. The flow along the walls adjacent to a corner are found to be away from the corner.

4) The strength of the secondary flows may be influenced by an interaction of the relative boundary layer thicknesses and the geometry of the corner. The two effects cannot be separated; however, immediately at the corner the geometry of the corner predominates.

5) The evidence of this study suggests that in a developing flow with boundary layers and a zero turbulence level free stream, the secondary flow may connect the two regions of flow, and is not limited to the boundary layers exclusively.

6) The distribution of turbulence quantities within the boundary layers is found to be very similar to the distribution in fully developed flow.

7) The similarity of the turbulence distribution implies that the mechanism of vorticity production in developing flow does not differ fundamentally from that of fully developed flow.

5.2 Recommendations for Further Study

As is evident in the chapter on results and discussion, the evidence from which some of the preceding conclusions are drawn is not as sound as is desirable. Consequently, the following recommendations in regard to any further studies of secondary flows in a developing flow situation are set down in the hopes that the difficulties and omissions found in this study will be overcome.

For any further study upon the subject of secondary flows in a developing flow, it is recommended that:

1) Probe design should be as precise as possible, yet inherently simple and easy to manipulate. Measurements must be quickly taken and duplicatable.

2) A simple configuration of the probe and its support should be maintained to allow rigorous blockage corrections.

3) The vertical as well as the horizontal components of secondary flows should be measured.

4) The turbulence field should be well defined with the expectation of performing a momentum balance and a vorticity balance. This would require data suitably accurate and sufficient to obtain second derivatives with respect to all three spatial coordinates.

REFERENCES

1. Arya, S.P.S. and Plate, E.J., Hot-Wire Measurements of Turbulence in a Thermally Stratified Flow. U.S. Army Grant DA-AMC-28-043-65-G20, CEM 67-68SPSA-EJP-11, Colorado State University, Fort Collins, (February 1968).

2. Brundrett, E. and Baines, W.D., The Production and Diffusion of Vorticity of Duct Flow, Journal of Fluid Mechanics, 19, (1964), 375.

3. Champagne, F.H., Turbulence Measurements with Inclined Hot Wires. D1-82-0491 Boeing Scientific Research Laboratories, Flight Sciences Laboratory Report No. 103, (December 1965). (Also see Journal of Fluid Mechanics, 28, (1966) 153, 177.)

4. Chiu, Chao-Lin and McSparron, J.E., Effect of Secondary Currents on Sediment Transport in a Corner, Journal of the Hydraulics Division, ASCE, 92, Proc. Paper 4905, (1966) 57.

5. Deissler, R.G. and Taylor, M.F., Analysis of Turbulent Flow and Heat Transfer in Noncircular Passages, NACA-TN 4384, (1958).

6. Delleur, J.W., Flow Direction Measurement with Hot Wire Anemometers. Presented at the Hydraulics Division Conference, ASCE, Tucson, Arizona, (August 25, 1965).

7. Delleur, J.W. and McManus, D.S., Secondary Flows in Straight Open Channels, Proc. 6th Mid-Western Conference on Fluid Mechanics, Austin, Texas, (September 1959), 81.

8. Einstein, H.A. and Li, H., Secondary Currents in Straight Channels, American Geophysical Union, Trans., 39, No. 6, (December 1958).

9. Finn, C.L. and Sandborn, V.A., Design of a Constant Temperature Hot-Wire Anemometer. U.S. Army Grant DA-AMC-28-043-65-G20, NASA, NGR-06-002-038, CER66-67CLF36, Colorado State University, Fort Collins, (March 1967).

10. Gessner, F.B., Turbulence and Mean-Flow Characteristics of Fully Developed Flow in Rectangular Channel. Ph.D. dissertation, Purdue University, (January 1964). (Also see Journal of Fluid Mechanics, 23, (1965), 689.)

11. Hinze, J.O., Turbulence. McGraw-Hill, New York, (1959).

12. Hoagland, L.C., Fully Developed Turbulent Flow in Straight Rectangular Ducts - Secondary Flow; Its Cause and Effect on the Primary Flow. Ph.D. dissertation, Massachusetts Institute of Technology, (1960).

13. Lamb, H., Hydrodynamics, Dover, New York, (1945).

14. Leopold, L.B., Watman, M.G. and Miller, J.P., Fluvial Processes in Geomorphology, W.H. Freeman, San Francisco, (1964).

15. Leutheusser, H.J., Turbulent Flow in Rectangular Ducts, Journal of the Hydraulics Division, ASCE, 89, (1963), 1.

16. Liggett, J.A., Chiu, C.L. and Miao, L.S., Secondary Currents in a Corner, Journal of the Hydraulics Division, ASCE, 91, (1965).

17. Ludwieg, H. and Tillmann, W., Investigation of the Wall Shearing Stress in Turbulent Boundary Layer, NACA-TM 1285, (1950).

18. Mager, A., Generalization of Boundary Layer Momentum-Integral Equations to Three Dimensional Flow Including Those of a Rotating System, NACA Report 1067, (1952).

19. Maslen, S.H., Transverse Velocities in Fully Developed Flows, Quarterly Journal of Applied Mathematics, 16, (1958), 173.

20. Nikuradse, J., Untersuchangen über die Geschwindigkeifsverteilung in Turbulenten Stromungen, VDI-Forschungsheft 281, Berlin (1926).

21. Plate, E.J. and Cermak, J.E., Micro-Meteorological Wind Tunnel Facility. Final Report, Fluid Dynamics and Diffusion Laboratory, Colorado State University, CER63EJP-JEC-9, (February 1963).

22. Pletcher, R.H. and McManus, H.N., Secondary Flow in the Entrance Section of a Straight Rectangular Duct, Proc. 8th Mid-Western Conference on Mechanics, (1963).

23. Prandtl, L., Über die ausgehildete Turbulenz, Verhandlungen des zweiten Internationalen Kongresses für Technische Mechanik, Zurich, (1926).

24. Schlichting, H., Boundary Layer Theory. 4th Ed., McGraw-Hill, New York, (1960).

25. Sears, W.R., Boundary Layers in Three-Dimensional Flow, Applied Mechanics Review, 7, (1954), 281.

26. Tieleman, H.W., Viscous Region of Turbulent Boundary Layer. U.S. Army Grant DA-AMC-28-043-65-G20, CER67-68HWT-21, Colorado State University, (December 1967).

27. Townsend, A.A., The Structure of Turbulent Shear Flow. University Press, Cambridge, (1956).

28. Tracy, H.J., Turbulent Flow in a Three-Dimensional Channel, Journal of the Hydraulics Division, ASCE, 91, (1965), 9.

29. Von Doenhoff, A.E. and Tetervin, N., Determination of General Relations for the Behavior of Turbulent Boundary Layers, NACA Report 772, (1943).

30. Webster, C.A., A Note on the Sensitivity to Yaw of a Hot-Wire Anemometer, Journal of Fluid Mechanics, 13, (1962), 307.

31. Zoric, D.L., Approach of Turbulent Boundary Layer to Similarity. U.S. Army Grant DA-AMC-28-043-65-G20, CER68-69DLZ-9, Colorado State University, Fort Collins, (September 1968).

APPENDIX A

DISCUSSION OF ROTATING HOT-WIRE ACCURACY FOR DETERMINING FLOW DIRECTION

APPENDIX A

DISCUSSION OF ROTATING HOT-WIRE ACCURACY FOR DETERMINING FLOW DIRECTION

In section 3.2.1, the method of flow direction measurement utilizing a rotating hot wire was described briefly. This method has been used successfully by Hoagland (12), Gessner (10), Brundrett and Baines (2), Pletcher and McManus (22), and Tracy (28). The same method was used in conjunction with a hot film by Liggett, Chiu, and Miao (16) to obtain measurements in water. The probe apparatus was, in each case mounted on a large, rigid traversing mechanism located outside the fluid flow confines. The conditions studied for this report did not permit the use of a rigid traversing bench. The reason for this was the physical size of the flow facility. Consequently, another means of probe support and orientation was sought.

Section 3.2.1 contains a brief description of several of the techniques that were investigated. Once a technique was operational, it was examined to determine its accuracy and dependability. Two of these methods subsequently used in the course of the experiment are discussed below.

Resolution

Delleur (6) has studied the ability of a rotating hot wire to determine flow direction in a turbulent stream. He concludes that flow directions may be determined within ± 0.05 degree in a flow with a turbulence level of $\sqrt{\overline{u_1^2}}/U_\infty = 0.10$ or less. Above $\sqrt{\overline{u_1^2}}/U_\infty = 0.12$ the resolution is limited to ± 0.10 degree. This is, of course,

provided the mechanism is equipped with a position indicator of sufficient resolution. The above values were obtained by repeating measurements several times. For this experiment described in the main text, the same technique was used.

Two wires of the same diameter, but different lengths, were rotated on the centerline of a 15 centimeter diameter pipe for air flowing at 6.1 meters per second with a turbulence level $\sqrt{u_1^2}/U_{\text{℄}}$ of approximately 9%. The wires were the same as those described in section 3.2.1 and 3.2.2. The wires were operated with a constant temperature anemometer, and the signal was averaged with time by the integration procedure previously described. It was possible to determine the position to within 0.0002 degree. The response of the wires is given in Fig. 43 in terms of the integrated hot-wire voltage versus an angular position relative to an arbitrary reference. The longer hot wire had a much greater sensitivity to angular motion in terms of a change in integrated voltage. The indicated symmetry was used to determine the direction of flow.

Several examples of repetition of wire position were obtained. It was soon apparent that it was possible to orient the hot wire in the flow with sufficient accuracy. Table IV lists the results of five of these repetition procedures for the longer wire and three for the shorter wire, which was subsequently discarded from any further consideration.

Platform Alignment

One of the techniques for wire alignment in the tunnel discussed briefly in section 3.2.1 employed the use of a secondary reference

line. It consisted of a wire of the same composition and diameter as the filament of the hot wire stretched across two supports 12.7 centimeters apart. Alignment of the reference line to the tunnel axis was made with a surveyors transit. Direct comparison of the hot-wire filament with the reference line was then required. Initially a 20 power microscope was positioned above the two wires and the hot wire rotated until the two wires, the reference line and the hot-wire filament, were parallel. This proved to be an adequate alignment method, but time consuming. For example, the probe alignment frequently required between two and three hours.

The second method of direct comparison between the reference line and the hot-wire filament was called the shadow graph techniques. It has been described in section 3.2.1.

Either of these methods depends upon four components; transit alignment, reference line alignment, hot-wire alignment, and hot-wire resolution - each predicated upon the one before. A simple calculation for transit alignment indicated an error of ± 0.005 degree or less in the line of sight.

Alignment of the reference line with the transit was examined by determining the reproducibility that could be expected. The transit was locked on an arbitrary position and a movable plastic platform equipped with a mirror and a scribed line was positioned 3.7 meters away. A scale was positioned one half this distance from the mirror such that it could be read through the mirror by changing the focus of the transit. The arrangement is shown in Fig. 44. The length of the scribed line was about 10 centimeters. The scribed line was

aligned with the transit by means of the adjustment screws, and the position was read on the scale through the mirror. The scribed line position was then altered and the procedure repeated. Table V contains the tabulated results of this procedure. The values presented suggest a standard deviation of 0.0053 cm with the maximum deviation being ± 0.1 cm. If it is assumed rotation of the mirror occurred about the same axis as rotation of the scribed line, then the values in Table V represent twice the change in arc length that would be experienced by the scribed line at the same radius. Thus, the maximum deviation of ± 0.1 cm corresponds to ± 0.016 degree.

Hot-Wire Alignment

Alignment of the hot-wire filament with the reference line was determined in a similar fashion. The microscope method described above produced a value of ± 0.026 degree for the maximum deviation from the mean over a series of 10 repetitions for the longer wire.

The magnification of the microscope was 20. The shadow graph technique achieved a magnification of 32 ± 6 depending upon how far from the tunnel floor the probe was located since the screen was fixed to the top of the tunnel. Table VI lists position values for the shadow graph repetition experiments. Each unit of the HP dial mounted on the drive motor corresponded to 0.0002 degree of probe rotation. The maximum deviation listed in Table VI then corresponds to ± 0.024 degree.

Overall Error

Using the following values for each of the four error components

transit	0.005^{o}
reference	0.016^{o}
filament	0.024^{o}
resolution	0.020^{o}

and considering them to be random, the square root of the sum of their squares is then ± 0.035 degree for an overall maximum probable error in any one alignment.

During application to secondary flow measurement in the wind tunnel, the method of position monitoring was changed from the direct observation of the numbers on the several dials of the gear train to the potentiometer arrangement described in section 3.2.1. This provided for a readout in terms of voltage from the potentiometer, but it added to the error to be expected in a measurement. This was due to the construction of the potentiometer, bacause it was insensitive to any angular change in probe direction less than 0.04 degree. Hence, the total maximum probable error to be expected in any one measurement reported is ± 0.053 degree.

Section 3.2.1 mentioned that the shadow graph technique was used to determine the direction of the free stream with respect to the geometrical centerline of the wind tunnel. Five such measurements at station x_1 = 12.2 meters and 71 centimeters from the floor indicated the two coincided. Four of the five were zero with the fifth being 0.05 degree. Thus, the free stream was subsequently used as a reference direction for aligning the probe. This provided the

opportunity to check the reproducibility of the entire system and compare it with the values predicted above.

Measurement of the flow direction angle, α, was repeated at the following points with the indicated results.

U_∞	x_3/d_3	x_2/d_2	α	
3.1 m/s	0	0.028	0.20 deg	0.25 deg
6.1 m/s	0	0.028	0.20 deg	0.20 deg
12.2 m/s	0	0.028	0.20 deg	0.20 deg
6.1 m/s	0.63	0.028	1.05 deg	1.10 deg
12.2 m/s	0.63	0.028	1.10 deg	1.10 deg

Hence, the values for α were assumed accurate to the nearest 0.05 degree in view of the discussion above.

Measurements were normally taken in a sequence such that the probe remained at the same elevation from the floor. A check of the zero position between each lateral measurement position should give the same value of potentiometer reading. The data shows this to have been the case to within $\pm$ 0.04 degree.

APPENDIX B

TWO- AND THREE-DIMENSIONALITY OF WIND TUNNEL FLOWS

APPENDIX B

TWO- AND THREE-DIMENSIONALITY OF WIND TUNNEL FLOWS

A variety of fluid mechanic experiments have been performed in the Army Meteorological Wind Tunnel. For example, studies of the action of winds on buildings in the atmospheric surface layer, instaneous and continuous diffusion from line and point sources with a variety of stratification and roughness conditions, and basic boundary layer research have been conducted in this facility. In most cases, the flow is assumed to be two-dimensional in nature. This precipitates a simplification in the governing equations and often relieves the problem of determining the three-dimensional characteristics of the flow. The question naturally arises then, under what circumstances may the flow accurately and effectively be termed two-dimensional?

Tracy (28) suggested a value of five for the width to depth ratio required to assure that two-dimensional flow is closely approached in the central region. He determined that secondary flows which exist in the central region of a 6.1:1 aspect ratio duct were very small. The turbulence field was also reasonably uniform, but more characteristic of a three-dimensional flow.

The usual criterion is that the momentum transport is either constant, or zero in one of the three coordinate directions. For true two-dimensional flow restricted to the x_1-x_2 plane, the turbulent shearing stresses are all zero except for $\overline{u_1 u_2}$, and gradients in the x_3 direction are nonexistent. At the midpoints of the walls $\overline{u_1 u_3}$ and $\overline{u_2 u_3}$ are zero and x_3 derivatives are zero because of

symmetry. This point, however, is indeed a point, and not an area of the flow, consequently, it is difficult in many cases to find and not really useful in terms of studying the flow over two or three-dimensional models in the flow field. In terms of the turbulence, the region of flow which may be used as an alternative to the exact point of symmetry is that region where $\overline{u_1u_3}$ and $\overline{u_2u_3}$ are minima, which occur at approximately $x_3/d_3 = 0.3$.

In terms of mean quantities two-dimensionality in the x_1-x_2 plane requires that $\partial U_3/\partial x_3 = 0$, that is, either U_3 is constant or equal to zero. In a boundary layer, it is interesting to examine this term as it enters the momentum integral equation. For a region sufficiently removed from the side boundaries and near the floor, the momentum equation in the x_1 direction can be written as

$$U_1 \frac{\partial U_1}{\partial x_1} + U_2 \frac{\partial U_1}{\partial x_2} = U_\infty \frac{\partial U_\infty}{\partial x_1} - \frac{1}{\rho} \frac{\partial \tau_{1,2}}{\partial x_2} \qquad \text{(B-1)}$$

with the usual boundary layer approximations. The continuity equation is retained in its three-dimensional form as

$$\frac{\partial U_1}{\partial x_1} + \frac{\partial U_2}{\partial x_2} + \frac{\partial U_3}{\partial x_3} = 0 \quad . \qquad \text{(B-2)}$$

An order of magnitude study revealed that $U_3 \frac{\partial U_1}{\partial x_3}$ was one order smaller than either of the remaining convective terms, and that $\tau_{1,3}$ may be neglected for the same reason.

Following the same development as that given by von Kármán, with the addition of the $\partial U_3/\partial x_3$ term to the continuity equation, the momentum integral equation for this case is

$$\frac{d\theta}{dx_1} + (H+2)\frac{\theta}{U_\infty}\frac{dU_\infty}{x_1} + \frac{1}{U_\infty^2}\int_o^h \frac{\partial U_3}{\partial x_3}(U_\infty - U_1)d\eta = \frac{C_f}{2} \qquad \text{(B-3)}$$

where the following definitions have been employed:

h = some point such that $h > x_2 = \delta$

η = integration variable for x_2

$C_f = \dfrac{\tau_o}{\frac{1}{2}\rho U_\infty^2}$, skin friction

$\delta^* = \dfrac{1}{U_\infty}\displaystyle\int_o^h (U_\infty - U_1)d\eta$, displacement thickness

$\theta = \dfrac{1}{U_\infty^2}\displaystyle\int_o^h (U_\infty^2 - U_1^2)d\eta$, momentum thickness

$H = \dfrac{\delta^*}{\theta}$, shape factor.

When $\partial U_\infty/\partial x_1 = 0$, or for a zero external pressure gradient, equation (B-3) becomes

$$\frac{d\theta}{dx_1} + \frac{1}{U_\infty^2}\int_o^h \frac{\partial U_3}{\partial x_3}(U_\infty - U_1)d\eta = \frac{C_f}{2} \qquad \text{(B-4)}$$

Von Kármán's momentum integral equation for two-dimensional flow and zero pressure gradient is in section 4.2:

$$\frac{d\theta}{dx_1} = \frac{C_f}{2} \qquad \text{(B-5)}$$

The obvious difference between equations (B-4) and (B-5) is the term

$$K = \frac{1}{U_\infty^2} \int_0^h \frac{\partial U_3}{\partial x_3} (U_\infty - U_1) d\eta \qquad \text{(B-6)}$$

which represents the additional momentum loss in a developing boundary layer due to the three-dimensionality of the flow field. Specifically, it represents the loss or gain, in momentum in terms of convection of momentum in the transverse direction, x_3 . In a two-dimensional flow $\partial U_3/\partial x_3 = 0$, thus, the convection of momentum in the transverse direction is either constant or zero, and K does not contribute. The value of K has been determined from the secondary flow measurements obtained for $U_\infty = 6.1$ meters per second and is plotted in Fig. 54 as a function of x_3/d_3 . The point where $K = 0$ is $x_3/d_3 = 0.29$ which corresponds closely to the point $x_3/d_3 = 0.3$ where $\overline{u_1 u_3}$, is a minimum.

In section 4.2, values of C_f determined by several means were presented. C_f determined from equation (B-4) is given below with the corresponding values at $x_1 = 12.2$ m and $x_3 = 0$ for $U_\infty = 6.1$ m/s taken from Table II.

Eq. (4-1)	0.00326
Eq. (4-2)	0.00257
Clauser's method	0.00154
Eq. (B-4)	0.00206

Thus K , a correction term to be added to von Kármán's momentum integral equation, is seen to be in the proper direction,

but appears to be too large compared to the Ludwieg and Tillmann value; and too small compared to the value from Clauser's method.

APPENDIX C

TURBULENCE CALCULATIONS

APPENDIX C

TURBULENCE CALCULATIONS

The equations and operation procedures for single and cross-wire turbulence measurements have been well documented in the literature and will not be rigorously presented here. What is presented below is included only to indicate the application of a recent result due to Arya and Plate (1) which relates the two sensitivities of a single inclined wire.

The mean-square voltage response from a hot wire inclined (yawed) in a turbulent flow is

$$\left(\sqrt{\overline{e_{1,2}^2}}\right)^2 = \overline{e_{1,2}^2} = a_1^2\overline{u_1^2} + a_1 a_2 \overline{u_1 u_2} + a_2^2\overline{u_2} \quad . \qquad \text{(C-1)}$$

a_1 and a_2 are usually termed the wire sensitivities and are related to the mean velocity of the flow and angle of inclination by

$$a_1 = \frac{\partial E}{\partial U} \qquad \text{(C-2)}$$

$$a_2 = \frac{1}{U}\frac{\partial E}{\partial \phi} \qquad \text{(C-3)}$$

where the mean voltage, E, is related to U through a calculation curve as in Fig. 20. When a single inclined wire is used which rotates, a_2 can be determined independently of a_1. Tieleman (26) and Zoric (31) followed this procedure and gave a discussion of its consequences. With a rigid cross wire, the common assumption is that the responses of the two inclined wires are identical, and it is further assumed commonly that a_1 and a_2 are equal in magnitude.

The first assumption is reasonable if the two wires are matched in their characteristics. The second assumption is reasonable provided the wires are operated at the correct angle of inclination.

Arya and Plate (1) have observed that over a significant range of yaw angle about 45 degrees, the relation

$$a_2 = \frac{(1-k^2)\ \cot\phi}{1+k^2\ \cot^2\phi}\ a_1 \qquad \text{(C-4)}$$

is valid. The k appearing in equation (C-4) is the same as given in Hinze's (11) form of the effective cooling velocity for hot wires.

$$U_{eff}^2 = U_{tot}^2\ (\sin^2\phi + k^2\ \cos^2\phi) \quad . \qquad \text{(C-5)}$$

Webster (30) and Champagne (3) have studied the variation of k with wire sizes and velocities. Webster did not obtain any consistent variation and suggested an average value of 0.2. Champagne observed a definite trend although it was based on less data. For the two wires used in this experiment, values of k from Champagne were $k_1 = 0.15$ and $k_2 = 0.14$.

The equation corresponding to equation (4-8) for the second wire is

$$\overline{e_{2,1}^2} = b_1^2\overline{u_1^2} + b_1 b_2 \overline{u_1 u_2} + b_2^2\ \overline{u_2^2} \quad . \qquad \text{(C-6)}$$

Given an independent determination of $\overline{u_1^2}$, equations (C-1) and (C-6) may be solved to give $\overline{u_1 u_2}$ and $\overline{u_2^2}$. This procedure was followed to obtain the components of the stress tensor, except $\overline{u_2 u_3}$. This was computerized and required an analytic form of the wire

calibration curve from which $\partial E/\partial U$ could be obtained. For this an equation of the form of "King's Law",

$$E^2 - E_o^2 = B\, U^m$$

was fitted to the hot-wire calibration curves by a least squares curve fitting process.

TABLES

TABLE I ADDITIONAL CONTRIBUTIONS

Reference	Duct Shape	D_h	L/D_h	R_e	U_{max}	Measurements				Turbulence					
						Isovels	Friction Factor	Wall Shear	Secondary Flow	$\overline{u_1^2}$	$\overline{u_2^2}$	$\overline{u_3^2}$	$\overline{u_1u_2}$	$\overline{u_1u_3}$	$\overline{u_2u_3}$
2	□	3 in.	260	8.3×10^4	66 fps	x				x	x	x	x	x	x
5	□ △	Calculated		2.4×10^4 90×10^4		x	x	x							
10	□	8 in.	40	15×10^4 30×10^4	87	x		x							
	2:1		60	5×10^4 30×10^4	127	x		x	x	x	x	x	x	x	x
12	2:1 3:1	5 in.	75	7.5×10^4 2×10^4	60	x	x	x	x						
15	□	3 in.		8.2×10^4 9.2×10^4		x x	x x	x x							
16	∨	6.6 in.		2.2×10^5	2.6	x		x	x						
22	3:1	6 in.	10.3 39.6	38.2×10^4 12.6×10^4	157.9	x			x	x					
28	6.4:1	8.7 in.	30	7.2×10^5	40	x			x	x	x	x	x	x	x
Author	□	6 ft	6.7		20	x	x	x	x	x	x	x	x	x	x

TABLE II BOUNDARY LAYER PARAMETERS
U_∞ = 6.1 m/s

x_1(m)	x_3(cm)	$(C_f x10^3)^1$	$(C_f x10^3)^2$	δ(cm)	δ^*(cm)	θ(cm)	H
3	0	2.67	--	21.6	3.68	2.74	1.343
6.1	0	2.63	1.68	31.6	4.88	3.76	1.297
9.1	0	2.60	1.62	38.5	5.51	4.28	1.284
10.7	0	2.62	1.54	41.6	5.74	4.52	1.270
12.2	0	2.57	1.54	43.8	5.98	4.70	1.276
13.7	0	2.36	1.51	44.9	6.62	5.05	1.310
	0	3.26					
12.2	0		1.65				
12.2	30.5		1.92				
12.2	45.8		1.86				
12.2	61.0		1.80				
12.2	76.3		1.72				
12.2	84.0		1.72				
12.2	91.5		1.70				

1 Calculated from equation (4-2)

2 Calculated using Clauser's method.

TABLE III ORIGINAL DATA

x_3 (in.)	x_2 (in.)	U_∞ (fps)	U_1 (fps)	α (deg)	U_3 (fps)
0	1	10	6.65	-0.20	-0.023
	12	10	9.32	-0.15	-0.024
	1	20	13.3	-0.20	-0.047
	12	20	19.0	0.0	0.0
	1	40	26.6	-0.20	-0.093
	12	40	39.0	-0.05	-0.034
12	1	10	6.9	-0.15	-0.018
	2		7.5	-0.25	-0.033
	9		9.2	+0.35	0.056
	12		9.6	-0.35	-0.059
	18		10.05	-0.10	-0.017
	1	20	14.0	-0.70	-0.171
	2		15.2	-0.60	-0.160
	9		18.8	-0.40	-0.132
	12		19.6	-0.30	-0.102
	18		19.9	+0.05	+0.018
	1	40	29.0	-0.70	-0.354
	2		32.4	-0.65	-0.366
	9		37.8	-0.30	-0.196
	12		39.4	-0.20	-0.138
	18		40.0	+0.05	+0.035
	32	20	20.05	0.0	0.0
		40	39.96	0.0	0.0
18	2	10	7.5	-0.25	-0.033
	9		9.12	+0.30	+0.048
	1	20	13.9	-0.60	-0.146
	2		15.1	-0.90	-0.141
	9		18.8	-0.30	-0.098
	1	40	26.2	-0.35	-0.160
	2		29.4	-0.80	-0.412
	9		35.7	-0.15	-0.093
	32	20	20.06	0.0	0.0

TABLE III ORIGINAL DATA - Continued

x_3 (in.)	x_2 (in.)	U_∞ (fps)	U_1 (fps)	α (deg)	U_3 (fps)
24	1	10	6.79	-0.90	-0.107
	2		7.43	-0.85	-0.110
	6		8.62	+0.15	+0.023
	9		9.18	-0.80	-0.128
	12		9.67	+0.10	+0.017
	18		10.0	-0.30	-0.052
	1	20	13.8	-1.10	-0.265
	2		15.0	-1.05	-0.158
	6		17.7	0.0	0
	9		18.8	-0.25	-0.082
	12		19.6	+0.05	+0.017
	18		20.0	+0.35	+0.122
	1	40	27.5	-1.10	-0.528
	2		29.4	-1.00	-0.511
	6		33.8	-0.05	-0.029
	9		36.3	-0.20	-0.127
	12		37.8	+0.15	+0.099
	18		40.0	+0.15	+0.105
30	1	10	6.68	-1.30	-0.152
	2		7.39	-0.70	-0.090
	3		7.81	-0.30	-0.041
	6		8.5	+0.15	+0.022
	9		8.7	-0.40	-0.061
	12		8.8	-0.40	-0.063
	1	20	13.6	-1.25	-0.297
	2		14.9	-0.70	-0.182
	3		15.6	-0.30	-0.081
	6		16.3	+0.30	+0.085
	9		15.9	-0.10	-0.028
	12		15.9	-0.30	-0.083
	1	40	28.0	-1.30	-0.635
	2		30.5	-0.70	-0.372
	3		31.9	-0.40	-0.223
	6		34.4	+0.10	+0.060
	9		35.3	-0.30	-0.184
	12		35.7	-0.40	-0.249

TABLE III ORIGINAL DATA - Continued

x_3 (in.)	x_2 (in.)	U_∞ (fps)	U_1 (fps)	α (deg)	U_3 (fps)
33	1	10	6.70	-1.05	-0.122
	2		7.39	-0.15	-0.019
	3		7.61	-0.05	-0.007
	6		8.22	+0.15	+0.022
	9		8.12	-0.40	-0.057
	12		7.98	-0.40	-0.056
	1	20	13.6	-1.15	-0.273
	2		14.9	-0.15	-0.039
	3		15.6	+0.40	+0.109
	6		16.35	+0.45	+0.128
	9		15.9	-0.60	-0.183
	12		15.9	-0.45	-0.125
	1	40	27.9	-1.05	-0.510
	2		30.2	-0.15	-0.079
	3		31.5	+0.05	+0.027
	6		32.9	+0.10	+0.056
	9		32.4	-0.90	-0.141
	12		32.9	-0.40	-0.230

TABLE IV HOT-WIRE RESOLUTION

Probe	Zero Angle	Zero Angle Repeat	Difference
1	20.59°	20.59°	0°
1	20.59°	20.59°	0°
1	20.59°	20.55°	-0.04°
1	121.44°	121.44°	0°
1	121.44°	121.45°	0.01°
2	110.73°	111.17°	0.44°
2	110.73°	108.72°	-2.01°
2	110.73°	110.20°	-0.53°

1 wire length = 12.7 mm

2 wire length = 2.54 mm

TABLE V REFERENCE LINE REPRODUCIBILITY

Trial	Scale Rdg	Deviation from Mean
1	18.2 cm	0
2	18.2	0
3	18.2	0
4	18.3	0.1 cm
5	18.1	-0.1 cm
Mean	18.2	
6	12.9 cm	-0.1
7	13.0	0
8	13.0	0
9	12.9	-0.1
10	13.0	0
11	13.1	0.1
12	13.0	0
13	12.9	-0.1
14	13.1	0.1
15	13.1	0.1
Mean	13.0	

TABLE VI SHADOW GRAPH REPRODUCIBILITY

Trial	HP Dial	Deviation from Mean
1	305	-55
2	395	35
3	240	-120
4	310	-50
5	340	-20
6	330	-30
7	480	120
8	380	20
9	400	40
10	440	80
Mean	362	

FIGURES

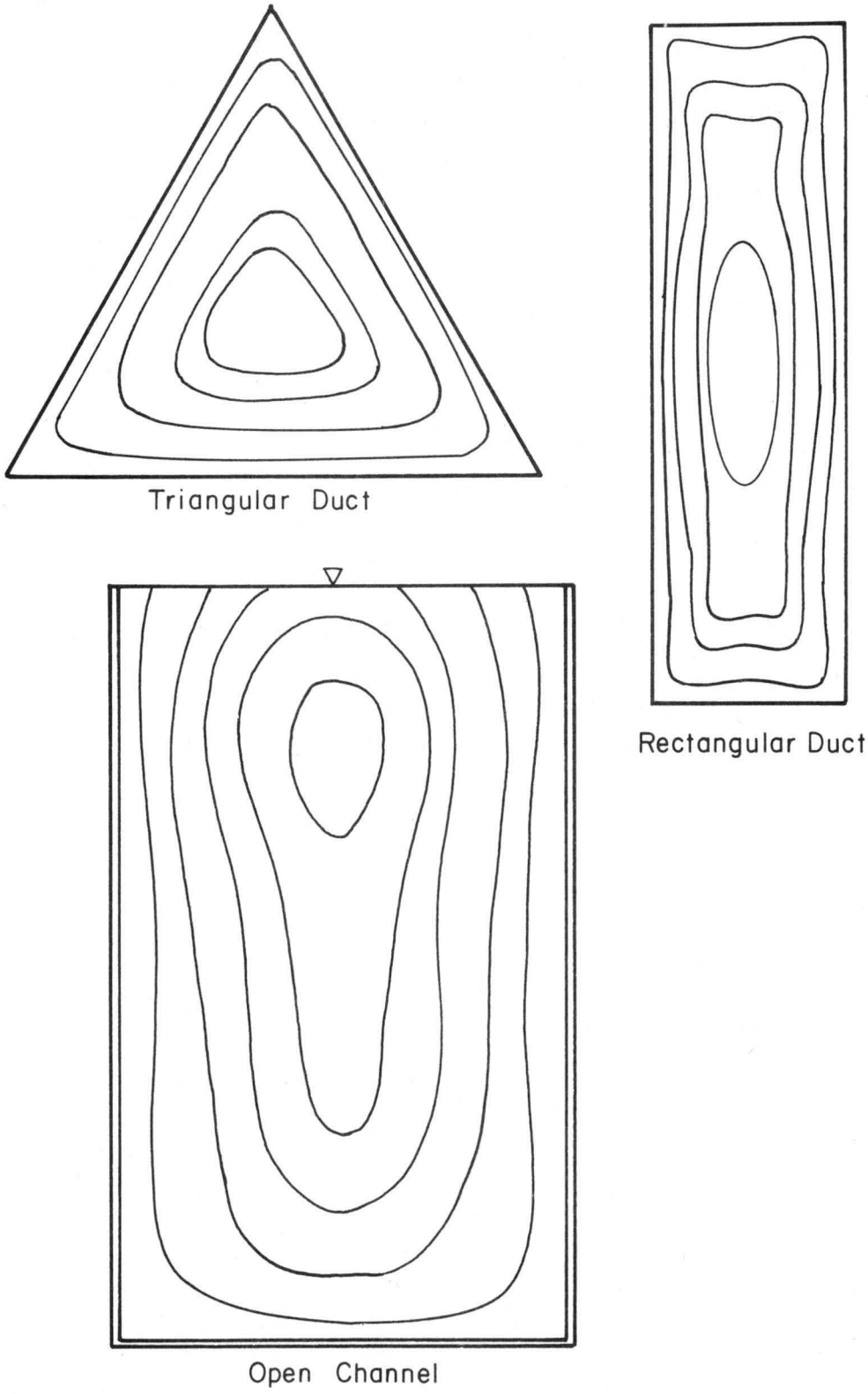

Fig. 1. Isovels of various cross section, (20), (23)

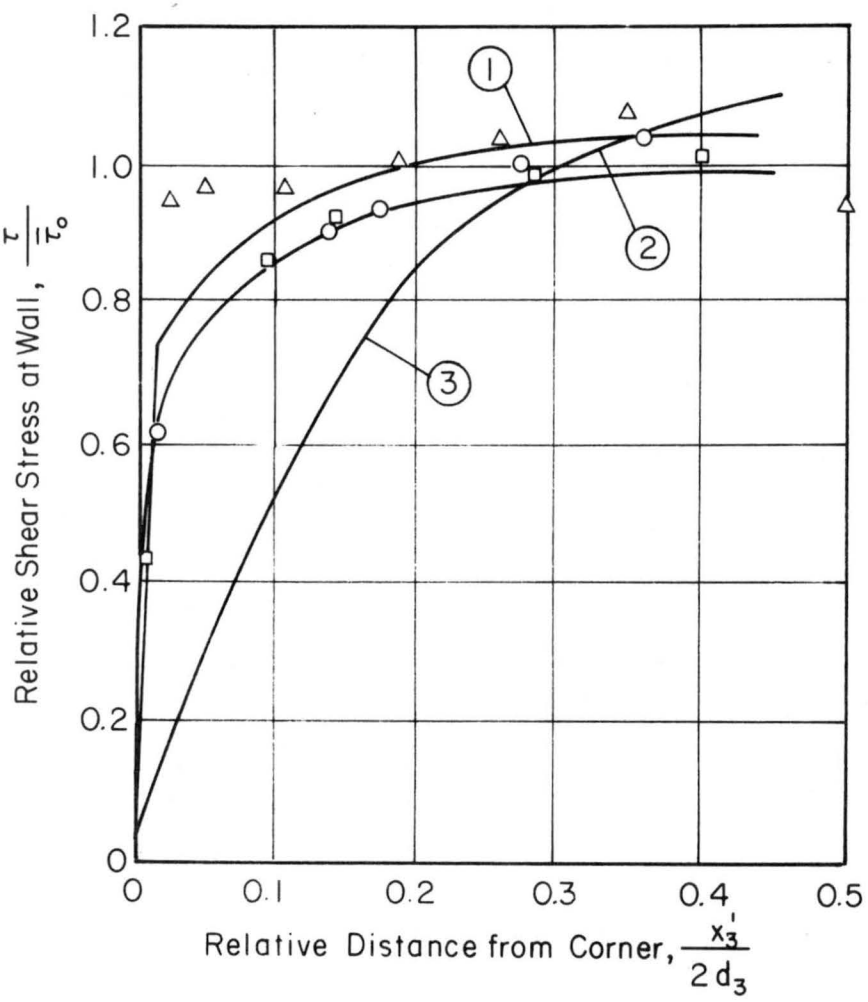

Fig. 2. Wall shear stress in a corner. (1) Leutheusser, experimental; (2) Liggett, Chiu and Miao, calculated; (3) Deissler and Taylor, calculated; ⊙ Liggett, Chiu and Miao, experimental; ⊡ Hoagland, experimental; △ Author, experimental

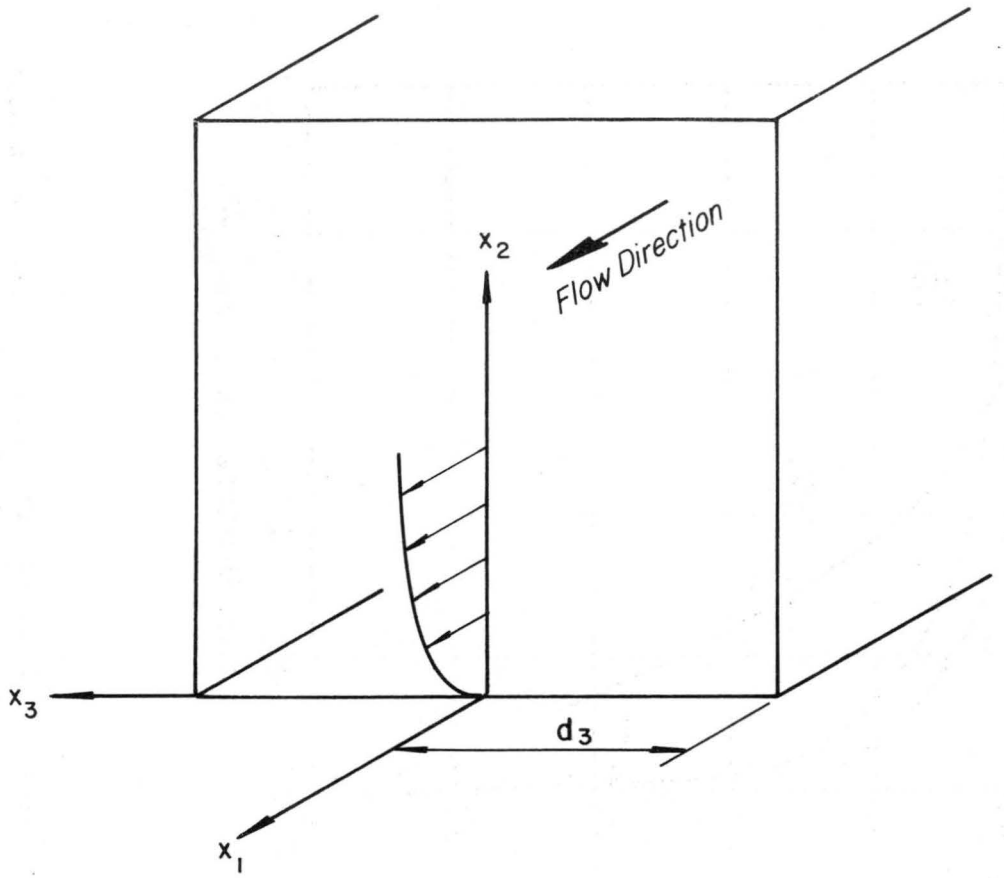

Fig. 3. Definition sketch of coordinate system

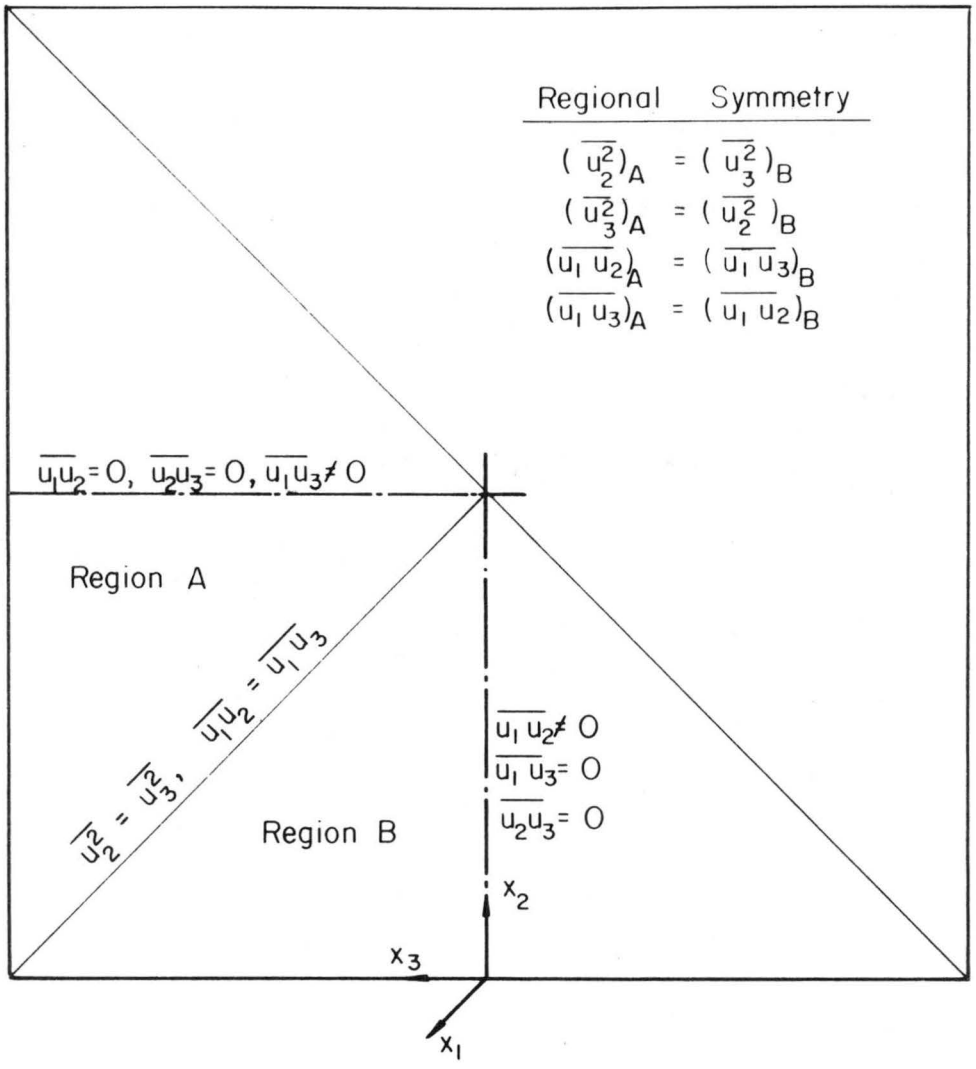

Fig. 4. Symmetry conditions for turbulent stresses in a square duct

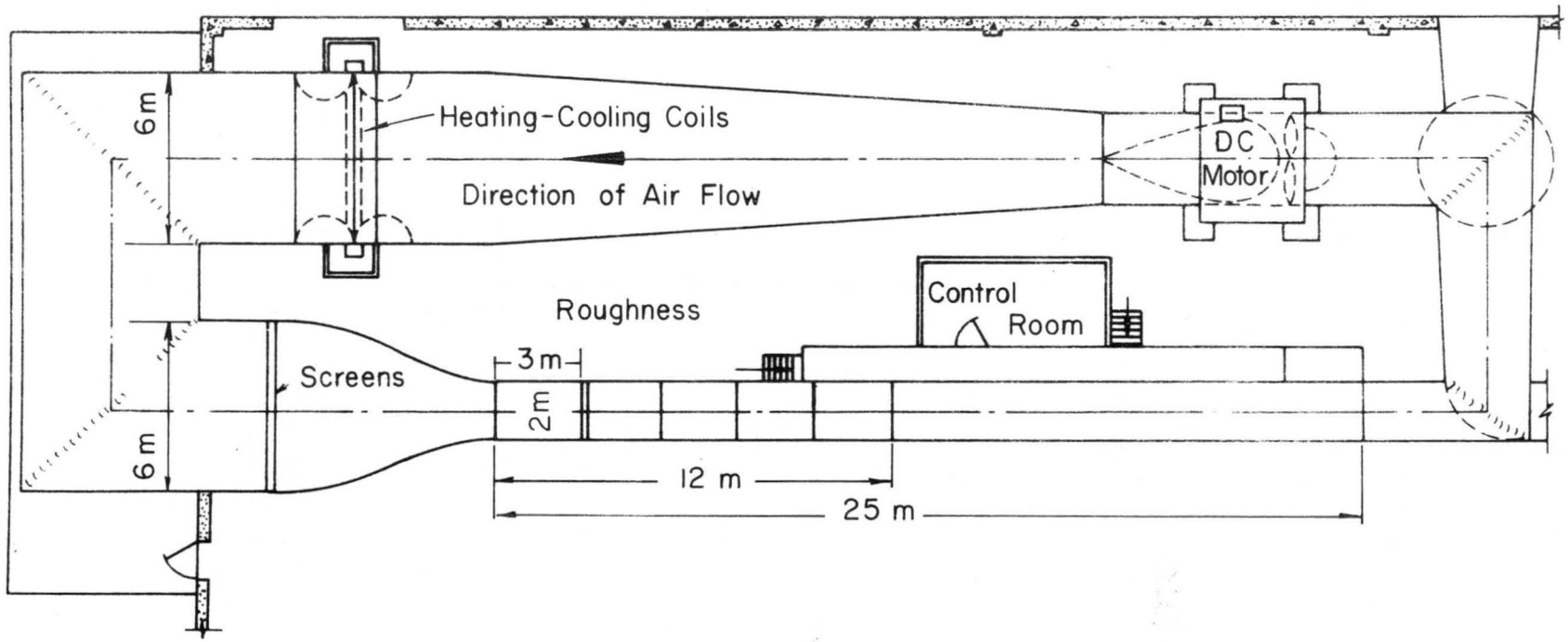

Fig. 5. Wind tunnel

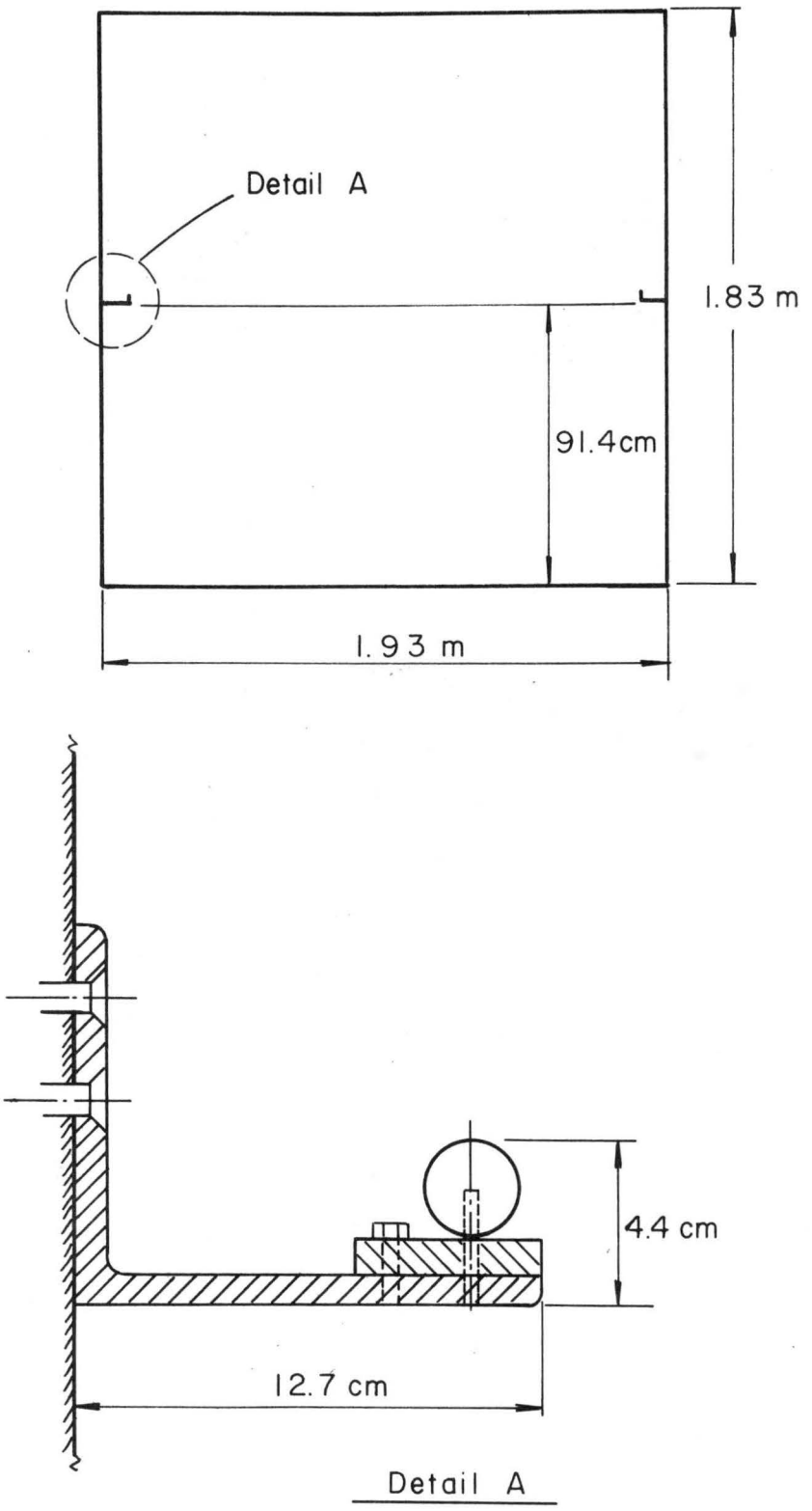

Fig. 6. Wind tunnel cross section at station 12.2 m

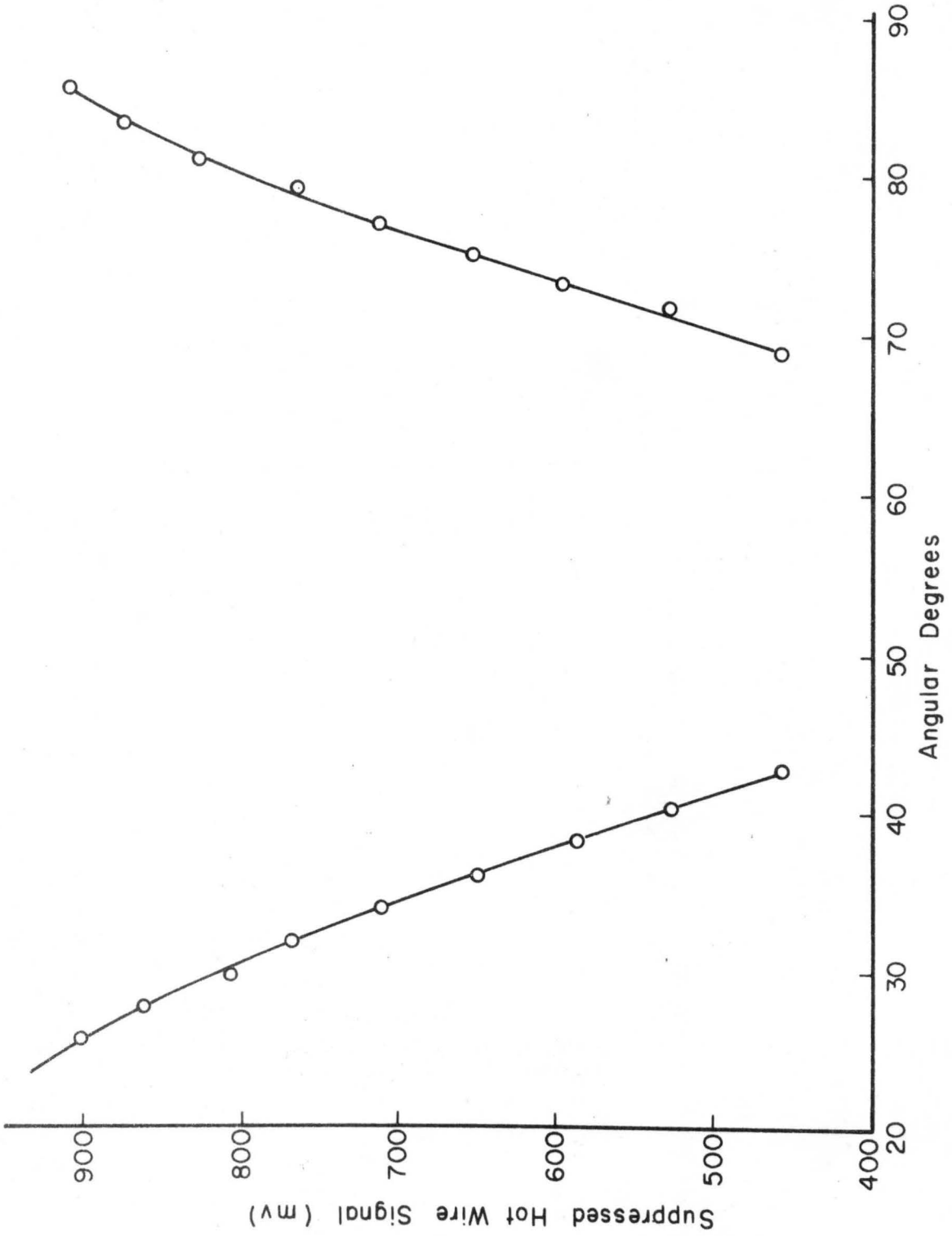

Fig. 7. Rotating hot wire signal

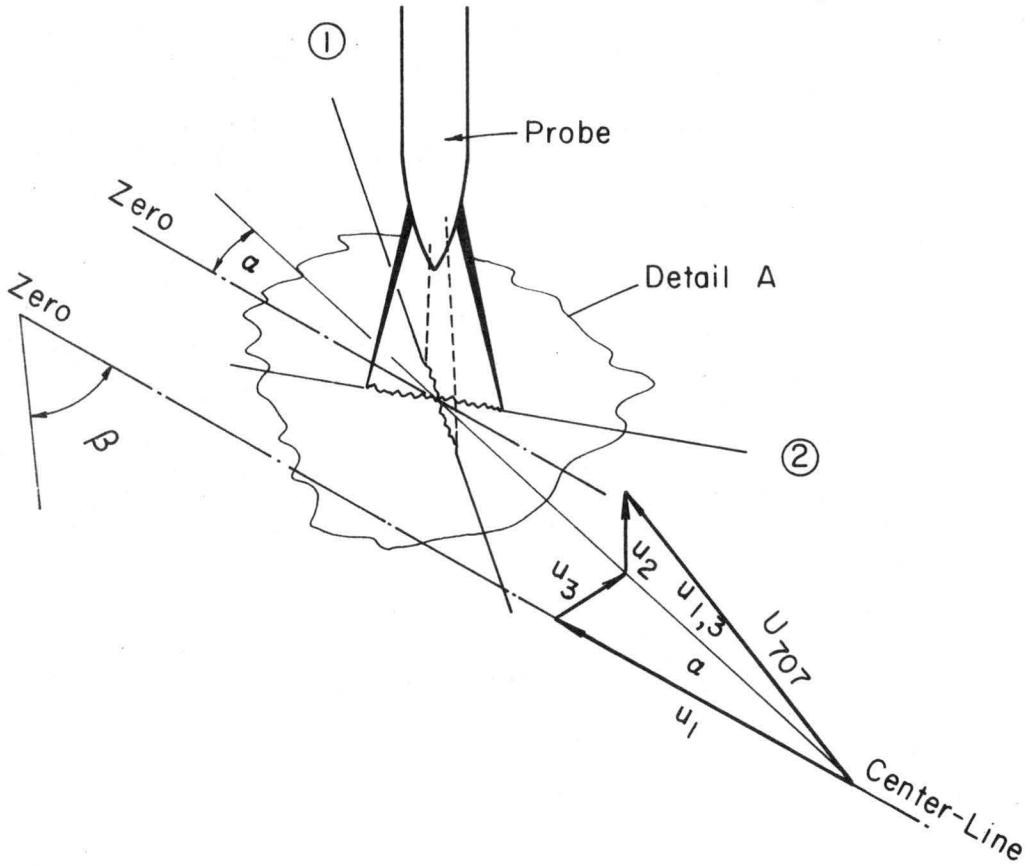

Detail A

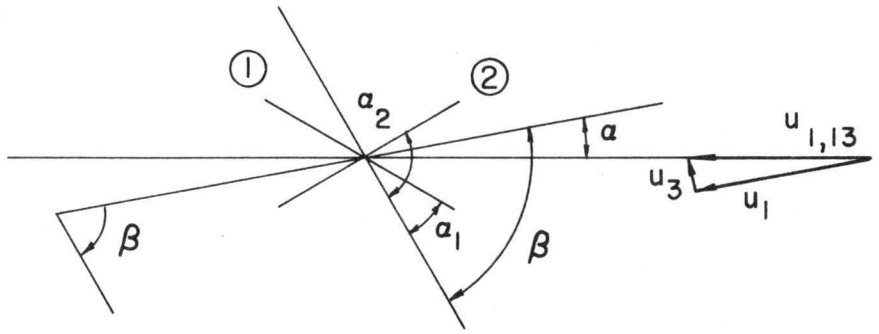

$$\alpha = \frac{\alpha_1+\alpha_2}{2} - \beta = \frac{\alpha_2-\alpha_1}{2} + \alpha_1 - \beta$$

Fig. 8. Sketch of rotating hot wire in a three-dimensional flow

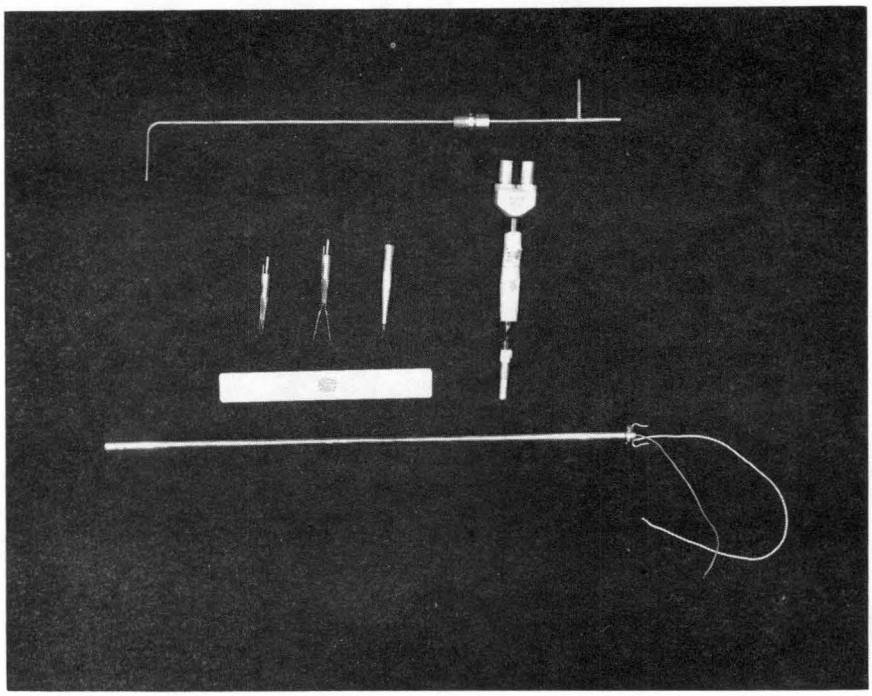

Fig. 9. Probes. Top to bottom, and left to right: pitot static tube, single hot wire, long single hot wire, x-wire, x-wire probe holder, six inch scale, and single wire probe holder

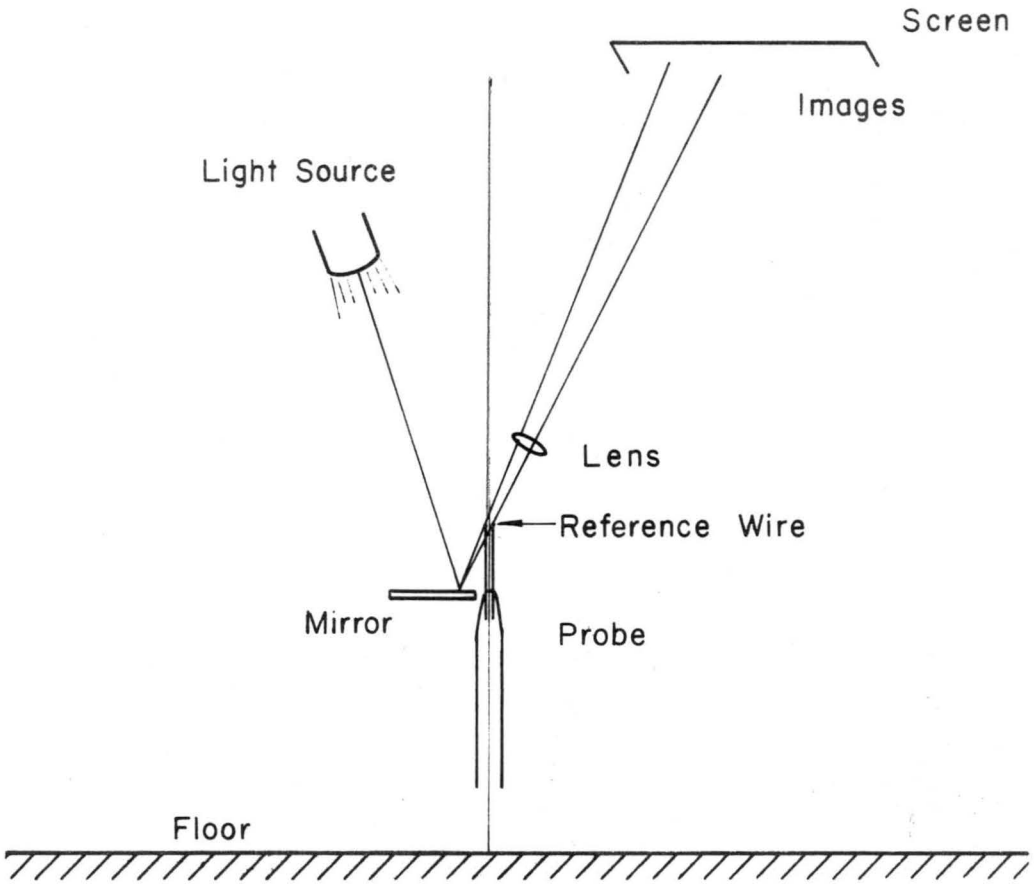

Fig. 10. Sketch of shadow graph technique

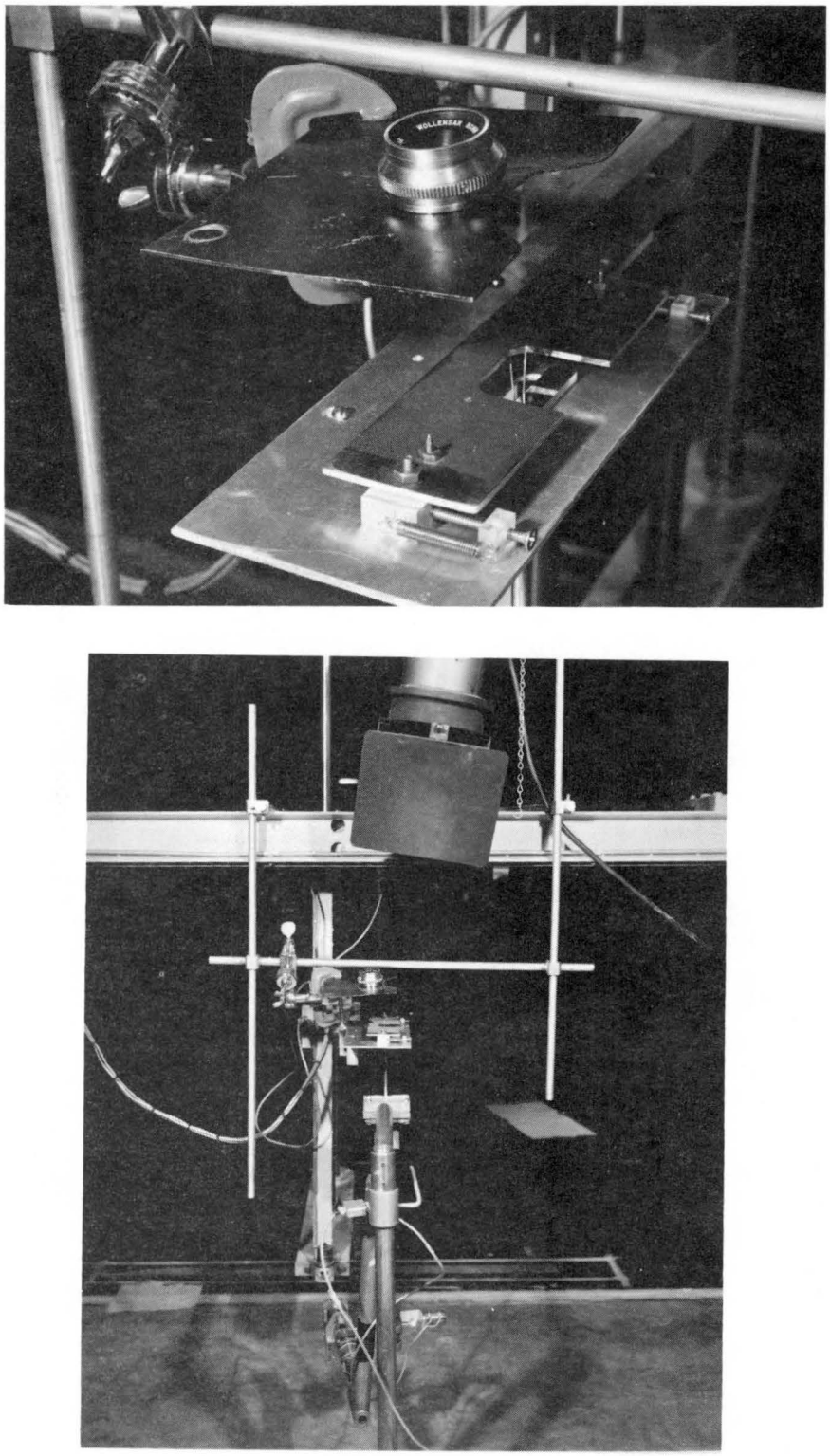

Fig. 11. Shadow graph technique

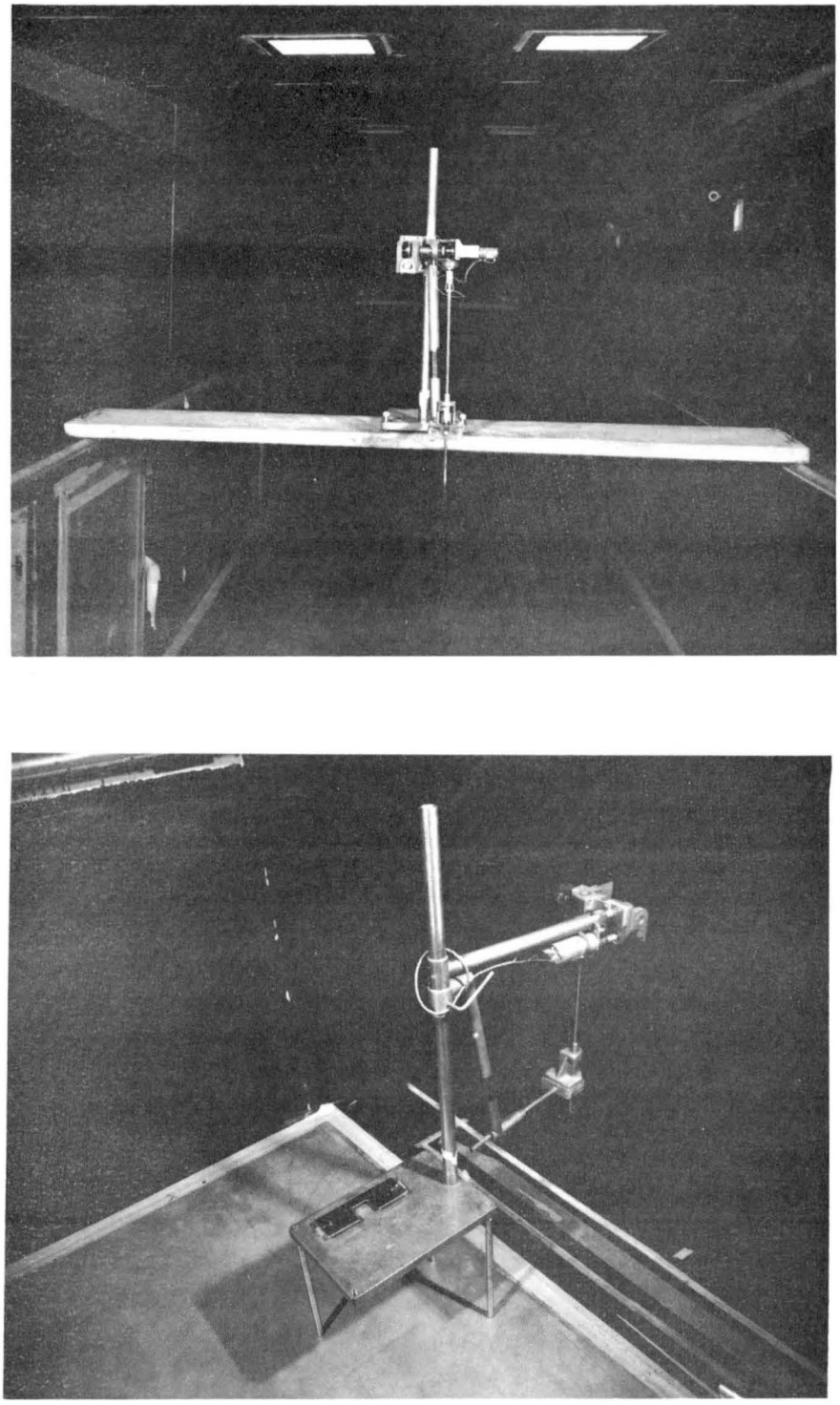

Fig. 12. Rotating probe and stand in wind tunnel

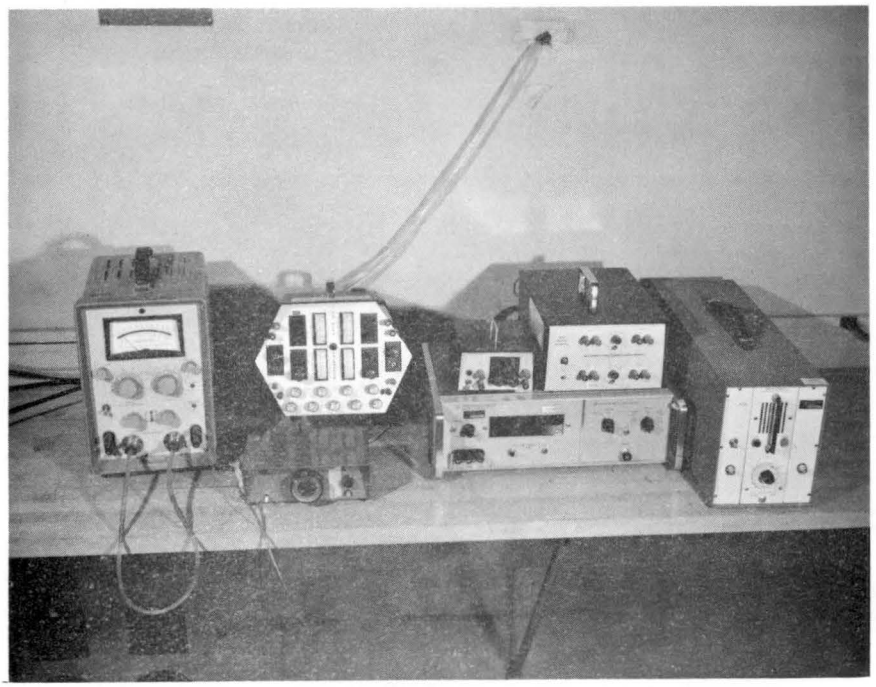

Fig. 13. Secondary flow instruments. Left to right: Tran-sonic pressure meter, rotating hot wire control, CSU anemometer, Hewlett Packard digital volt meter, CSU voltage source, CSU integrator, and Dynamics Corp. amplifier

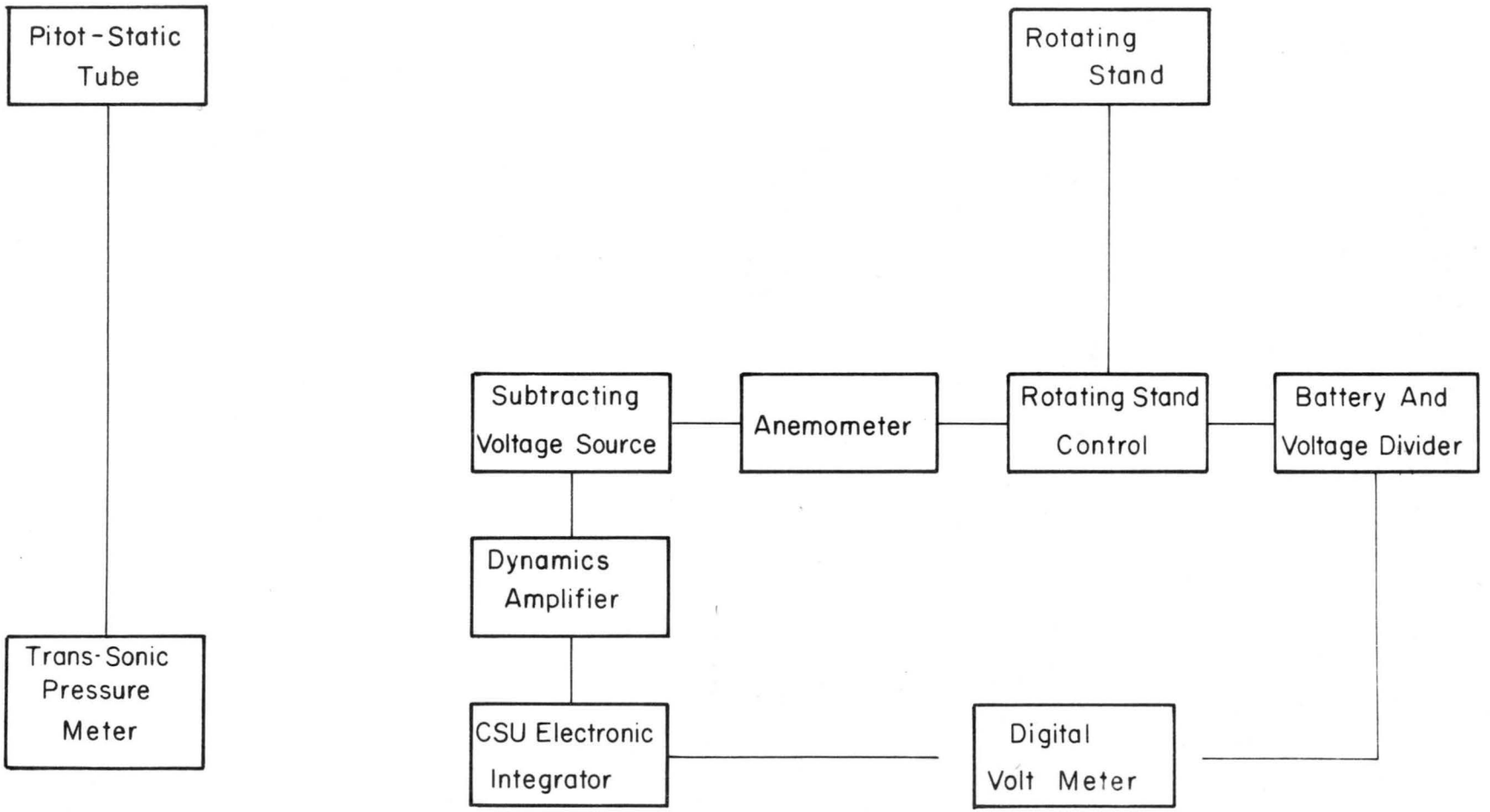

Fig. 14. Block diagram of secondary flow instrumentation

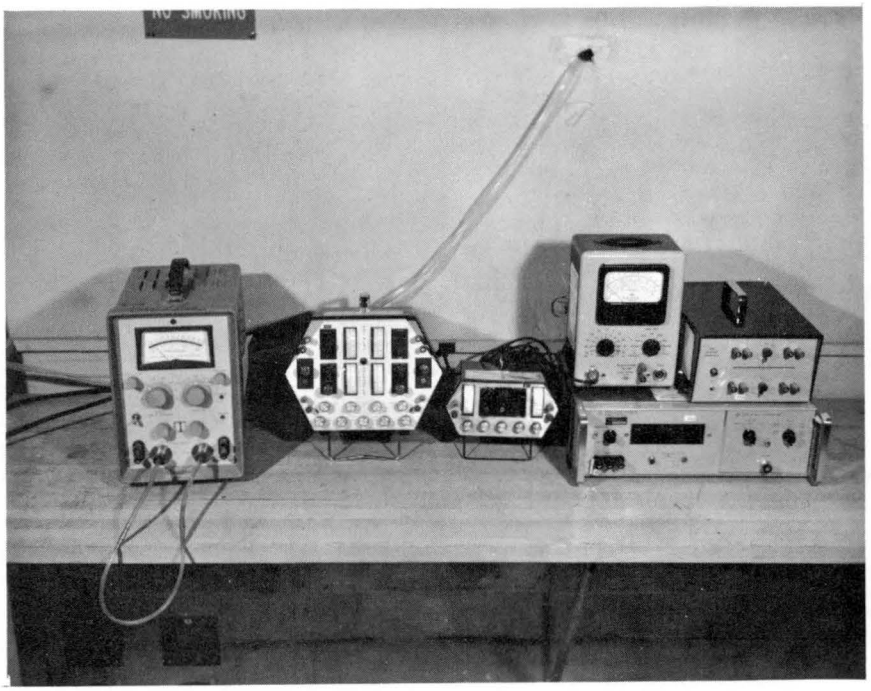

Fig. 15. Turbulence instrumentation. Left to right: Tran-sonic pressure meter, dual channel CSU anemometer, single channel CSU anemometer, B&K true RMS meter, Hewlett Packard digital volt meter, and CSU integrator.

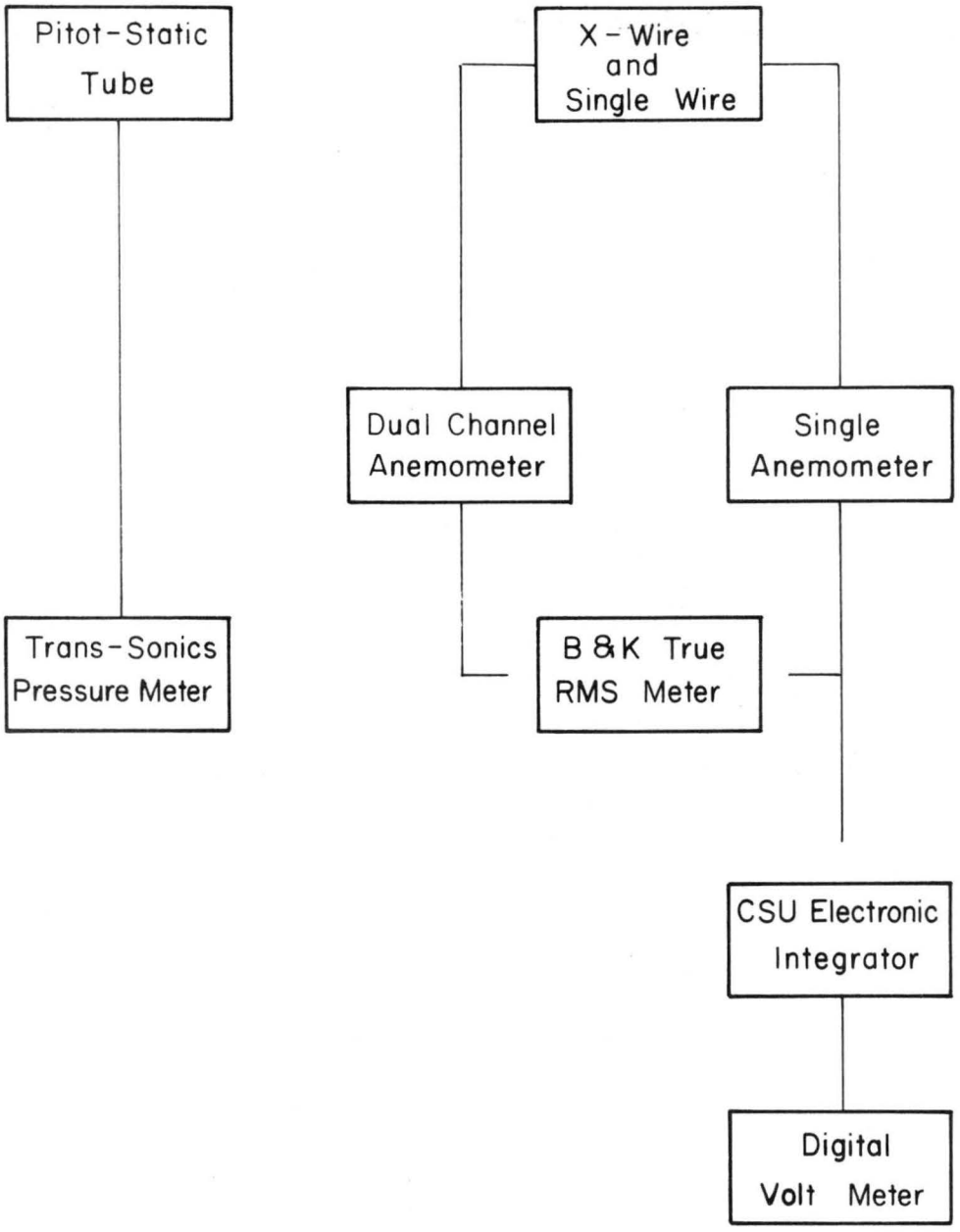

Fig. 16. Block diagram for turbulence instrumentation

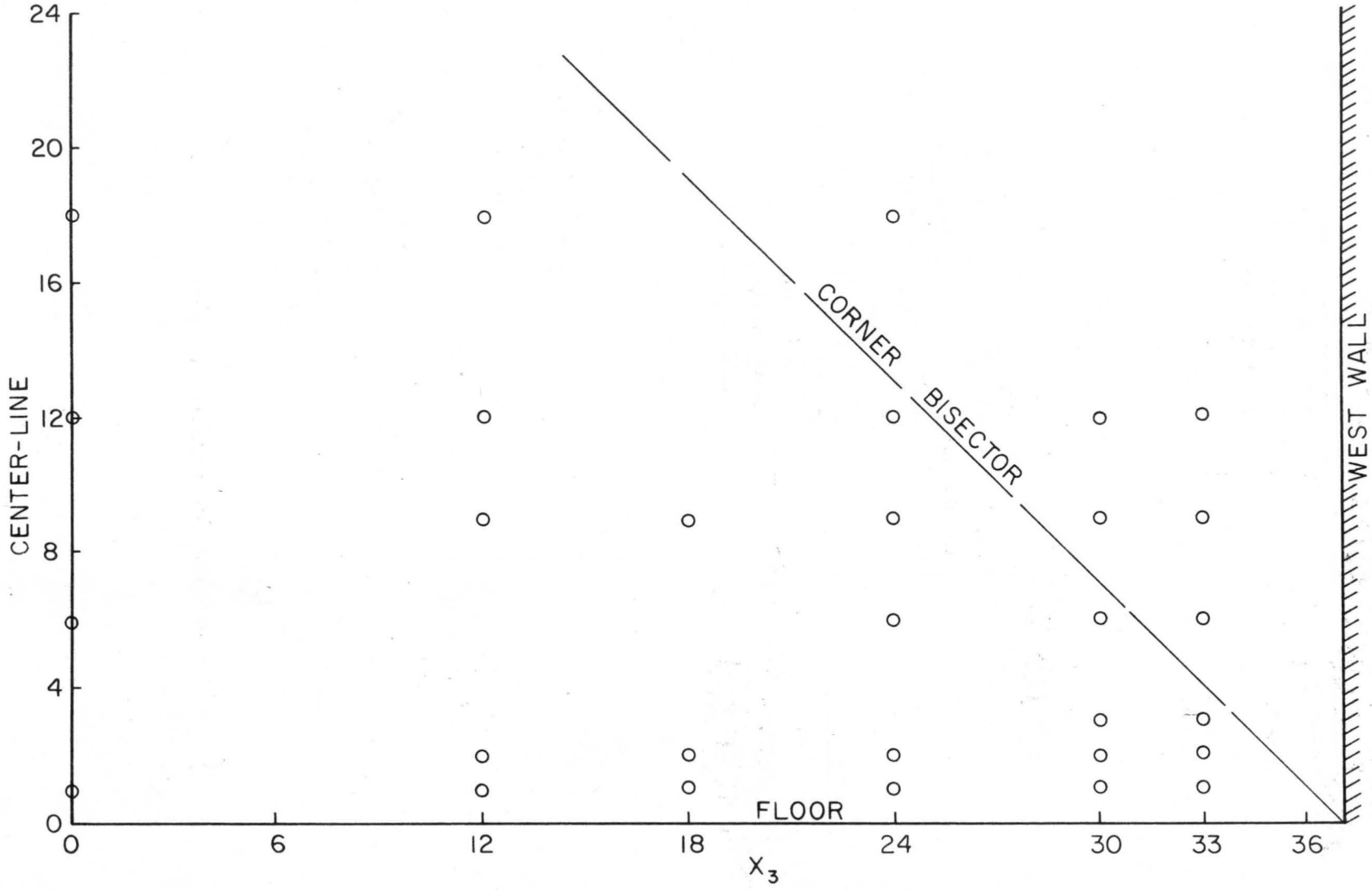

Fig. 17. Map of measurement points in cross section

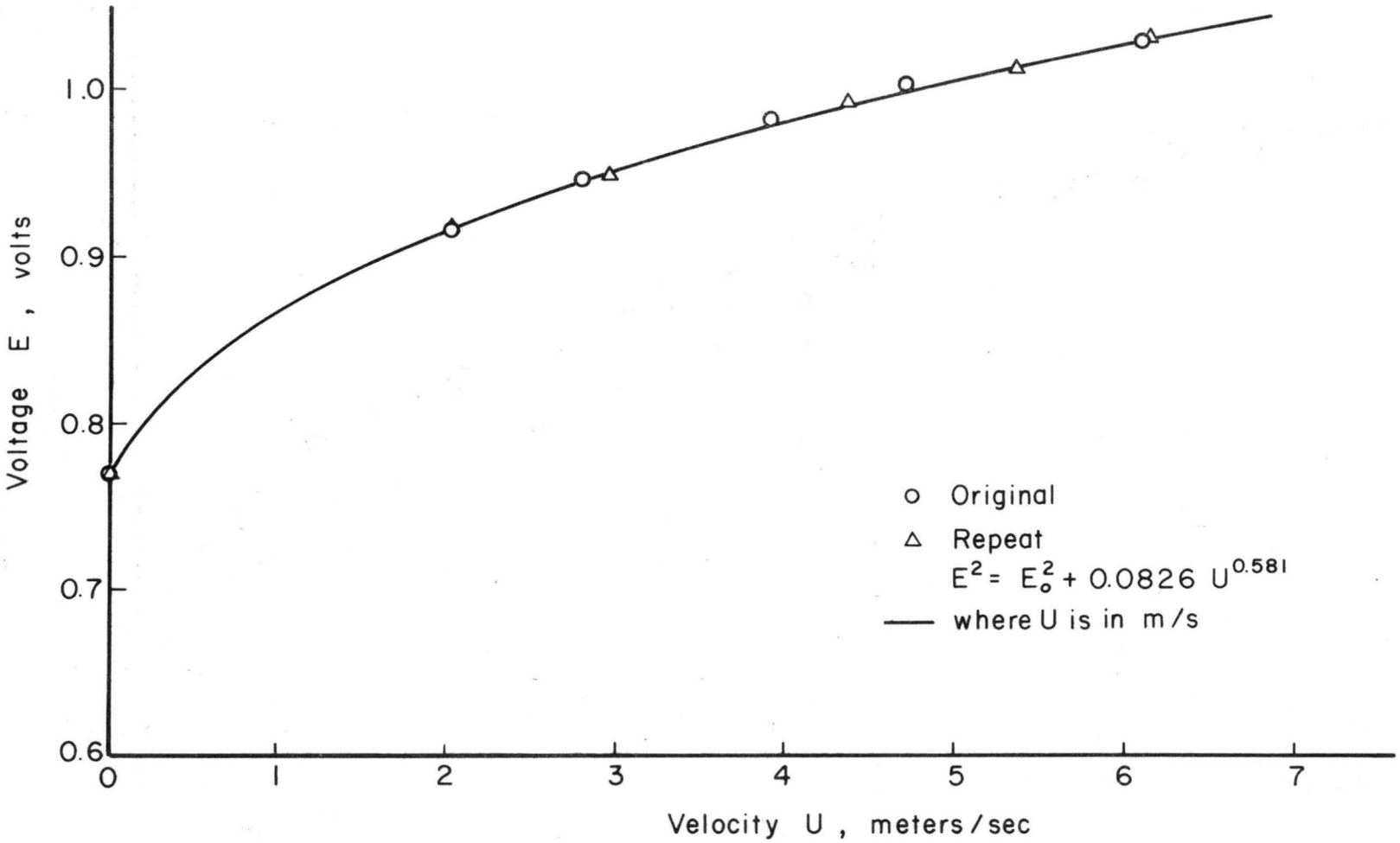

Fig. 18. Hot wire calibration curve

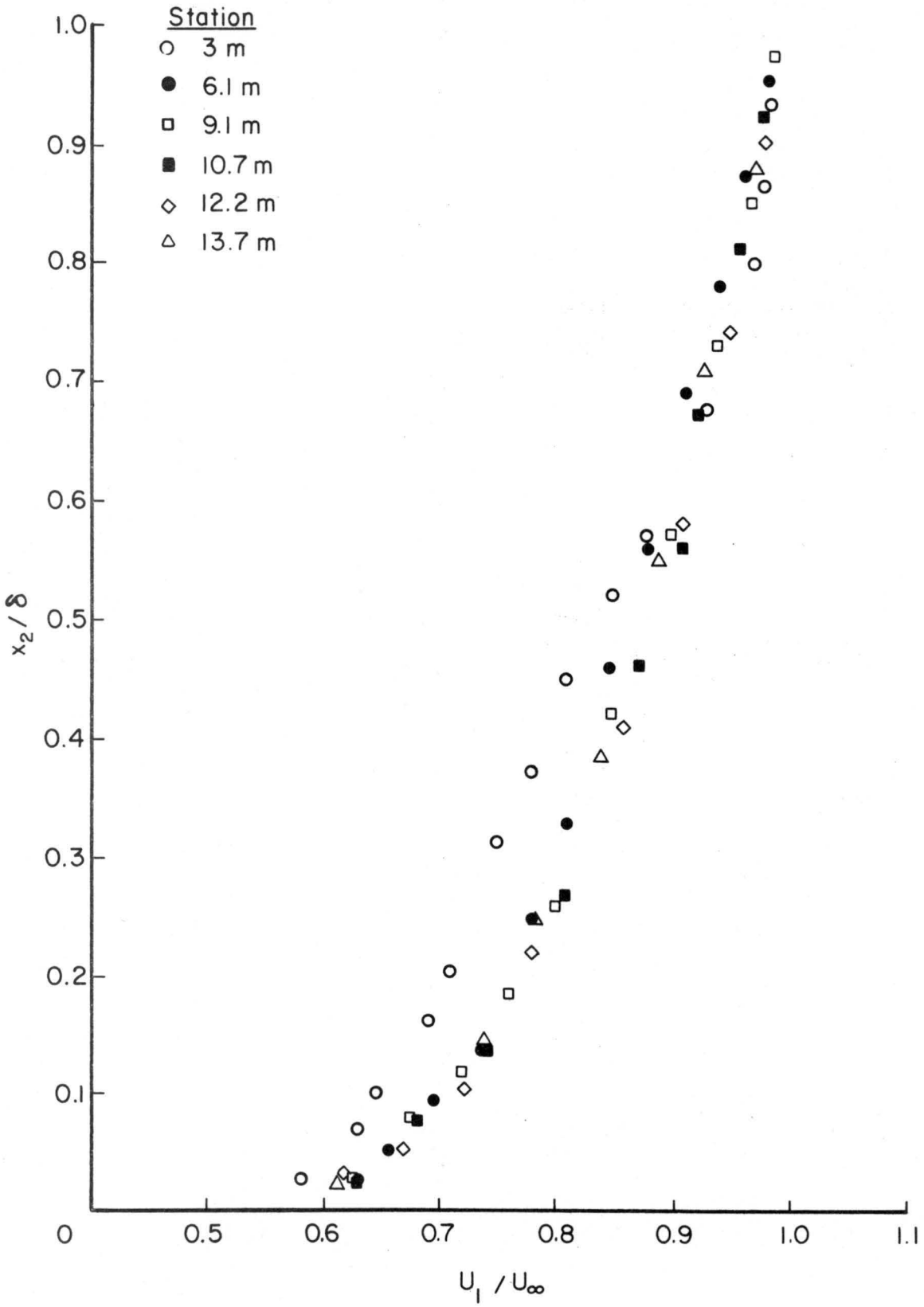

Fig. 19. Velocity profiles along centerline of wind tunnel

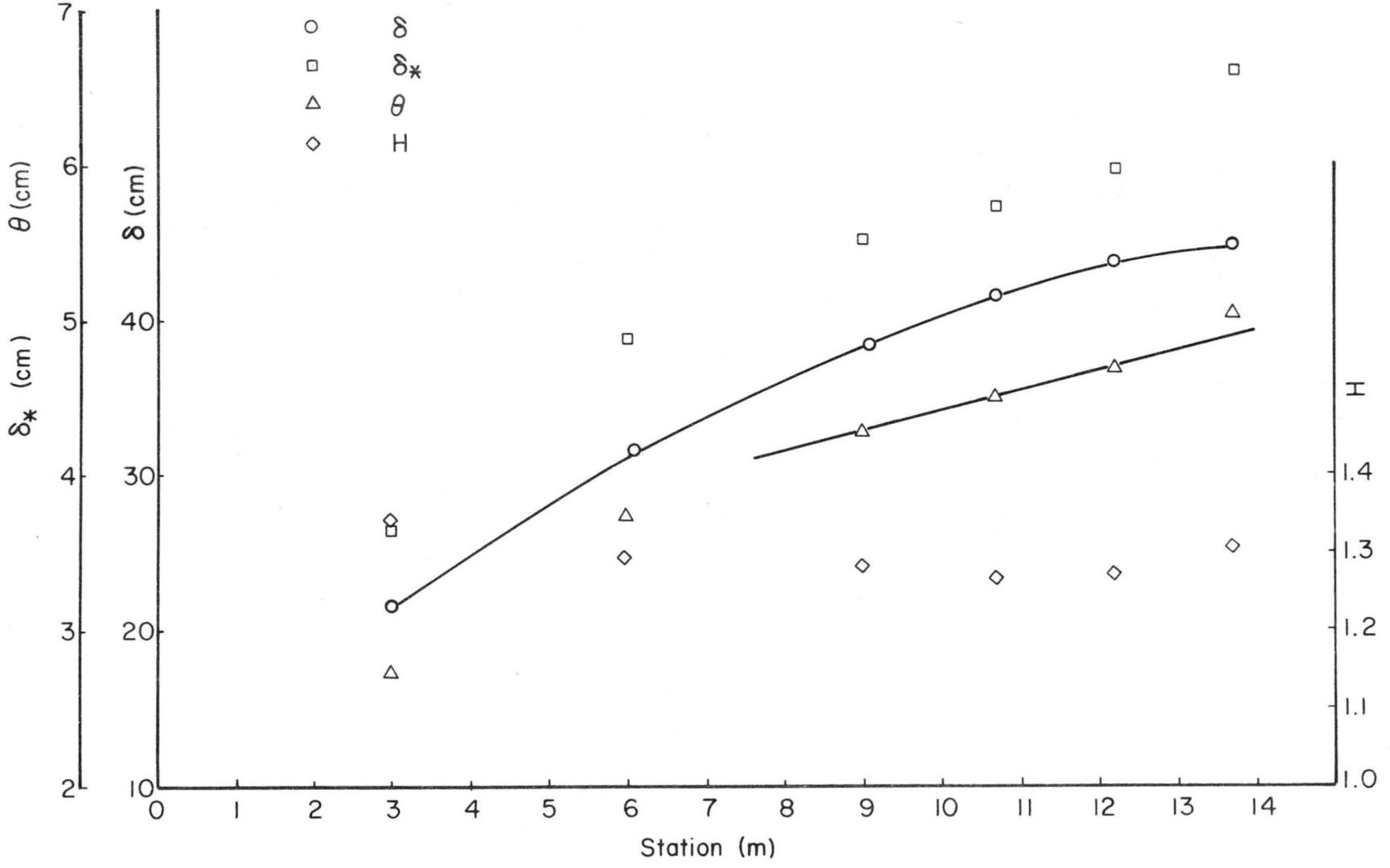

Fig. 20. Boundary layer parameters

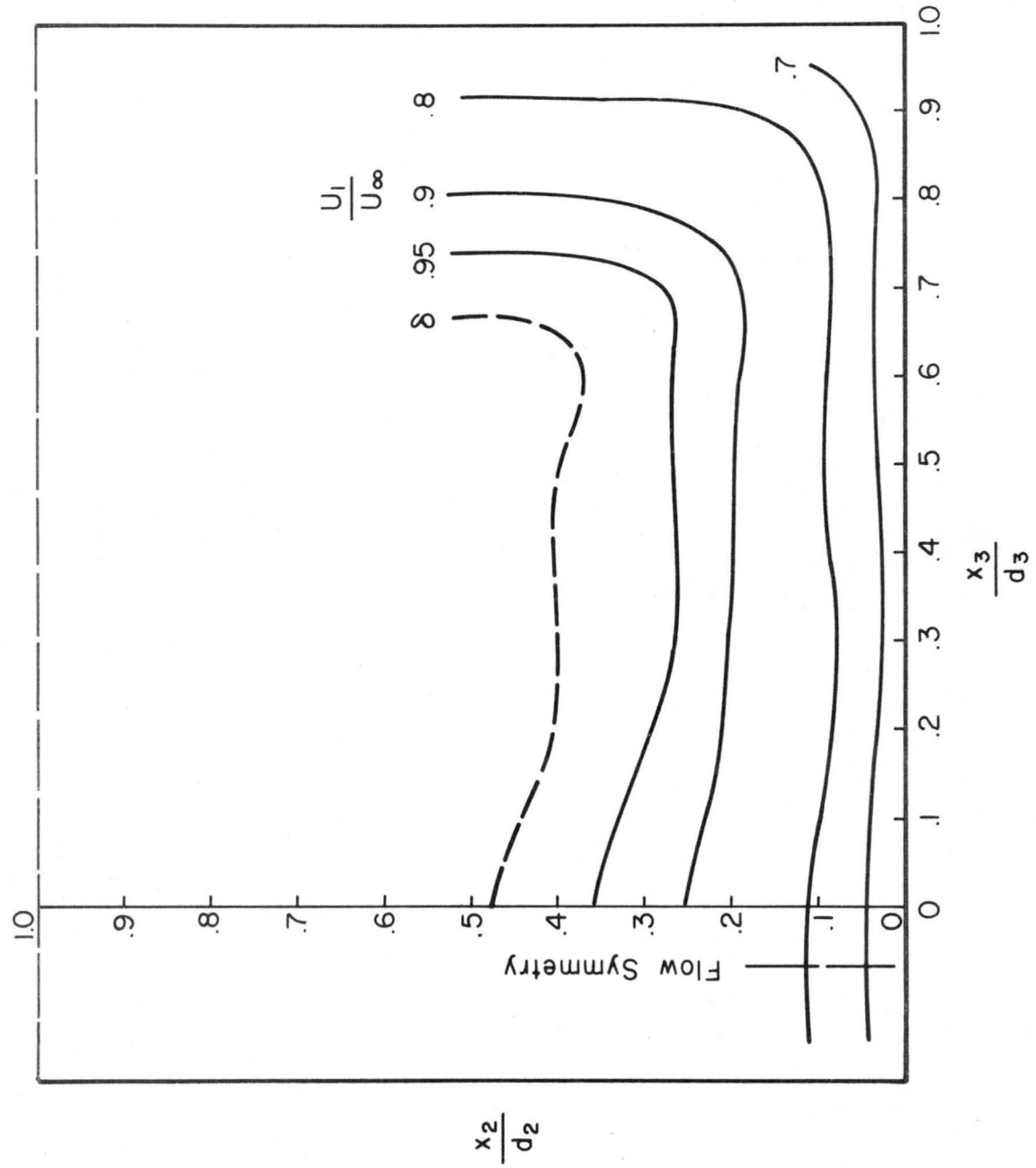

Fig. 21. Isovels

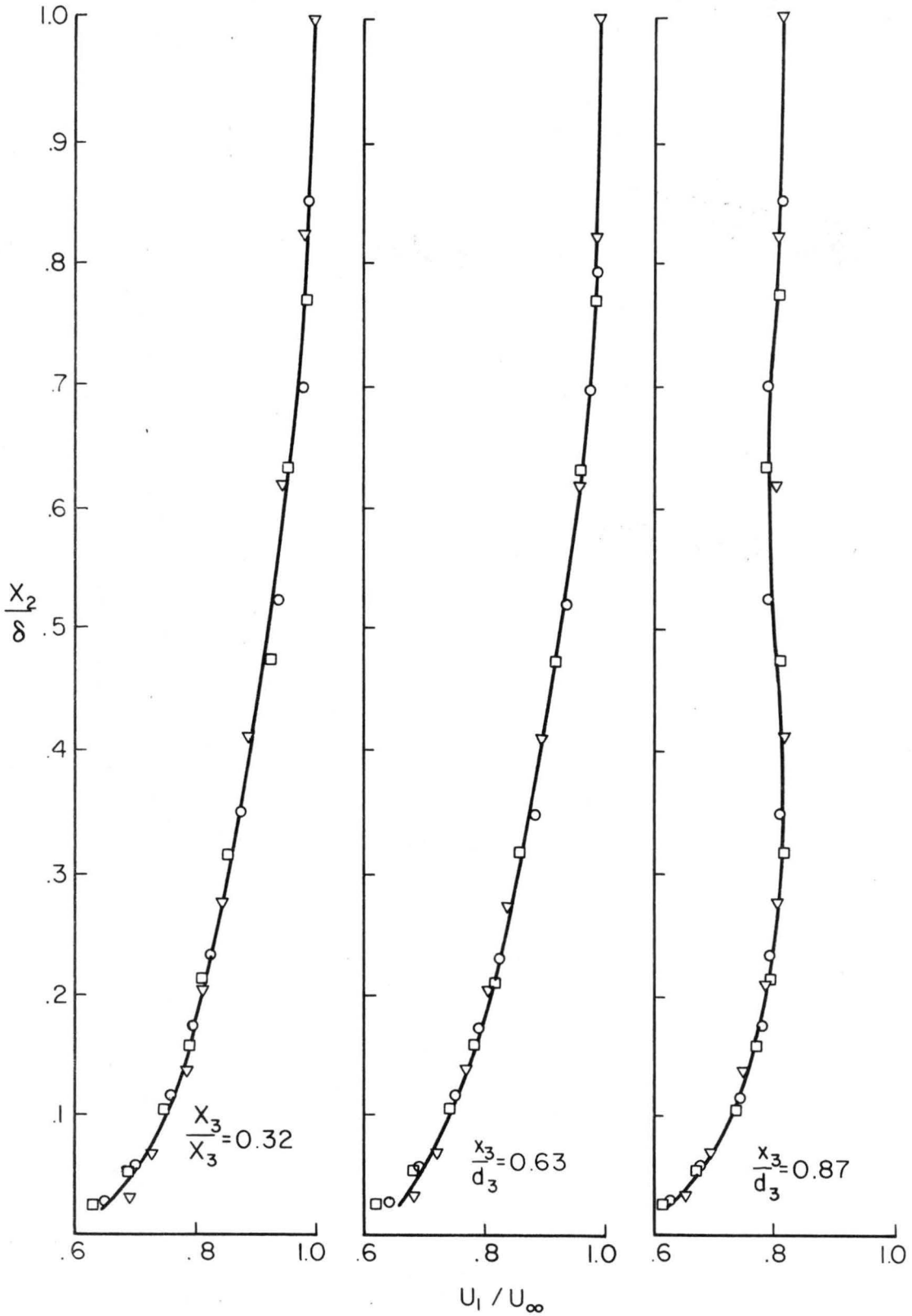

Fig. 22. Velocity profiles in cross section, x_1 = 12.2 m

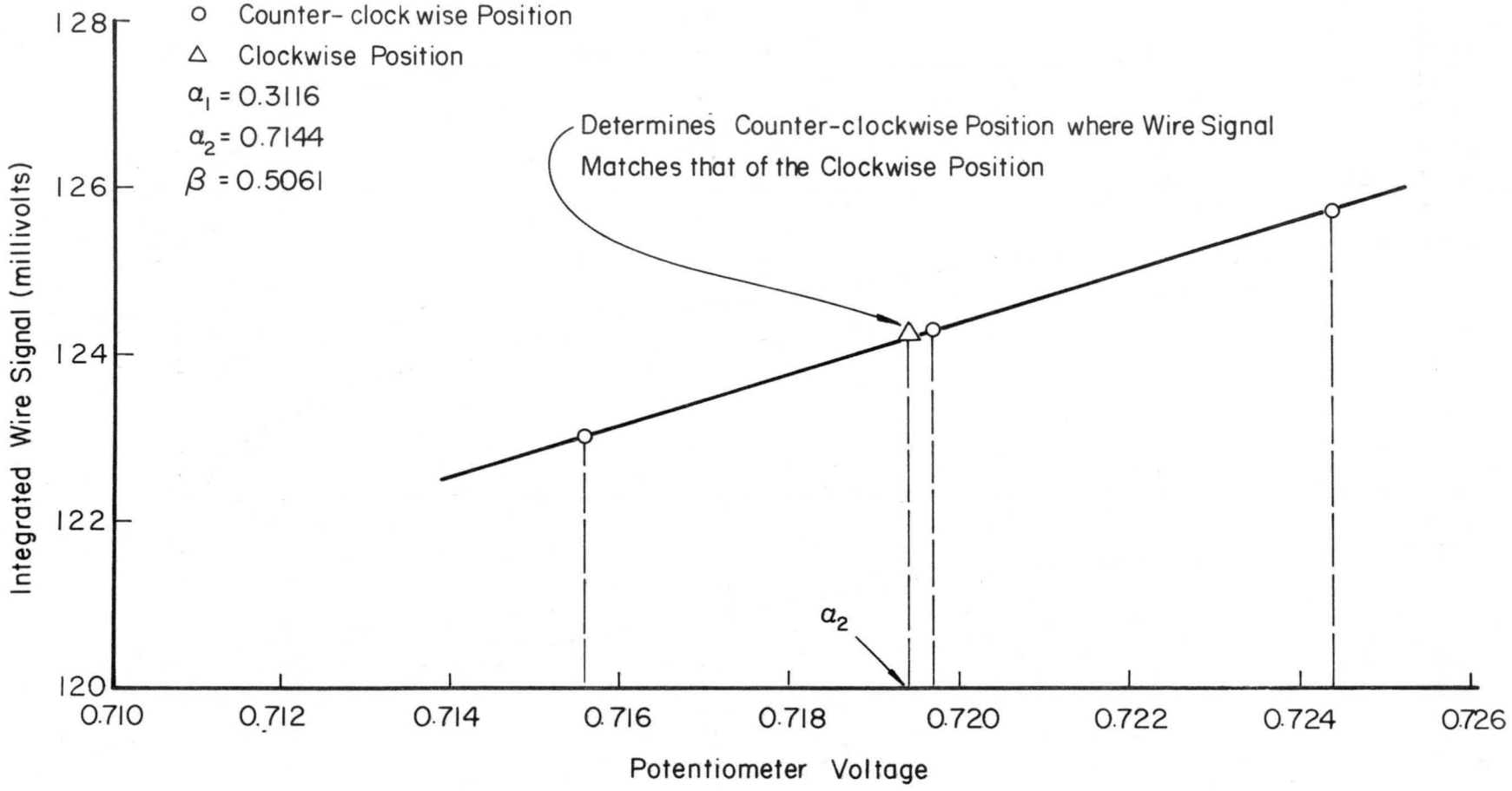

Fig. 23. Typical secondary flow data for determination of α

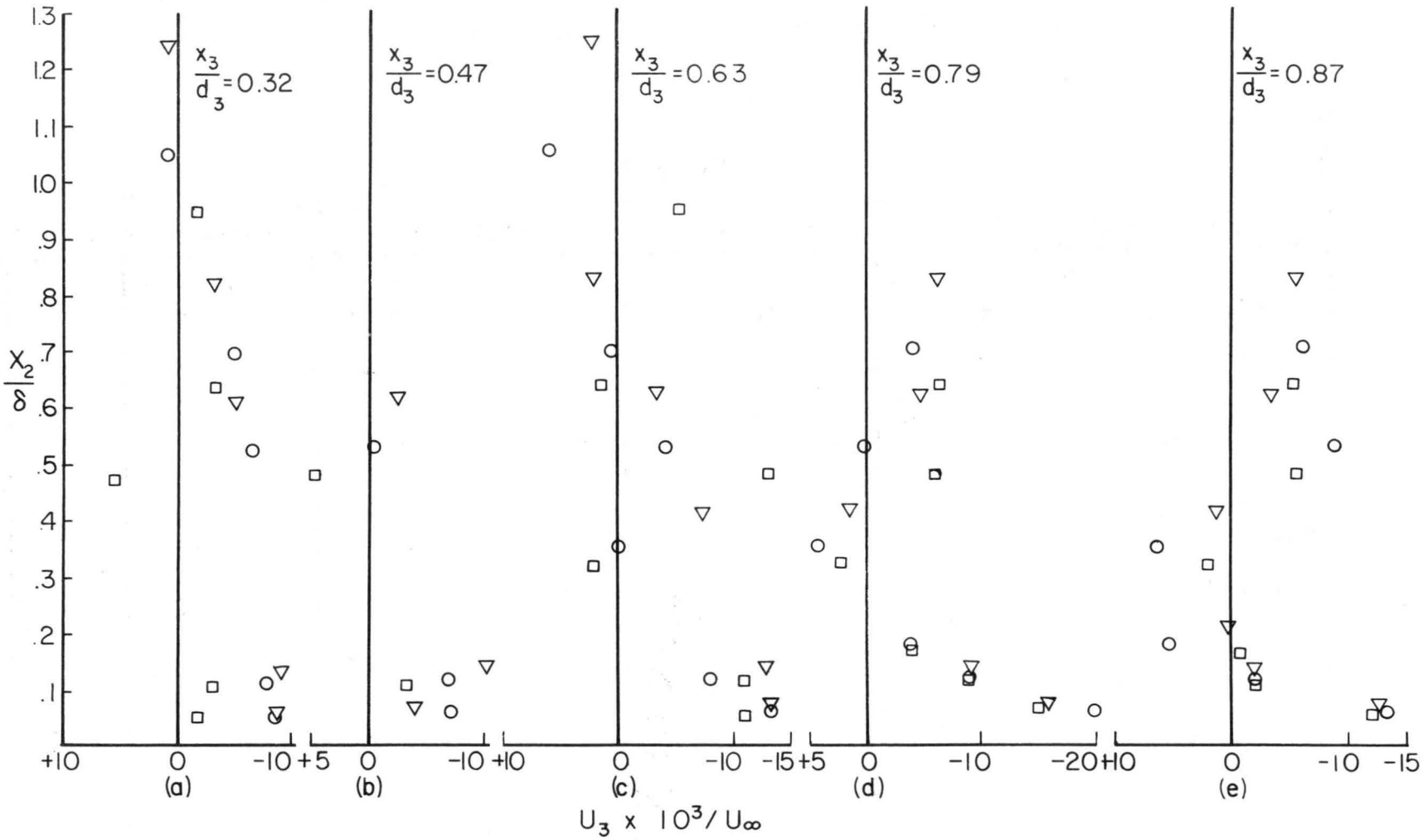

Fig. 24. Horizontal secondary flow components; U_3/U_∞ vs x_2/δ

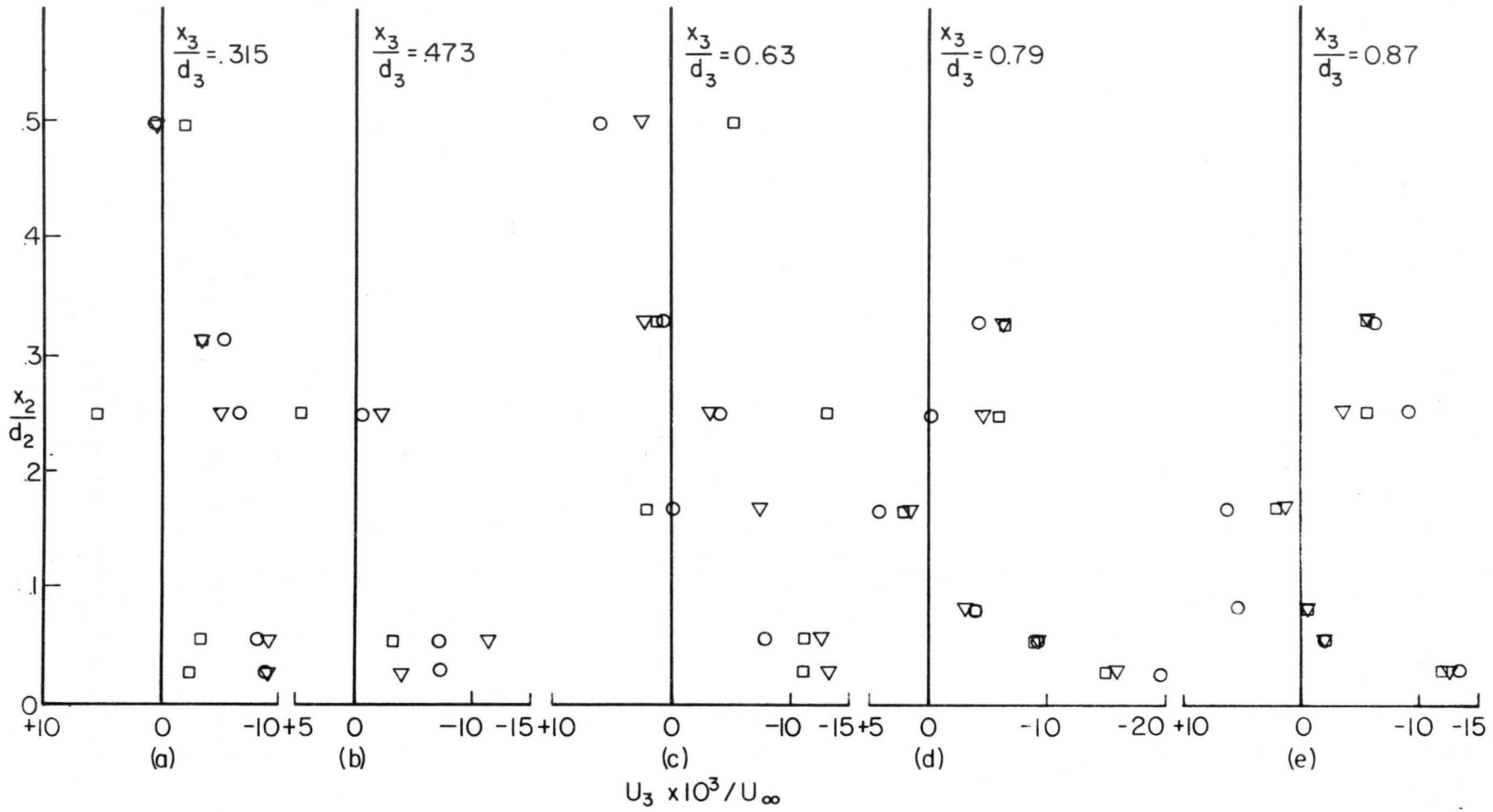

Fig. 25. Horizontal secondary flow components; U_3/U_∞ vs x_2/d_2

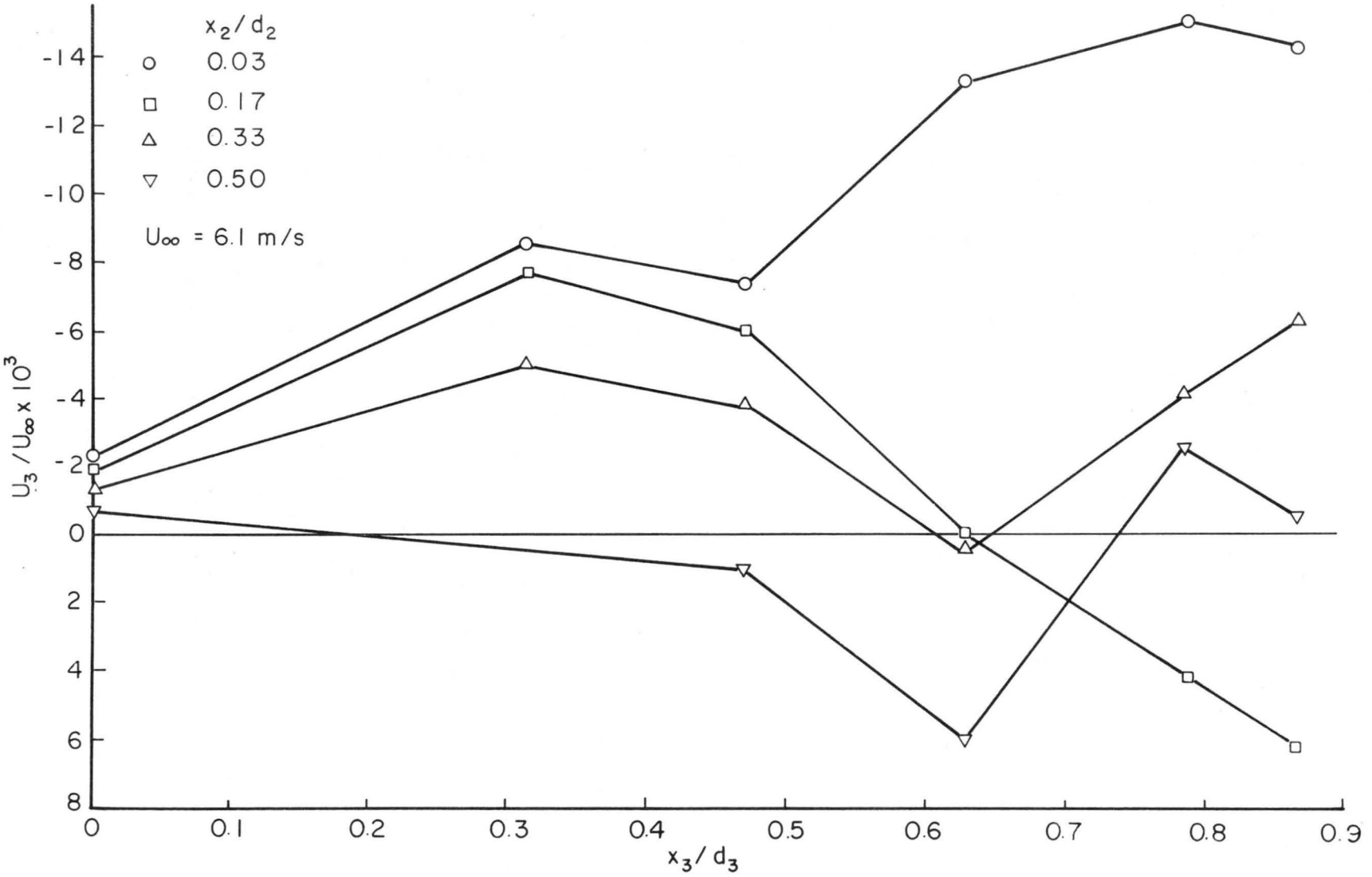

Fig. 26. Horizontal secondary flow components; U_3/U_∞ vs x_3/d_3

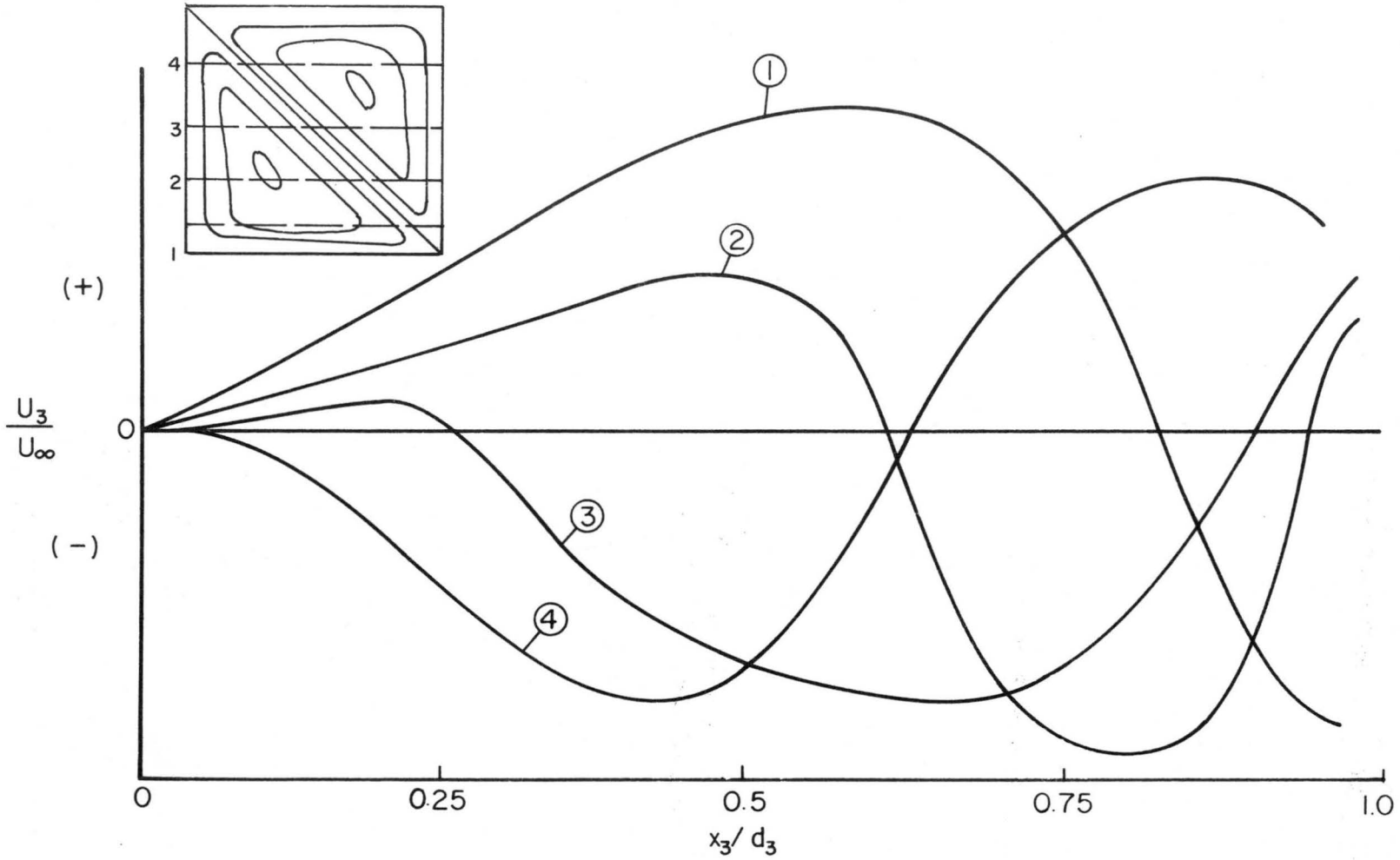

Fig. 27. Idealized horizontal secondary flow components; U_3/U_∞ vs x_3/d_3

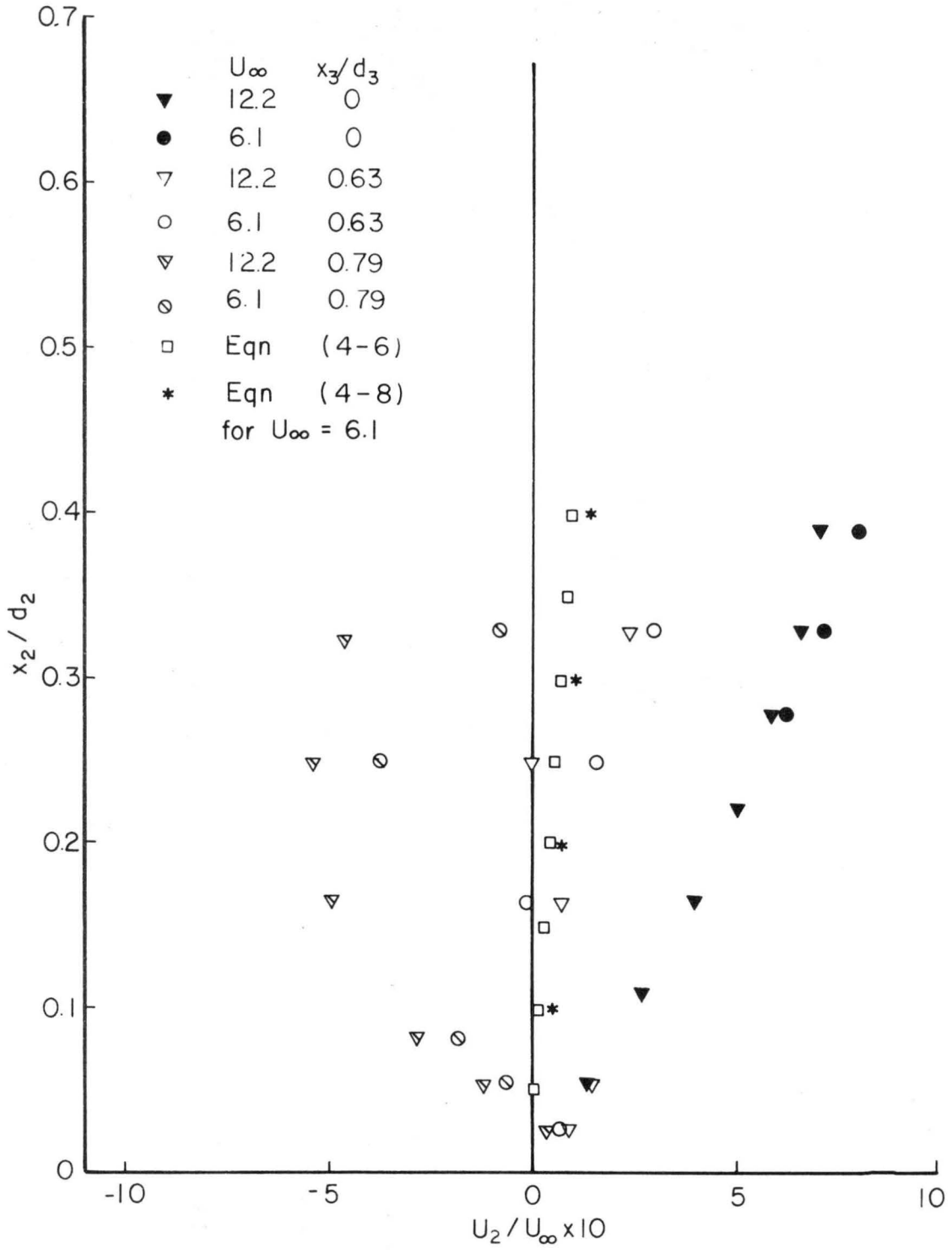

Fig. 28. Calculated vertical secondary flow components; U_2/U_∞ vs x_2/d_2

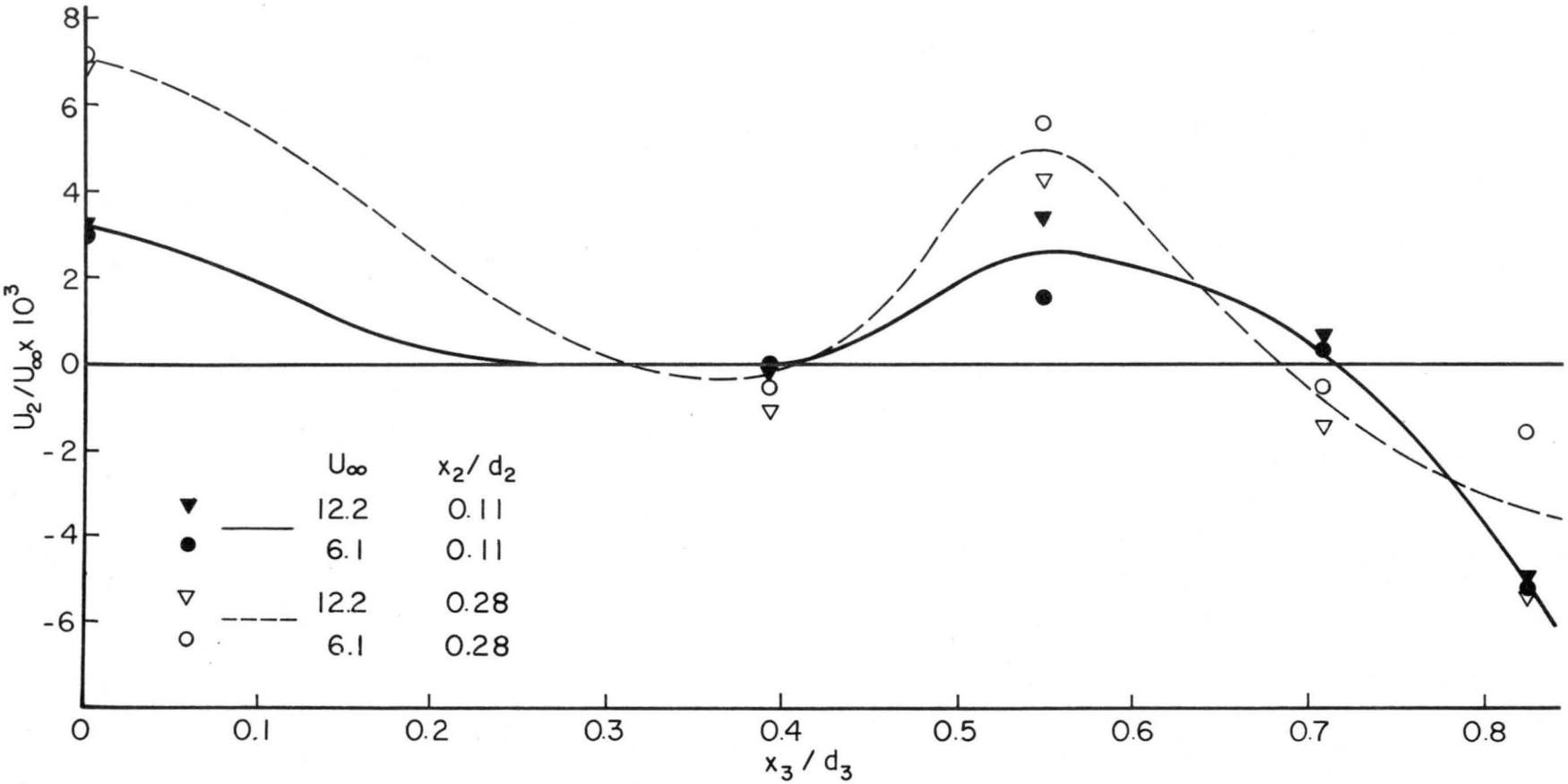

Fig. 29. Calculated vertical secondary flow components; U_2/U_∞ vs x_3/d_3

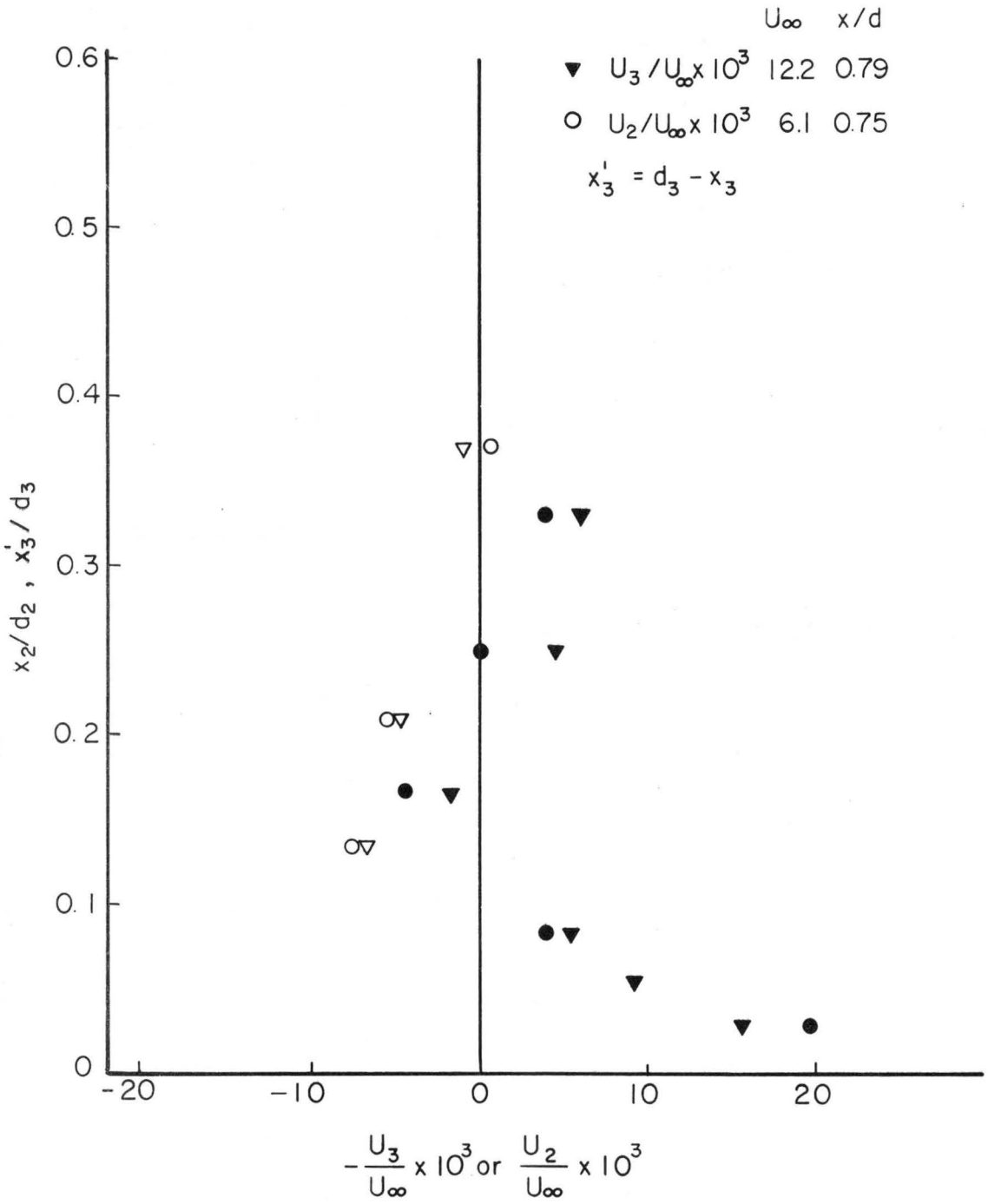

Fig. 30. Corner symmetry

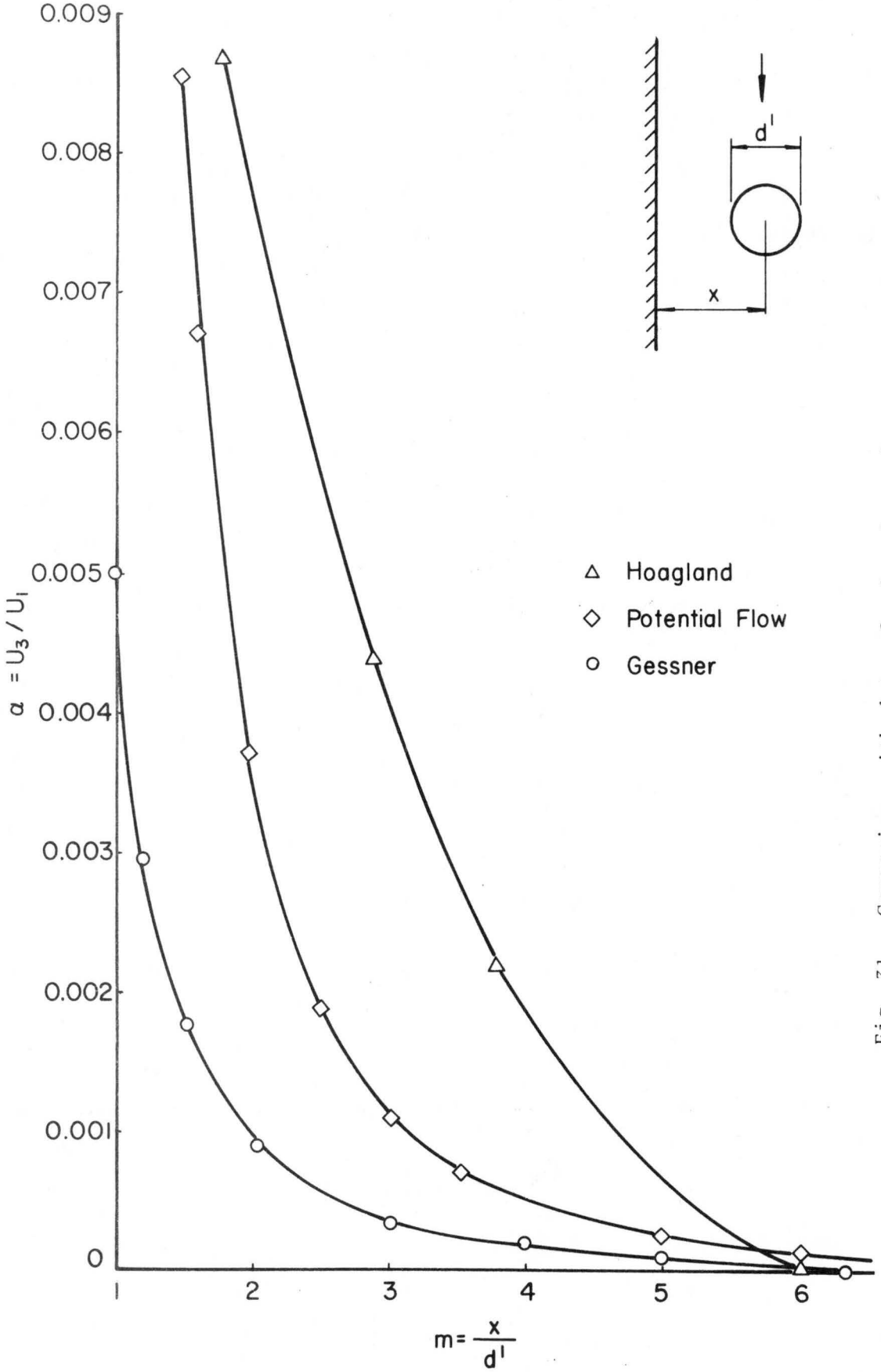

Fig. 31. Comparison with data of other investigators

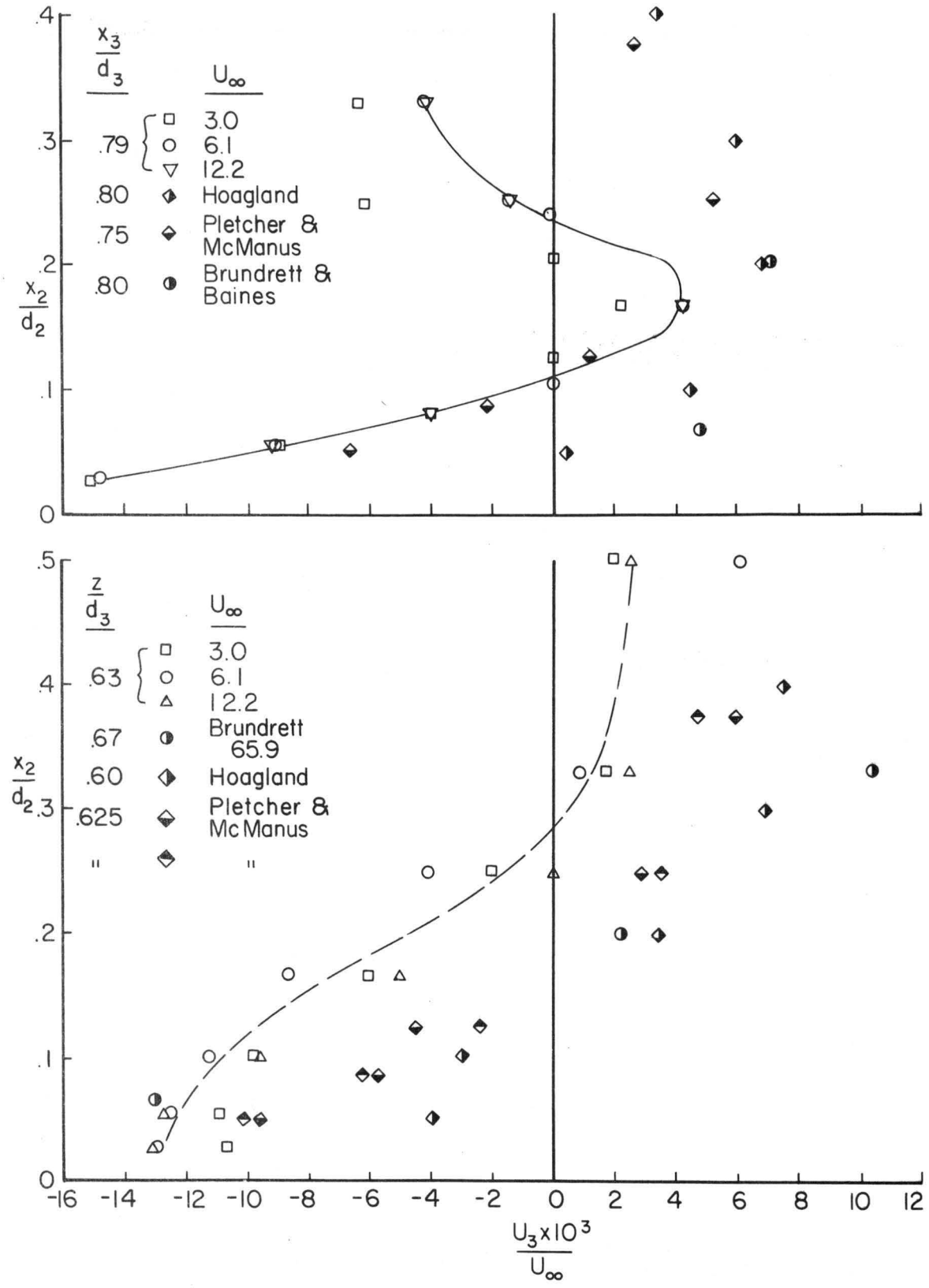

Fig. 32. Comparison with data of other investigators

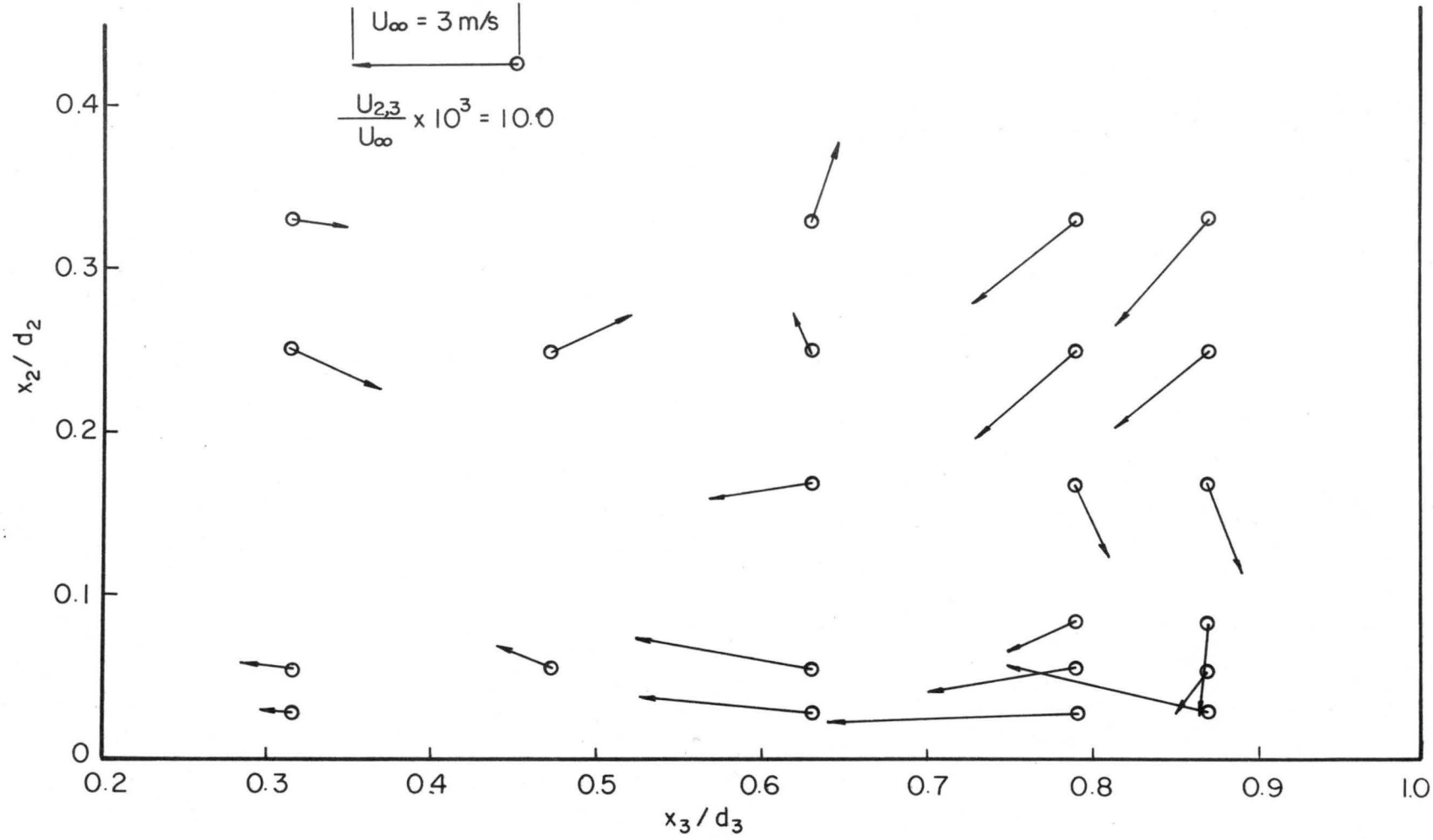

Fig. 33. Resultant secondary flow in cross section, U_∞ = 3 m/s

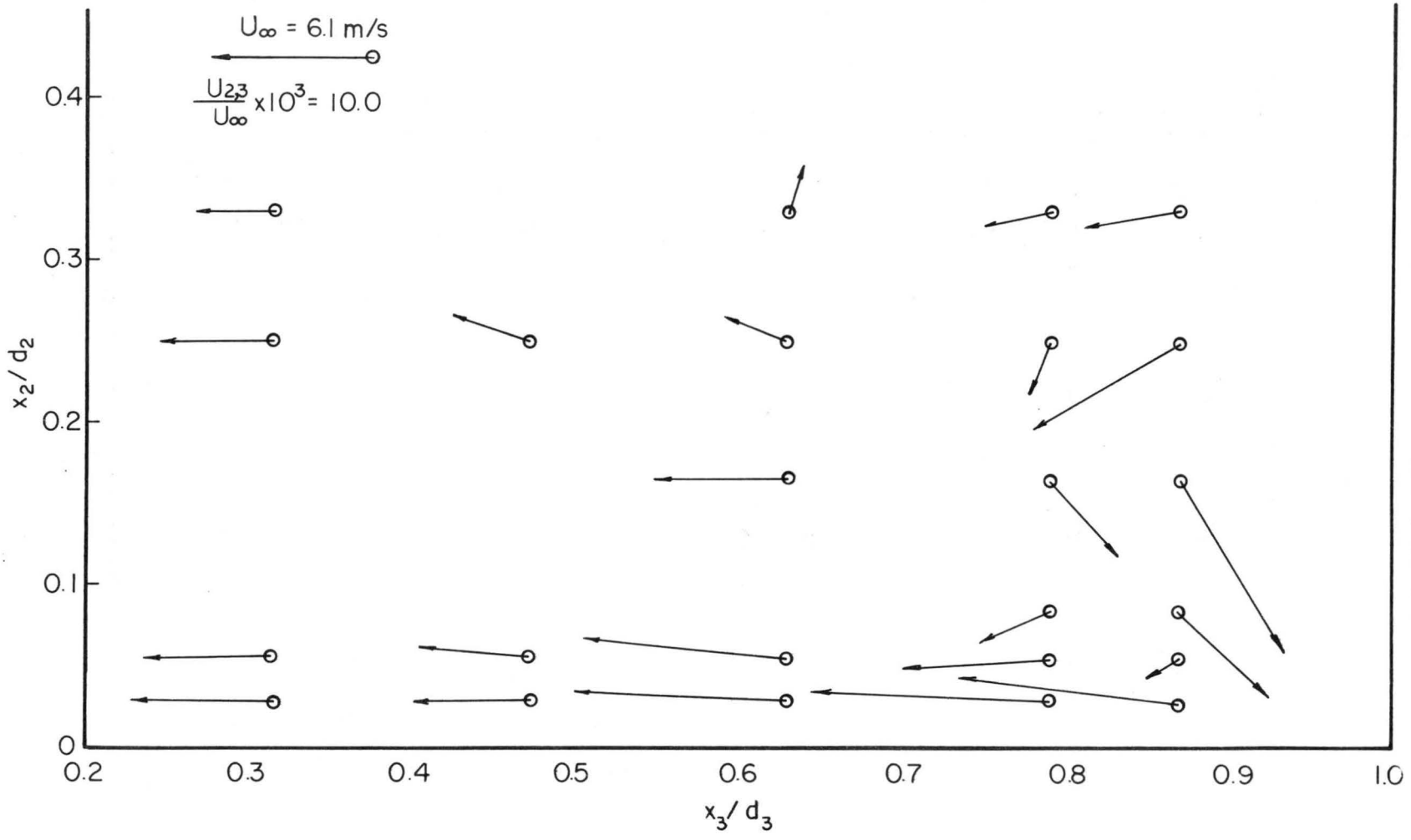

Fig. 34. Resultant secondary flow in cross section, U_∞ = 6.1 m/s

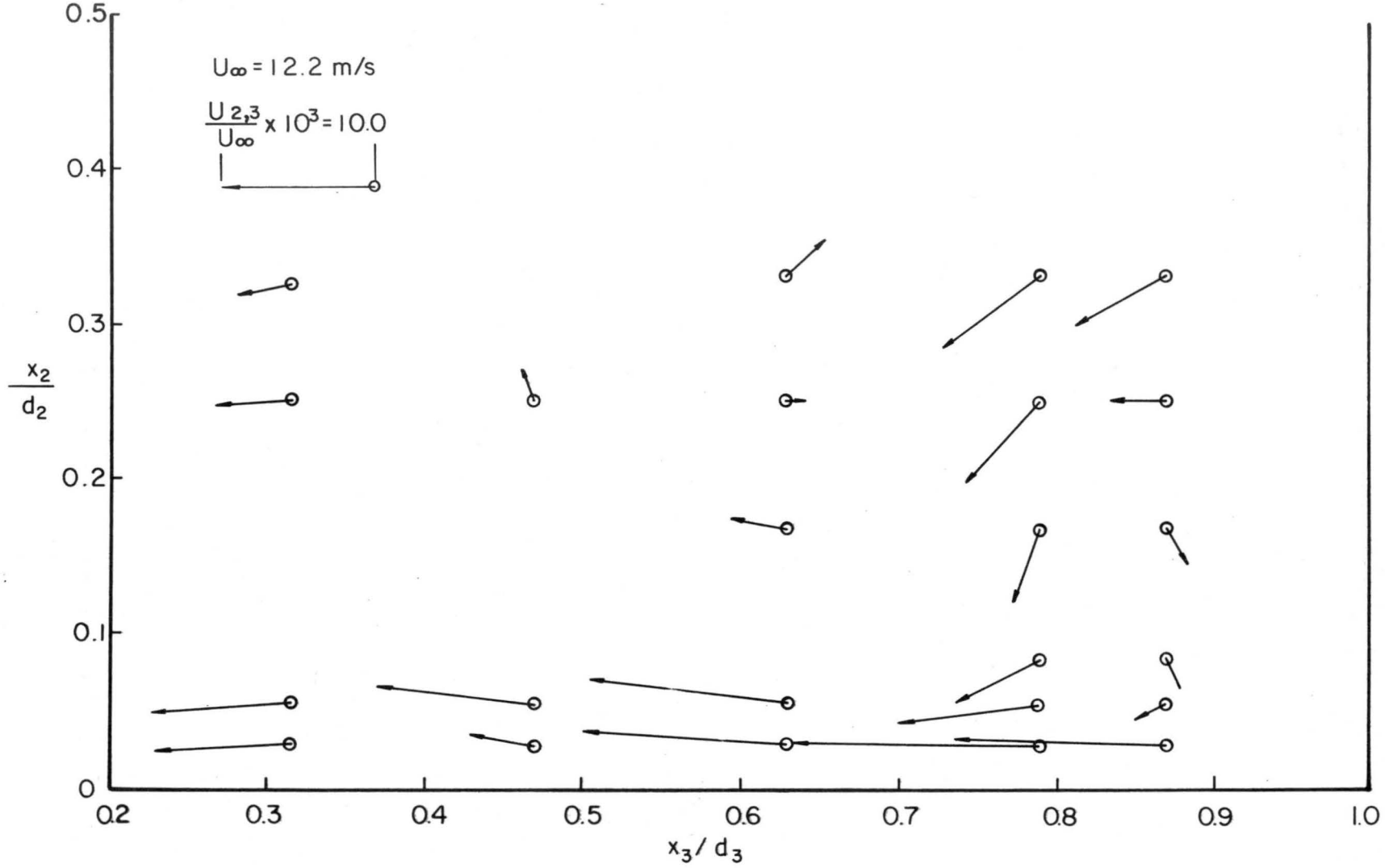

Fig. 35. Resultant secondary flow in cross section, U_∞ = 12.2 m/s

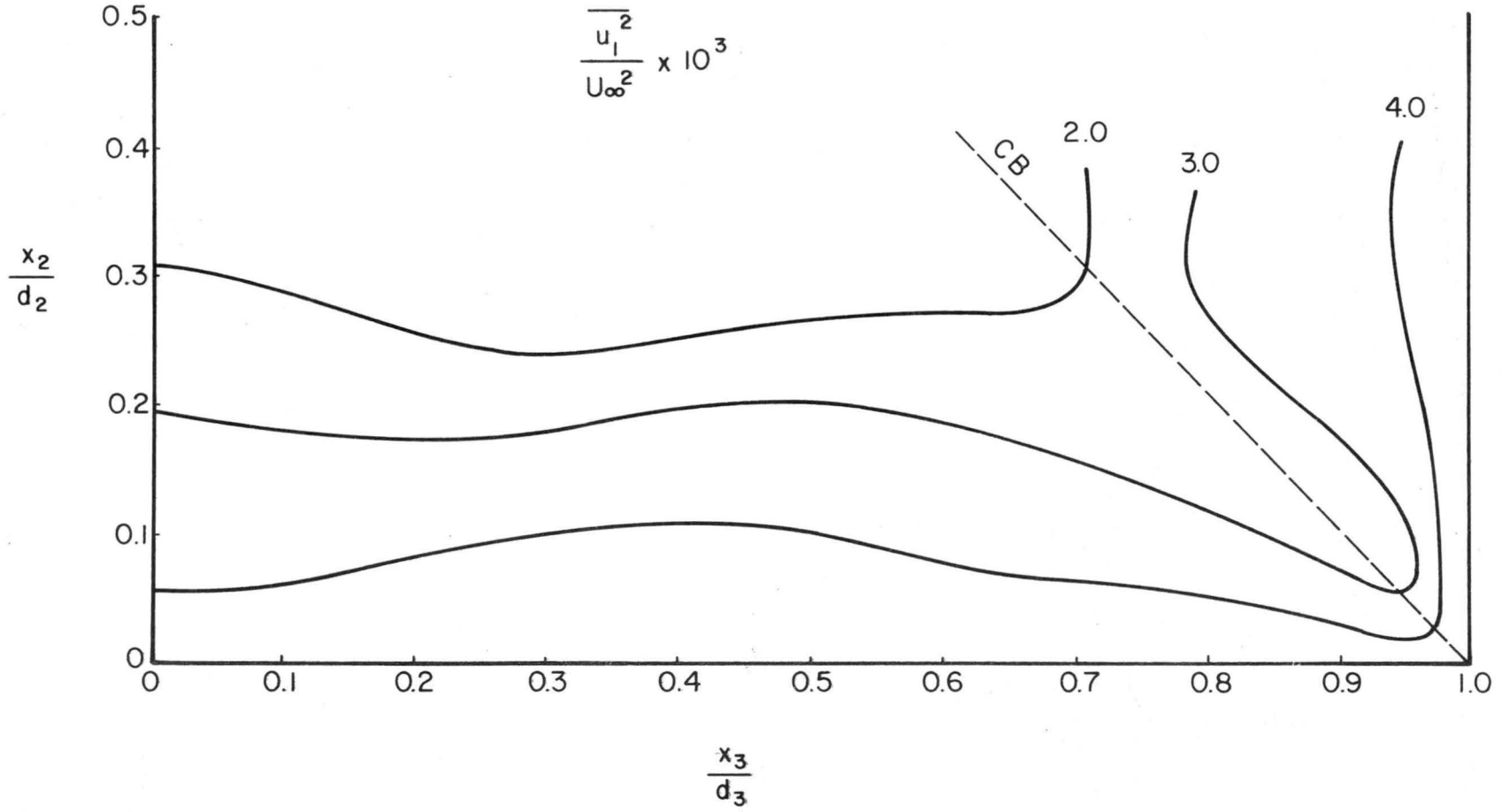

Fig. 36. Distribution of $\overline{u_1^2}/U_\infty^2$

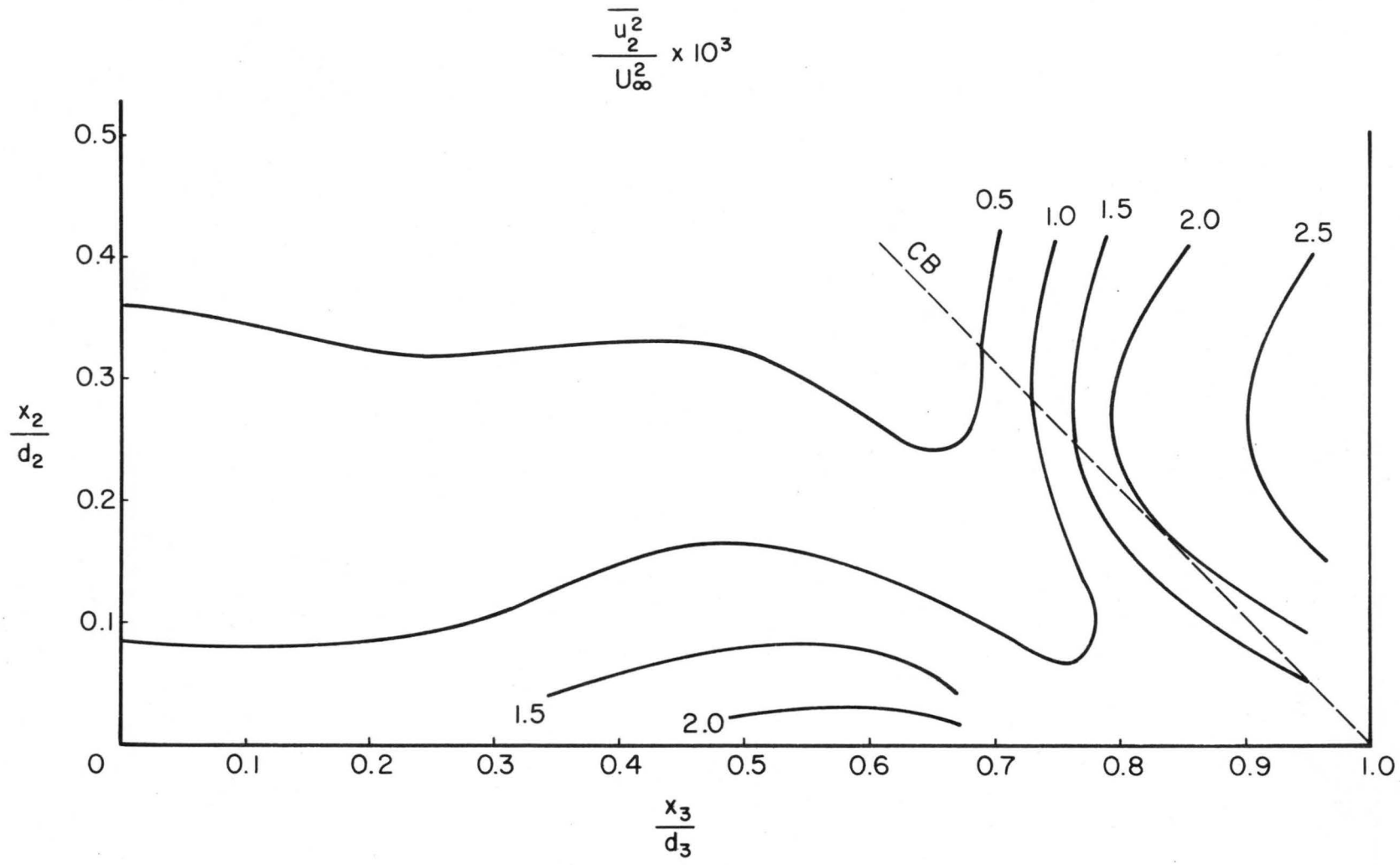

Fig. 37. Distribution of $\overline{u_2^2}/U_\infty^2$

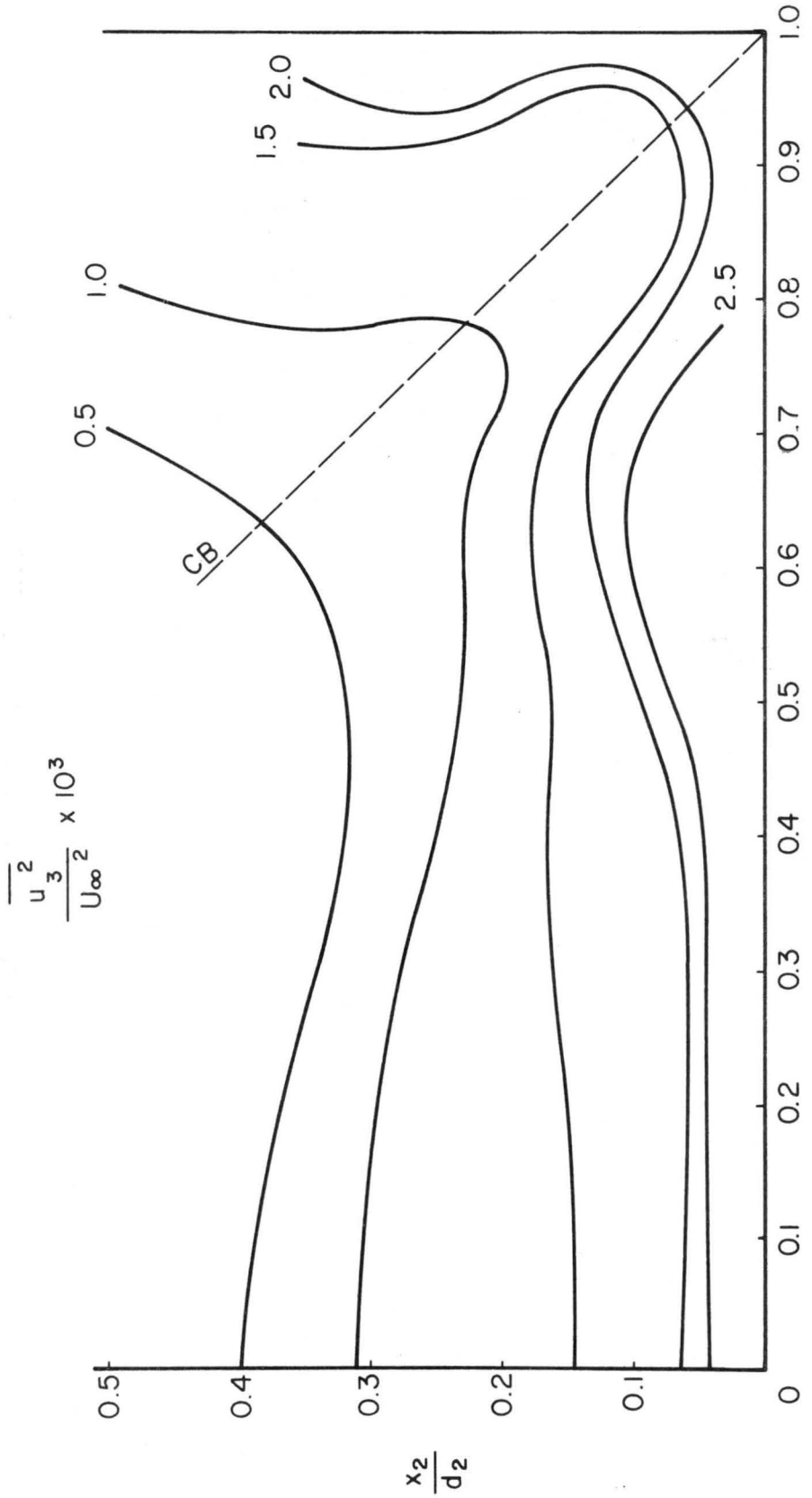

Fig. 38. Distribution of $\overline{u_3^2}/U_\infty^2$

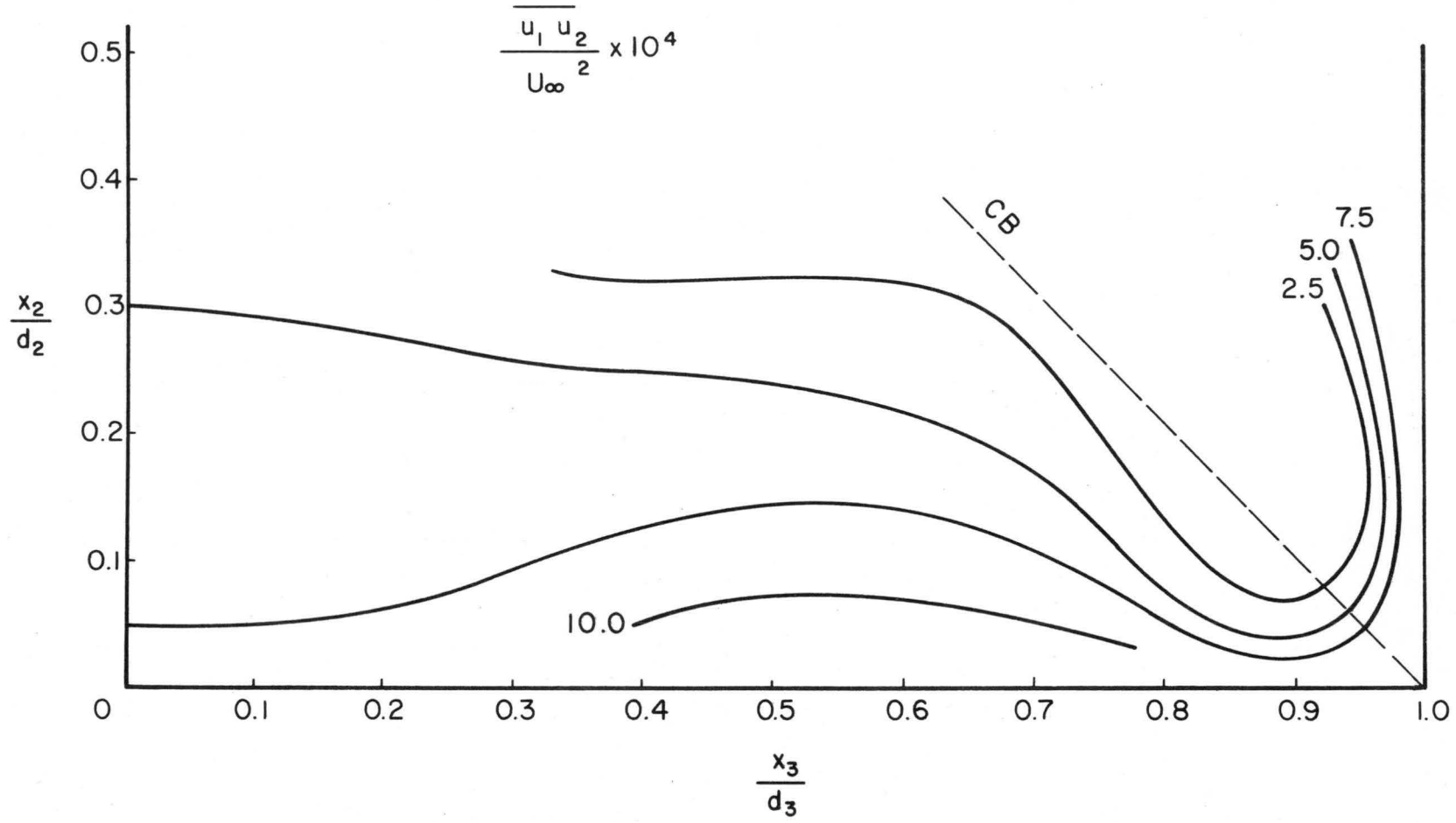

Fig. 39. Distribution of $\overline{u_1 u_2}/U_\infty^2$

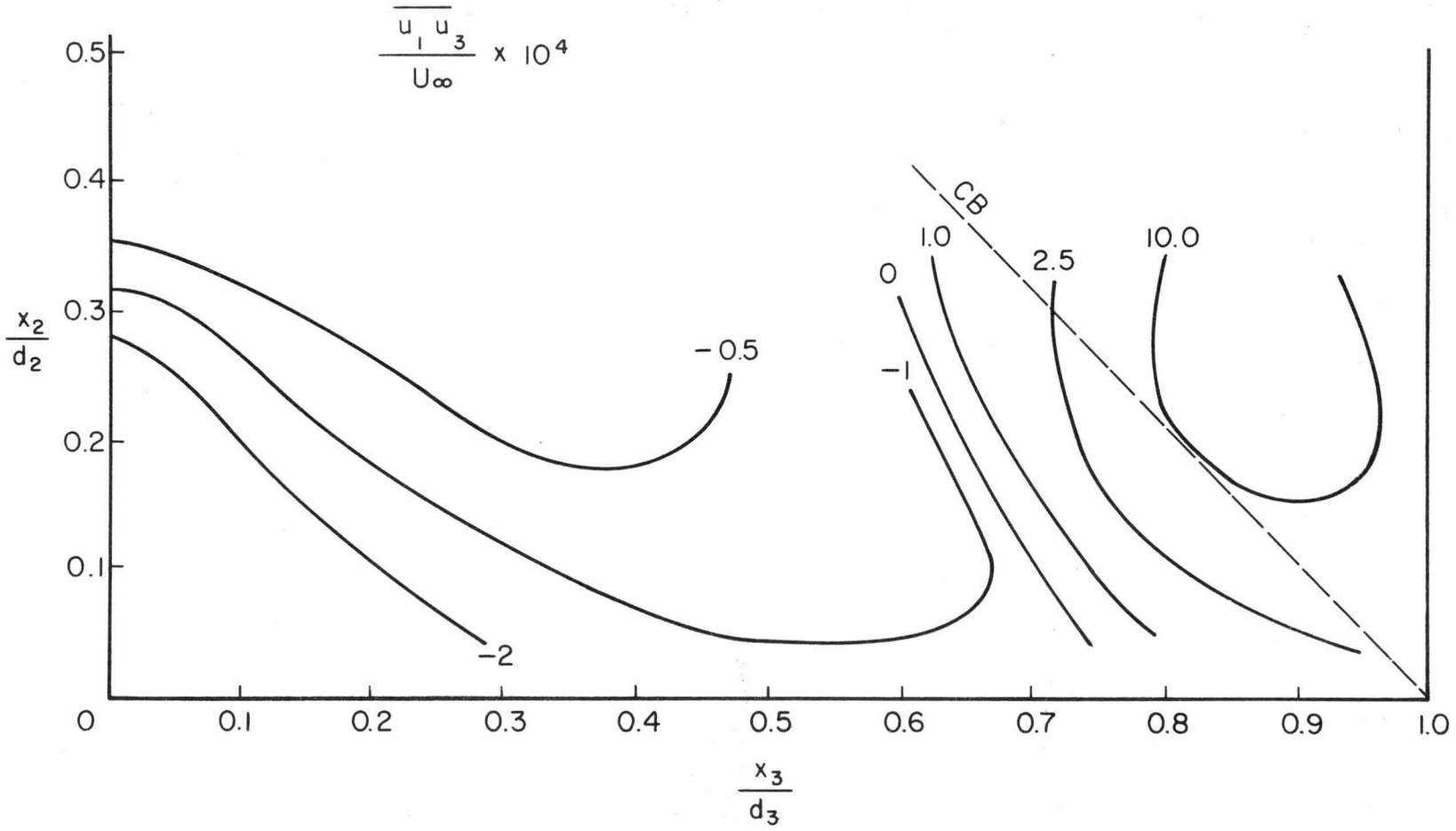

Fig. 40. Distribution of $\overline{u_1 u_3}/U_\infty^2$

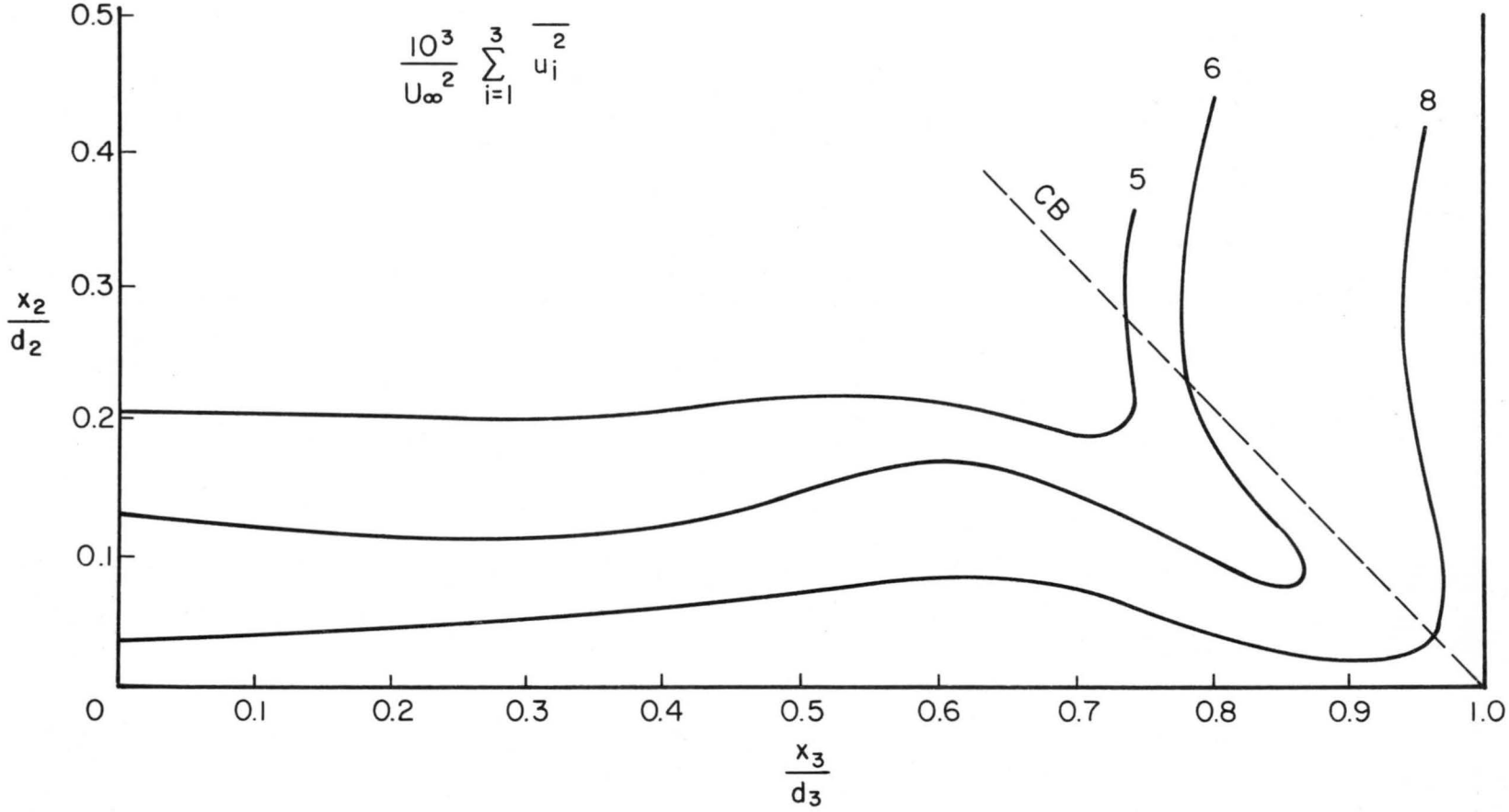

Fig. 41. Distribution of $1/U_\infty^2 \sum_{i=1}^{3} \overline{u_i^2}$

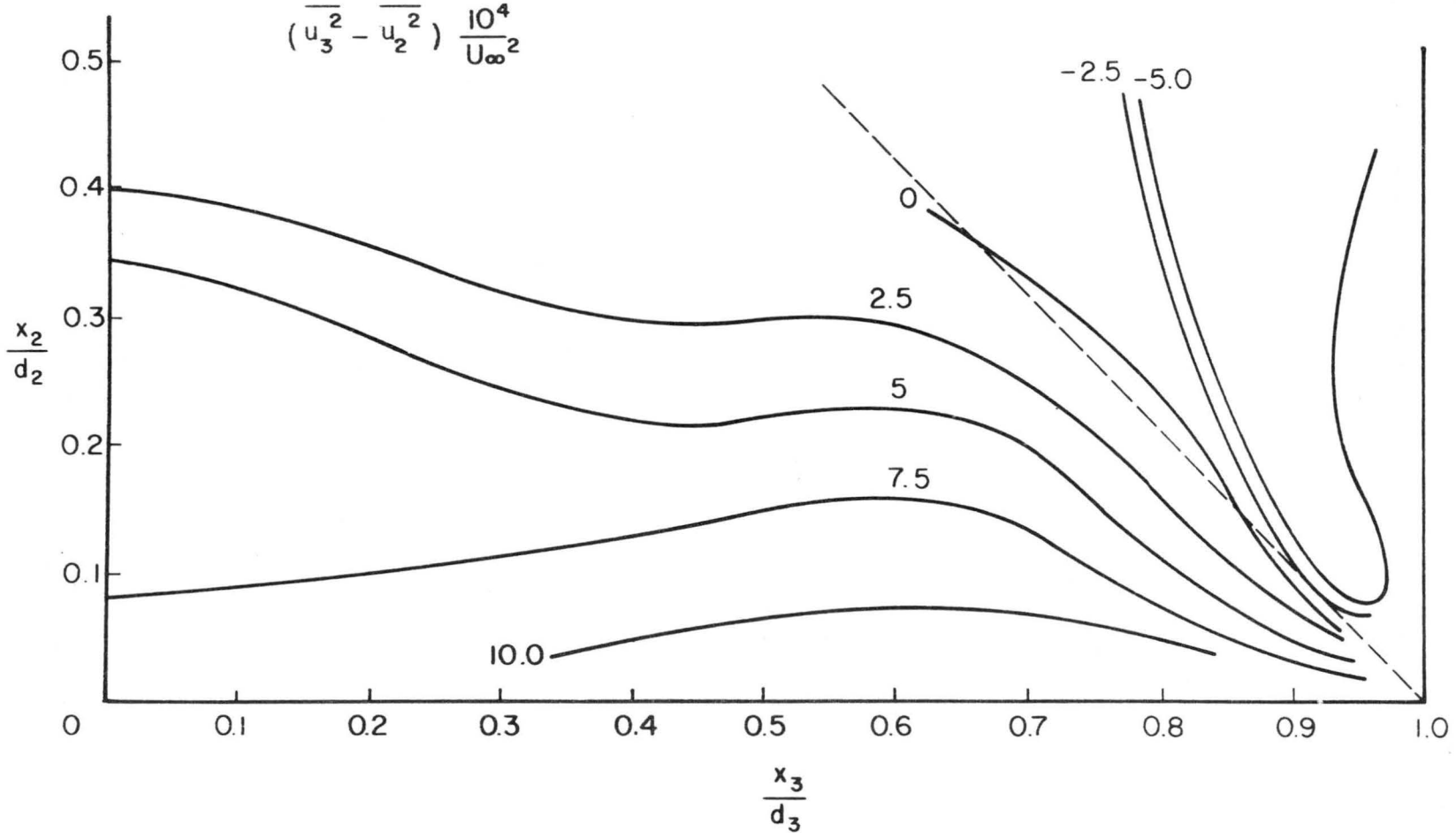

Fig. 42. Distribution of $(\overline{u_3^2}-\overline{u_2^2})/U_\infty^2$

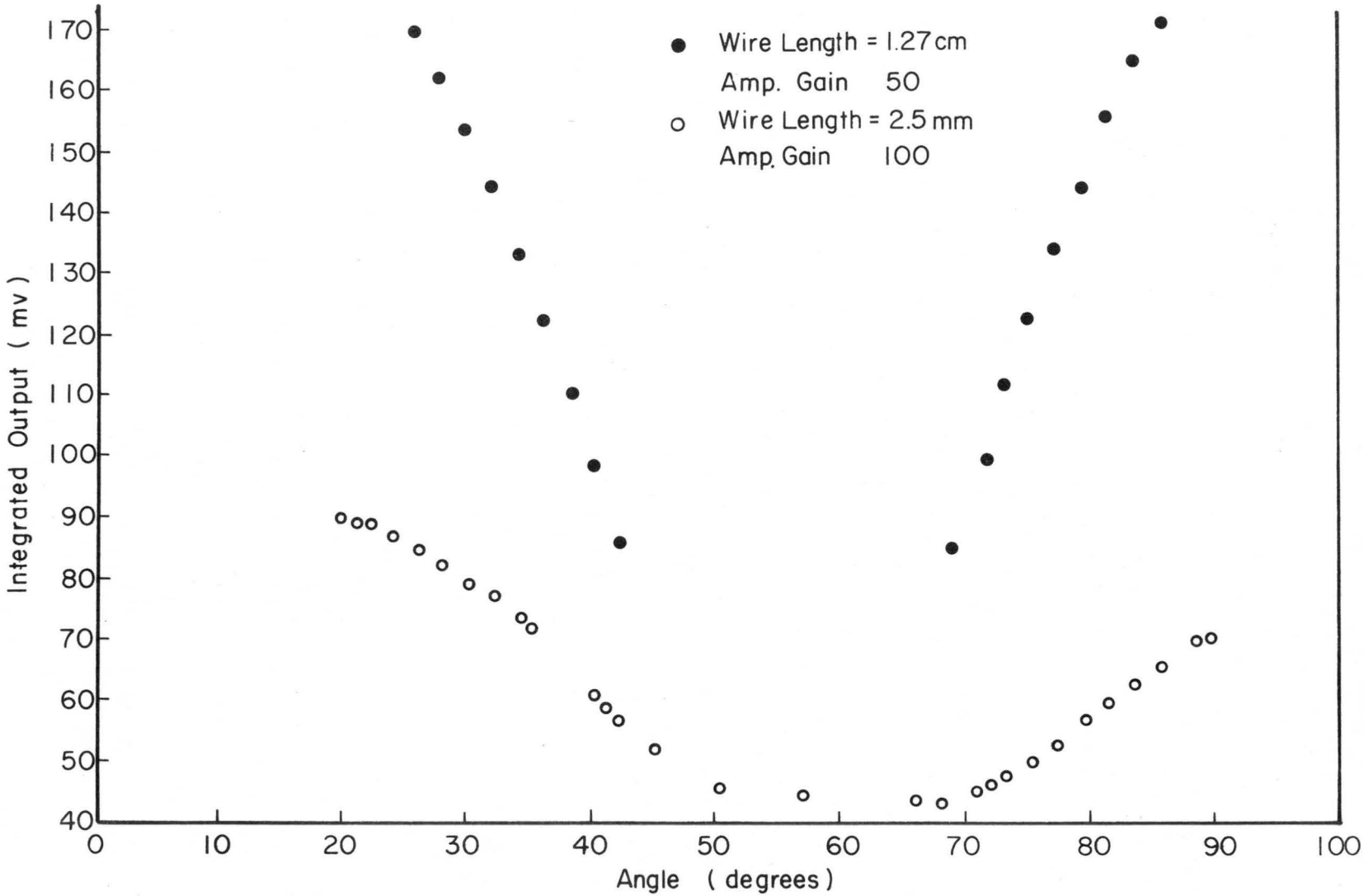

Fig. 43. Rotating hot wire response

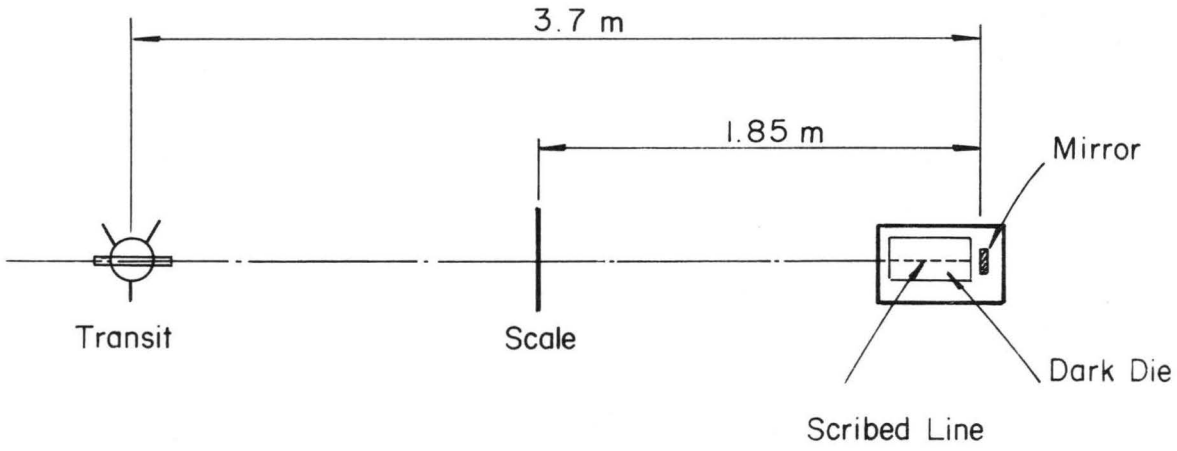

Fig. 44. Sketch of secondary reference line alignment

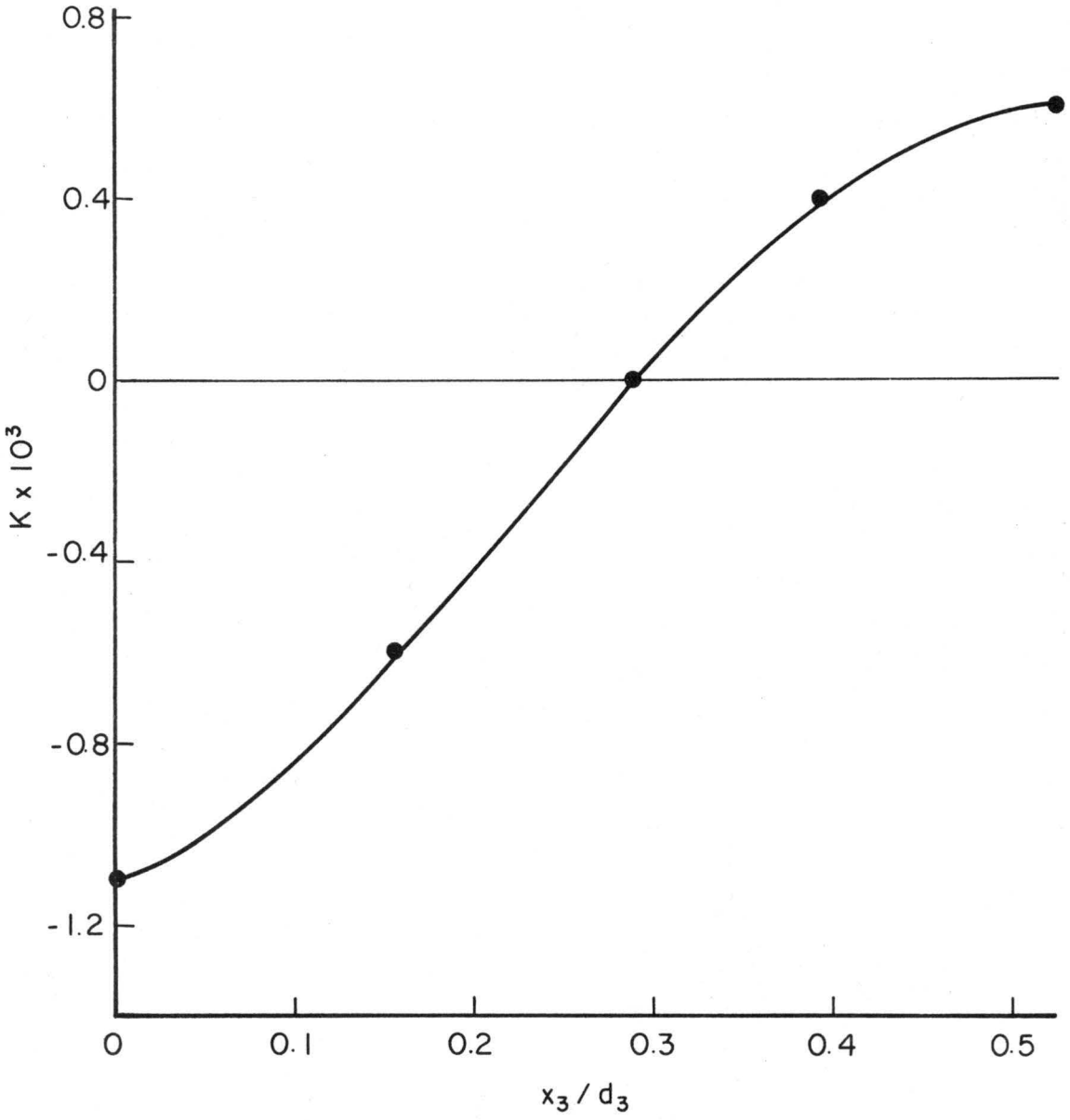

Fig. 45. Correction factor to momentum integral equation

Unclassified
Security Classification

DOCUMENT CONTROL DATA - R&D

(Security classification of title, body of abstract and indexing annotation must be entered when the overall report is classified)

1. ORIGINATING ACTIVITY *(Corporate author)*

Fluid Dynamics and Diffusion Laboratory
College of Engineering, Colorado State University
Fort Collins, Colorado 80521

2a. REPORT SECURITY CLASSIFICATION

Unclassified

2b. GROUP

3. REPORT TITLE

Secondary Flow in a Boundary Layer

4. DESCRIPTIVE NOTES *(Type of report and inclusive dates)*

Technical Report

5. AUTHOR(S) *(Last name, first name, initial)*

Veenhuizen, S. D. and Meroney, R. N.

6. REPORT DATE	7a. TOTAL NO. OF PAGES	7b. NO. OF REFS
June 1969	124	31

8a. CONTRACT OR GRANT NO.	9a. ORIGINATOR'S REPORT NUMBER(S)
N00014-68-A-0493	CER68-69SDV-RNM28
b. PROJECT NO. NR 062-414/6-6-68 (Code 438)	9b. OTHER REPORT NO(S) *(Any other numbers that may be assigned this report)*
c.	
d.	

10. AVAILABILITY/LIMITATION NOTICES

Distribution of this report is unlimited

11. SUPPLEMENTARY NOTES	12. SPONSORING MILITARY ACTIVITY
	Office of Naval Research U.S. Department of Defense Washington, D. C.

13. ABSTRACT

The secondary flow in a developing boundary layer of a square duct is investigated experimentally. Measurements of the horizontal components of secondary flow were made for three free stream Reynolds numbers based upon the hydraulic diameter of 3.6×10^5, 7.2×10^5, and 1.4×10^6. Measurements of the developing boundary layer parameters and turbulence quantities in a corner were made for the intermediate Reynolds number.

A criterion for two dimensionality of wind tunnel flow is examined and a correction for three dimensionality is evaluated from the experimental data.

DD FORM 1 JAN 64 1473

Unclassified
Security Classification

14. KEY WORDS	LINK A		LINK B		LINK C	
	ROLE	WT	ROLE	WT	ROLE	WT
Secondary flow						
Boundary layer						
Three dimensional flow						

INSTRUCTIONS

1. ORIGINATING ACTIVITY: Enter the name and address of the contractor, subcontractor, grantee, Department of Defense activity or other organization *(corporate author)* issuing the report.

2*a*. REPORT SECURITY CLASSIFICATION: Enter the overall security classification of the report. Indicate whether "Restricted Data" is included. Marking is to be in accordance with appropriate security regulations.

2*b*. GROUP: Automatic downgrading is specified in DoD Directive 5200.10 and Armed Forces Industrial Manual. Enter the group number. Also, when applicable, show that optional markings have been used for Group 3 and Group 4 as authorized.

3. REPORT TITLE: Enter the complete report title in all capital letters. Titles in all cases should be unclassified. If a meaningful title cannot be selected without classification, show title classification in all capitals in parenthesis immediately following the title.

4. DESCRIPTIVE NOTES: If appropriate, enter the type of report, e.g., interim, progress, summary, annual, or final. Give the inclusive dates when a specific reporting period is covered.

5. AUTHOR(S): Enter the name(s) of author(s) as shown on or in the report. Enter last name, first name, middle initial. If military, show rank and branch of service. The name of the principal author is an absolute minimum requirement.

6. REPORT DATE: Enter the date of the report as day, month, year; or month, year. If more than one date appears on the report, use date of publication.

7*a*. TOTAL NUMBER OF PAGES: The total page count should follow normal pagination procedures, i.e., enter the number of pages containing information.

7*b*. NUMBER OF REFERENCES: Enter the total number of references cited in the report.

8*a*. CONTRACT OR GRANT NUMBER: If appropriate, enter the applicable number of the contract or grant under which the report was written.

8*b*, 8*c*, & 8*d*. PROJECT NUMBER: Enter the appropriate military department identification, such as project number, subproject number, system numbers, task number, etc.

9*a*. ORIGINATOR'S REPORT NUMBER(S): Enter the official report number by which the document will be identified and controlled by the originating activity. This number must be unique to this report.

9*b*. OTHER REPORT NUMBER(S): If the report has been assigned any other report numbers *(either by the originator or by the sponsor)*, also enter this number(s).

10. AVAILABILITY/LIMITATION NOTICES: Enter any limitations on further dissemination of the report, other than those imposed by security classification, using standard statements such as:

(1) "Qualified requesters may obtain copies of this report from DDC."

(2) "Foreign announcement and dissemination of this report by DDC is not authorized."

(3) "U. S. Government agencies may obtain copies of this report directly from DDC. Other qualified DDC users shall request through _____."

(4) "U. S. military agencies may obtain copies of this report directly from DDC. Other qualified users shall request through _____."

(5) "All distribution of this report is controlled. Qualified DDC users shall request through _____."

If the report has been furnished to the Office of Technical Services, Department of Commerce, for sale to the public, indicate this fact and enter the price, if known.

11. SUPPLEMENTARY NOTES: Use for additional explanatory notes.

12. SPONSORING MILITARY ACTIVITY: Enter the name of the departmental project office or laboratory sponsoring *(paying for)* the research and development. Include address.

13. ABSTRACT: Enter an abstract giving a brief and factual summary of the document indicative of the report, even though it may also appear elsewhere in the body of the technical report. If additional space is required, a continuation sheet shall be attached.

It is highly desirable that the abstract of classified reports be unclassified. Each paragraph of the abstract shall end with an indication of the military security classification of the information in the paragraph, represented as *(TS)*, *(S)*, *(C)*, *or (U)*.

There is no limitation on the length of the abstract. However, the suggested length is from 150 to 225 words.

14. KEY WORDS: Key words are technically meaningful terms or short phrases that characterize a report and may be used as index entries for cataloging the report. Key words must be selected so that no security classification is required. Idenfiers, such as equipment model designation, trade name, military project code name, geographic location, may be used as key words but will be followed by an indication of technical context. The assignment of links, rules, and weights is optional.

DISTRIBUTION LIST FOR UNCLASSIFIED
TECHNICAL REPORTS ISSUED UNDER
CONTRACT N00014-68-A-TASK 062-414
0493-0001

Technical Library
Building 131
Aberdeen Proving Ground, Maryland 21005

Defense Documentation Center (20)
Cameron Station
Alexandria, Virginia 22314

Technical Library
Naval Ship Research and
Development Center
Annapolis Division
Annapolis Maryland 21402

Professor Bruce Johnson
Engineering Department
Naval Academy
Annapolis, Maryland 21402

Library
Naval Academy
Annapolis, Maryland 21402

Professor W. P. Graebel
Department of Engineering
Mechanics
The University of Michigan
College of Engineering
Ann Arbor, Michigan 48104

Professor W. R. Debler
Department of Engineering Mechanics
University of Michigan
Ann Arbor, Michigan 48108

Dr. Francis Ogilvie
Department of Naval Architecture
and Marine Engineering
University of Michigan
Ann Arbor, Michigan 48108

Professor S. D. Sharma
Department of Naval Architecture
and Marine Engineering
University of Michigan
Ann Arbor, Michigan 48108

Professor W. W. Willmarth
Department of Aerospace Engineering
University of Michigan
Ann Arbor, Michigan 48108

Professor Finn C. Michelsen
Naval Architecture and Marine
Engineering
445 West Engineering Bldg.
University of Michigan
Ann Arbor, Michigan 48104

AFOSR (REM)
1400 Wilson Boulevard
Arlington, Virginia 22204

Dr. J. Menkes
Institute for Defense Analyses
400 Army-Navy Drive
Arlington, Virginia 22204

Professor S. Corrsin
Mechanics Department
The Johns Hopkins University
Baltimore, Maryland 20910

Professor O. M. Phillips
The Johns Hopkins University
Baltimore, Maryland 20910

Professor L. S. G. Kovasznay
The Johns Hopkins University
Baltimore, Maryland 20910

Librarian
Department of Naval Architecture
University of California
Berkeley, California 94720

Professor P. Lieber
Department of Mechanical Engineering
University of California
Institute of Engineering Research
Berkeley, California 94720

Professor M. Holt
Division of Aeronautical Sciences
University of California
Berkeley, California 94720

Professor J. V. Wehausen
Department of Naval Architecture
University of California
Berkeley, California 94720

Professor J. R. Paulling
Department of Naval Architecture
University of California
Berkeley, California 94720

Professor E. V. Laitone
Department of Mechanical Engineering
University of California
Berkeley, California 94720

School of Applied Mathematics
Indiana University
Bloomington, Indiana 47401

Commander
Boston Naval Shipyard
Boston, Massachusetts 02129

Director
Office of Naval Research
Branch Office
495 Summer Street
Boston, Massachusetts 02210

Professor M. S. Uberoi
Department of Aeronautical Engineering
University of Colorado
Boulder, Colorado 80303

Naval Applied Science Laboratory
Technical Library
Bldg. 1 Code 222
Flushing and Washington Avenues
Brooklyn, New York 11251

Professor J. J. Foody
Chairman, Engineering Department
State University of New York
Maritime College
Bronx, New York 10465

Dr. Irving C. Statler, Head
Applied Mechanics Department
Cornell Aeronautical Laboratory, Inc.
P. O. Box 235
Buffalo, New York 14221

Dr. Alfred Ritter
Assistant Head, Applied Mechanics Dept.
Cornell Aeornautical Laboratory, Inc.
Buffalo, New York 14221

Professor G. Birkhoff
Department of Mathematics
Harvard University
Cambridge, Massachusetts 02138

Commanding Officer
NROTC Naval Administrative Unit
Massachusetts Institute of Technology
Cambridge, Massachusetts 02139

Professor N. Newman
Department of Naval Architecture and
Marine Engineering
Massachusetts Institute of Technology
Cambridge, Massachusetts 02139

Professor A. H. Shapiro
Department of Mechanical Engineering
Massachusetts Institute of Technology
Cambridge, Massachusetts 02139

Professor C. C. Lin
Department of Mathematics
Massachusetts Institute of Technology
Cambridge, Massachusetts 02139

Professor E. W. Merrill
Department of Mathematics
Masachusetts Institute of Technology
Cambridge, Massachusetts 02139

Professor M. A. Abkowitz
Department of Naval Architecture
and Marine Engineering
Massachusetts Institute of Technology
Cambridge, Massachusetts 02139

Professor G. H. Carrier
Department of Engineering and
Applied Physics
Harvard University
Cambridge, Massachusetts 02139

Professor E. Mollo-Christensen
Room 54-1722
Massachusetts Institute of Technology
Cambridge, Massachusetts 02139

Professor A. T. Ippen
Department of Civil Engineering
Massachusetts Institute of Technology
Cambridge, Massachusetts 02139

Commander
Charleston Naval Shipyard
U.S. Naval Base
Charleston, South Carolina 29408

A. R. Kuhlthau, Director
Research Laboratories for the
Engineering Sciences
Thorton Hall, University of Virginia
Charlottesville, Virginia 22903

Director
Office of Naval Research
Branch Office
219 Dearborn Street
Chicago, Illinois 60604

Library
Naval Weapons Center
China Lake, California 93557

Library MS 60-3
NASA Lewis Research Center
21000 Brookpark Road
Cleveland, Ohio 44135

Professor J. M. Burgers
Institute of Fluid Dynamics and
Applied Mathematics
University of Maryland
College Park, Maryland 20742

Acquisition Director
NASA Scientific and Technical
Information
P. O. Box 33
College Park, Maryland 20740

Professor Pai
Institute for Fluid Dynamics
and Applied Mathematics
University of Maryland
College Park, Maryland 20740

Technical Library
Naval Weapons Laboratory
Dahlgren, Virginia 22448

Computation & Analyses Laboratory
Naval Weapons Laboratory
Dahlgren, Virginia 22448

Professor C. S. Wells
LTV Research Center
Dallas, Texas 75222

Dr. R. H. Kraichnan
Dublin, New Hampshire 03444

Commanding Officer
Army Research Office
Box CM, Duke Station
Durham, North Carolina 27706

Professor A. Charnes
The Technological Institute
Northwestern University
Evanston, Illinois 60201

Dr. Martin H. Bloom
Polytechnic Institute of Brooklyn
Graduate Center, Dept. of Aerospace
Engineering and Applied Mechanics
Farmingdale, New York 11735

Technical Documents Center
Building 315
U.S. Army Mobility Equipment
Research and Development Center
Fort Belvoir, Virginia 22060

Professor J. E. Cermak
College of Engineering
Colorado State University
Ft. Collins, Colorado 80521

Technical Library
Webb Institute of Naval Architecture
Glen Cove, Long Island, New York 11542

Professor E. V. Lewis
Webb Institute of Naval Architecture
Glen Cove, Long Island, New York 11542

Library MS 185
NASA, Langley Research Center
Langley Station
Hampton, Virginia 23365

Dr. B. N. Pridmore Brown
Northrop Corporation
NORAIR-Div.
Hawthorne, California 90250

Dr. J. P. Breslin
Stevens Institute of Technology
Davidson Laboratory
Hoboken, New Jersey 07030

Mr. D. Savitsky
Stevens Institute of Technology
Davidson Laboratory
Hoboken, New Jersey 07030

Mr. C. H. Henry
Stevens Institute of Technology
Davidson Laboratory
Hoboken, New Jersey 07030

Professor J. F. Kennedy, Director
Iowa Institute of Hydraulic Research
State University of Iowa
Iowa City, Iowa 52240

Professor L. Landweber
Iowa Institute of Hydraulic Research
State University of Iowa
Iowa City, Iowa 52240

Professor E. L. Resler
Graduate School of
Aeronautical Engineering
Cornell University
Ithaca, New York 14851

Professor John Miles
c/o I.G.P.P.
University of California, San Diego
La Jolla, California 92038

Director
Scripps Institution of Oceanography
University of California
La Jolla, California 92037

Dr. B. Sternlicht
Mechanical Technology Incorporated
968 Albany-Shaker Road
Latham, New York 12110

Mr. P. Eisenberg, President
Hydronautics
Pindell School Road
Howard County
Laurel, Maryland 20810 (2)

Professor A. Ellis
University of California, San Diego
Department of Aerospace & Mech. Engrg. Sci.
La Jolla, California 92037

Mr. Alfonso Alcedan L., Director
Laboratorio Nacional De Hydraulics
Antigui Cameno A. Ancon
Casilla Jostal 682
Lima, Peru

Commander
Long Beach Naval Shipyard
Long Beach, California 90802

Professor John Laufer
Department of Aerospace Engineering
University Park
Los Angeles, California 90007

Professor J. Ripkin
St. Anthony Falls Hydraulic Lab.
University of Minnesota
Minneapolis, Minnesota 55414

Professor J. M. Killen
St. Anthony Falls Hydraulic Lab.
University of Minnesota
Minneapolis, Minnesota 55414

Lorenz G. Straub Library
St. Anthony Falls Hydraulic Lab.
Mississippi River at 3rd Avenue SE.
Minneapolis, Minnesota 55414

Dr. E. Silberman
St. Anthony Falls Hydraulic Lab.
University of Minnesota
Minneapolis, Minnesota 55414

Superintendent
Naval Postgraduate School
Library Code 0212
Monterey, California 93940

Professor A. B. Metzner
University of Delaware
Newark, New Jersey 19711

Technical Library
USN Underwater Weapons &
Research & Engineering Station
Newport, Rhode Island 02840

Technical Library
Underwater Sound Laboratory
Fort Trumbull
New London, Connecticut 06321

Professor J. J. Stoker
Institute of Mathematical Sciences
New York University
251 Mercer Street
New York, New York 10003

Engineering Societies Library
345 East 47th Street
New York, New York 10017

Office of Naval Research
New York Area Office
207 W. 24th Street
New York, New York 10011

Commanding Officer
Office of Naval Research
Branch Office
Box 39
FPO New York, New York 09510 (25)

Professor H. Elrod
Department of Mechanical Engineering
Columbia University
New York, New York 10027

Society of Naval Architects and
Marine Engineering
74 Trinity Place
New York, New York 10006

Professor S. A. Piascek
Department of Engineering Mechanics
University of Notre Dame
Notre Dame, Indiana 46556

United States Atomic Energy Commission
Division of Technical Information
Extension
P. O. Box 62
Oak Ridge, Tennessee 37830

Miss O. M. Leach, Librarian
National Research Council
Aeronautical Library
Montreal Road
Ottawa 7, Canada

Technical Library
Naval Ship Research and
Development Center
Panaman City, Florida 32401

Library
Jet Propulsion Laboratory
California Institute of Technology
4800 Oak Grove Avenue
Pasadena, California 91109

Professor M. S. Plesset
Engineering Division
California Institute of Technology
Pasadena, California 91109

Professor H. Liepmann
Department of Aeronautics
California Institute of Technology
Pasadena, California 91109

Technical Library
Naval Undersea Warfare Center
3202 E. Foothill Boulevard
Pasadena, California 91107

Dr. J. W. Hoyt
Naval Undersea Warfare Center
3202 E. Foothill Boulevard
Pasadena, California 91107

Professor T. Y. Wu
Department of Engineering
California Institute of Technology
Pasadena, California 91109

Director
Office of Naval Research
Branch Office
1030 E. Green Street
Pasadena, California 91101

Professor A. Acosta
Department of Mechanical Engineering
California Institute of Technology
Pasadena, California 91109

Naval Ship Engineering Center
Philadelphia Division
Technical Library
Philadelphia, Pennsylvania 19112

Technical Library (Code 249B)
Philadelphia Naval Shipyard
Philadelphia, Pennsylvania 19112

Professor R. C. Mac Camy
Department of Mathematics
Carnegie Institute of Technology
Pittsburgh, Pennsylvania 15213

Dr. Paul Kaplan
Oceanics, Inc.
Plainview, Long Island, New York 11803

Technical Library
Naval Missile Center
Point Mugu, California 93441

Technical Library
Naval Civil Engineering Lab.
Port Hueneme, California 93041

Commander
Portsmouth Naval Shipyard
Portsmouth, New Hampshire 03801

Commander
Norfolk Naval Shipyard
Portsmouth, Virginia 23709

Professor F. E. Bisshopp
Division of Engineering
Brown University
Providence, Rhode Island 02912

Dr. L. L. Higgins
TRW Space Technology Labs, Inc.
One Space Park
Redondo Beach, California 90278

Redstone Scientific Information Center
Attn: Chief, Document Section
Army Missile Command
Redstone Arsenal, Alabama 35809

Dr. H. N. Abramson
Southwest Research Institute
8500 Culebra Road
San Antonio, Texas 78228

Editor
Applied Mechanics Review
Southwest Research Institute
8500 Culebra Road
San Antonio, Texas 78206

Librarian
Naval Command Control Communications
Laboratory Center
San Diego, California 92152

Library & Information Services
General Dynamics-Convair
P. O. Box 1128
San Diego, California 92112

Commander (Code 246P)
Pearl Harbor Naval Shipyard
Box 400
FPO San Francisco, California 96610

Technical Library (Code H245C-3)
Hunters Point Division
San Francisco Bay Naval Shipyard
San Francisco, California 94135

Office of Naval Research
San Francisco Area Office
1076 Mission Street
San Francisco, California 94103

Dr. A. May
Naval Ordnance Laboratory
White Oak
Silver Spring, Maryland 20910

Fenton Kennedy Document Library
The Johns Hopkins University
Applied Physics Laboratory
8621 Georgia Avenue
Silver Spring, Maryland 20910

Librarian
Naval Ordnance Laboratory
White Oak
Silver Spring, Maryland 20910

Dr. Bryne Perry
Department of Civil Engineering
Stanford University
Stanford, California 94305

Professor Milton Van Dyke
Department of Aeronautical Engineering
Stanford University
Stanford, California 94305

Professor E. Y. Hsu
Department of Civil Engineering
Stanford University
Stanford, California 94305

Dr. R. L. Street
Department of Civil Engineering
Stanford University
Stanford, California 94305

Professor S. Eskinazi
Department of Mechanical Engineering
Syracuse University
Syracuse, New York 13210

Professor R. Pfeffer
Florida State University
Geophysical Fluid Dynamics Institute
Tallahassee, Florida 32306

Professor J. Foa
Department of Aeronautical Engineering
Rennsselaer Polytechnic Institute
Troy, New York 12180

Professor R. C. Di Prima
Department of Mathematics
Rennsselaer Polytechnic Institute
Troy, New York 12180

Dr. M. Sevik
Ordnance Research Laboratory
Pennsylvania State University
University Park, Pennsylvania 16801

Professor J. Lumley
Ordnance Research Laboratory
Pennsylvania State University
University Park, Pennsylvania 16801

Dr. J. M. Robertson
Department of Theoretical and
Applied Mechanics
University of Illinois
Urbana, Illinois 61803

Shipyard Technical Library
Code 130L7 Building 746
San Francisco Bay Naval Shipyard
Vallejo California 94592

Code L42
Naval Ship Research and
Development Center
Washington, D. C. 20007

Code 800
Naval Ship Research and
Development Center
Washington, D. C. 20007

Code 2027
U. S. Naval Research Laboratory
Washington, D. C. 20390 (6)

Code 438
Chief of Naval Research
Department of the Navy
Washington, D. C. 20360 (3)

Code 513
Naval Ship Research and
Development Center
Washington, D. C. 20007

Science & Technology Division
Library of Congress
Washington, D. C. 20540

ORD 913 (Library)
Naval Ordnance Systems Command
Washington, D. C. 20360

Code 6420
Naval Ship Engineering Center
Concept Design Division
Washington, D. C. 20360

Code 500
Naval Ship Research and
Development Center
Washington, D. C. 20007

Code 901
Naval Ship Research and
Development Center
Washington, D. C. 20007

Code 520
Naval Ship Research and
Development Center
Washington, D. C. 20007

Code 0341
Naval Ship Systems Command
Department of the Navy
Washington, D. C. 20360

Code 2052 (Technical Library)
Naval Ship Systems Command
Department of the Navy
Washington, D. C. 20360

Mr. J. L. Schuler (Code 03412)
Naval Ship Systems Command
Department of the Navy
Washington, D. C. 20360

Dr. J. H. Huth (Code 031)
Naval Ship Systems Command
Department of the Navy
Washington, D. C. 20360

Code 461
Chief of Naval Research
Department of the Navy
Washington, D. C. 20360

Code 530
Naval Ship Research and
Development Center
Washington, D. C. 20360

Code 466
Chief of Naval Research
Department of the Navy
Washington, D. C. 20360

Office of Research and Development
Maritime Administration
441 G. Street, NW.
Washington, D. C. 20235

Code 463
Chief of Naval Research
Department of the Navy
Washington, D. C. 20360

National Science Foundation
Engineering Division
1800 G. Street, NW.
Washington, D. C. 20550

Dr. G. Kulin
National Bureau of Standards
Washington, D. C. 20234

Department of the Army
Coastal Engineering Research Center
5201 Little Falls Road, NW.
Washington, D. C. 20011

Code 521
Naval Ship Research and
Development Center
Washington, D. C. 20007

Code 481
Chief of Naval Research
Department of the Navy
Washington, D. C. 20390

Code 421
Chief of Naval Research
Department of the Navy
Washington, D. C. 20360

Commander
Naval Ordnance Systems Command
Code ORD 035
Washington, D. C. 20360

Librarian Station 5-2
Coast Guard Headquarters
1300 E. Street, NW.
Washington, D. C. 20226

Division of Ship Design
Maritime Administration
441 G. Street, NW.
Washington, D. C. 20235

HQ USAF (AFRSTD)
Room 1D 377
The Pentagon
Washington, D. C. 20330

Commander
Naval Ship Systems Command
Code 6644C
Washington, D. C. 20360

Code 525
Naval Ship Research and
Development Center
Washington, D. C. 20007

Dr. A. Powell (Code 01)
Naval Ship Research and
Development Center
Washington, D. C. 20007

Director of Research Code RR
National Aeronautics & Space Admin.
600 Independence Avenue, SW.
Washington, D. C. 20546

Commander
Naval Ordnance Systems Command
Code 03
Washington, D. C. 20360

Code ORD 05411
Naval Ordnance Systems Command
Washington, D. C. 20360

AIR 5301
Naval Air Systems Command
Department of the Navy
Washington, D. C. 20360

AIR 604
Naval Air Systems Command
Department of the Navy
Washington, D. C. 20360

Dr. John Craven (PM 1100)
Deep Submergence Systems
Project
Department of the Navy
Washington, D. C. 20360

Code 522
Naval Ship Research and
Development Center
Washington, D. C. 20007

Commander
Naval Oceanographic Office
Washington, D. C. 20390

Chief of Research & Development
Office of Chief of Staff
Department of the Army
The Pentagon
Washington, D. C. 20310

Code 6342A
Naval Ship Systems Command
Department of the Navy
Washington, D. C. 20360

Code 468
Chief of Naval Research
Department of the Navy
Washington, D. C. 20360

Director
U. S. Naval Research Laboratory
Code 6170
Washington, D. C. 20390

Code 473
Chief of Naval Research
Department of the Navy
Washington, D. C. 20360

Code 6100
Naval Ship Engineering Center
Department of the Navy
Washington, D. C. 20360

Mr. Ralph Lacey (Code 6114)
Naval Ship Engineering Center
Department of the Navy
Washington, D. C. 20360

Dr. A. S. Iberall, President
General Technical Services, Inc.
451 Penn Street
Yeadon, Pennsylvania 19050

Dr. H. Cohen
IBM Research Center
P. O. Box 218
Yorktown Heights, New York 10598

Commanding General
U. S. Army Electronics Command
Attn: AMSEL-BL-DO, Mr. T. Pries
Fort Monmouth, New Jersey 07703

Professor E. Y. Hsu
Associate Professor of Fluid Mechanics
Stanford University
Department of Civil Engineering
Stanford, California 94305